Journal of Cardiovascular Magnetic Resonance®, 1(3), 257–294 (1999)

ABSTRACTS

Oral and Poster

Abstracts were presented at the annual meeting of the Society for Cardiovascular Magnetic Resonance in Atlanta, Georgia, January 22–24, 1999.

Magnetic Resonance Oximetry for Congenital Heart Disease

G.A. Wright, N. Merchant, G. Kim, J.A. Stainsby, X. Qi, G. Webb. *Toronto, Ontario, Canada*

Purpose: The goal of this study is to evaluate whether MRI measurements of blood oxygen saturation (%HbO_2) in the great vessels, primarily the superior vena cava (SVC) and pulmonary artery (PA), can characterize shunt severity in patients with simple intracardiac septal defects.

Methods: MR oximetry exploits the dependence of blood's signal decay time constant, T2, on %HbO_2. T2 measurements were made in the great vessels using a flow-insensitive, motion-compensated, magnetization-preparation sequence. These measurements were then transformed via the results of an in vitro calibration to %HbO_2 in each vessel. Shunt severity was determined from the change in %HbO_2 between the SVC and the PA, with a step-up of greater than 7%HbO_2, indicating a significant shunt. These measurements were repeated in 24 healthy subjects and 14 patients with atrial, atrioventricular, and ventricular septal defects. In the patient studies, results were compared to %HbO_2 measurements obtained from cardiac catheterization.

Results: MR %HbO_2 measurements compared favorably to those from cardiac catheterization. The mean difference between the two measures was 3.1%HbO_2, not deemed statistically significant in this study. Data from only one subject were rejected on the basis of poor quality, likely due to excessive respiratory motion. In the remaining studies, 23 of the 24 healthy subjects were correctly classified as not having significant shunts. In all 13 remaining patient studies, MR characterization of shunt significance matched that of cardiac catheterization.

Conclusions: MR oximetry is a promising method for the noninvasive assessment of oxygen saturation in the great vessels of the heart and, therefore, shunt severity in patients with congenital heart disease.

Real-Time Intravascular Magnetic Resonance Receiver Probe: Preliminary Observations with Three Prototype Catheters

P.A. Rivas, M.V. McConnell, G. Scott, C. Meyer, J.M. Pauly, D.G. Nishimura, A. Macovski, B.S. Hu. *Stanford, CA*

Purpose: Plaque imaging is important for the detection and monitoring of therapy in atherosclerotic heart disease. While intravascular ultrasound has proven to be a valuable adjunct in coronary interventions, tissue characterization is limited. MRI has been shown to image plaque components. However, given the need to resolve plaque structures of 80–200 μm, a significant increase in sensitivity is needed. Our goal is to improve the SNR for high-resolution images using intravascular receiver coils, while avoiding motion-related problems with real-time imaging.

Methods: Three receiver coils were assessed for sensitivity in saline: (1) opposed solenoids, (2) flexible twin lead, and (3) dipole antenna. Their sensitivity was assessed ex vivo in human arteries fixed in formalin with histologic correlation and in vivo in the rabbit. All sequences were performed on a GE 1.5-T system with 4 Gauss/cm gradients with a maximum slew rate of 150 mT/m/ms.

Results: In saline, the flexible twin-lead receiver coil provided the least falloff of sensitivity radial to the coil and was independent of loading conditions. *Ex vivo* images show down to 80 μm resolution with three distinct layers seen optimally with a T2-weighted fast spin-echo sequence. Real-time image acquisition and display were achieved at a temporal resolution of 50–200 msec with resultant trade-offs due to hardware constraints.

Conclusion: Real-time interactive intravascular MR imaging is a feasible imaging method. Further improvements in image quality are expected to make this a useful research and clinical tool.

References

1. Hurst G. Intravascular (catheter) NMR receiver probe: preliminary design analysis and application to canine iliofemoral imaging. *Magn Reson Med*, 1992; 24:343–357.
2. Atalar E. High resolution intravascular MRI and MRS by using a catheter receiver coil. *Magn Reson Med*, 1996; 36:596–605.
3. Ocali O. Intravascular magnetic resonance imaging using a loopless catheter antenna. *Magn Reson Med*, 1997; 37:112–118.

Dobutamine Stress Magnetic Resonance Imaging Is Superior to Dobutamine Stress Echocardiography for the Detection of Stress-Induced Wall Motion Abnormalities

E. Nagel, H.B. Lehmkuhl, U. Vogel, C. Klein, S. Schalla, W. Boksch, S. Dreysse, A. Ellmer, E. Frantz, E. Fleck. *Berlin, Germany*

Dobutamine stress echocardiography (DSE) has become a well-established tool for the noninvasive detection of myocardial ischemia. However, it is highly user dependent (1), and image quality is nondiagnostic in at least 10–15% of patients, reducing its overall diagnostic accuracy. Rapid magnetic resonance imaging allows the visualization of a complete cardiac cycle within a single breathhold. This allows similar stress protocols to be applied to MR as are currently used for DSE. We have recently shown that dobutamine stress MR (DSMR) is superior to DSE (2). The aim of the current study was to prove the hypothesis that these differences are mainly due to the superior image quality of DSMR in comparison to DSE.

In 209 patients (148 m, 61 f) scheduled for their primary diagnostic coronary angiography, DSE (Sonotron System 5) and DSMR (Philips ACS NT, 1.5 Tesla) were performed. MR images were obtained during breath holding in 3 short-axes, a 4- and a 2-chamber view using a standard turbo gradient echo sequence (TE: 4.3 ms, TR: 8 ms, temporal resolution: 35 ms (better under stress), spatial resolution: 1 × 1.2 × 8 mm). Patients were examined at rest and with increasing doses of dobutamine (5, 10, 20, 30, 40 μg/kg body weight for 3 minutes each) and up to 1 mg atropine until submaximal heart rate was reached. Regional wall motion was assessed visually by two independent observers for 16 segments per patient. Significant coronary artery disease was defined as a diameter stenosis of ≥50%. Image quality was graded according to the visibility of the endocardial border.

In 178 patients, a diagnostic DSE and DSMR could be obtained. Overall sensitivity was 74.3% for DSE and 88.7% for DSMR ($p < 0.05$); specificity was 69.8% and 85.7%, respectively ($p < 0.05$). Image quality was very good in 20% of DSE examinations and 69% of DSMR examination ($p < 0.05$), good in 31% and 13%, moderate in 41% and 16%, and nondiagnostic in 8% and 2%. In patients with echocardiographic good to very good image quality (51% of patients), sensitivity and specificity were similar between both stress tests; however, there was a highly significant improvement of sensitivity and specificity for patients with moderate echocardiographic image quality when examined with DSMR. The sensitivities for different vessel segments are shown in the table:

	Proximal		Medial		Distal	
	DSE	DSMR	DSE	DSMR	DSE	DSMR
LAD	78%	97%	71%	93%	71%	92%
RCx	68%	92%			69%	90%
RCA	73%	93%	76%	95%	72%	84%

Dobutamine stress MR tomography is superior to dobutamine stress echocardiography. These differences can be mainly explained by the superior quality of the MR images especially in the posterior circulation.

References

1. Hoffmann R, et al. Analysis of interinstitutional observer agreement in interpretation of dobutamine stress echocardiograms. *J Am Coll Cardiol,* 1996; 27:330–6.
2. Nagel E, et al. High dose dobutamine magnetic resonance imaging for the detection of myocardial ischemia. *Circulation* (in press).

Delineation of Induced Collateral Circulation in a Pig Model of Chronic Ischemia Based on Assessment of Functional Contractile Reserve

C.H. Lorenz, K.J. Lunn, M. Nolan, M. Taniuchi. *St. Louis, MO*

The recent clinical emergence of vascular growth factors for treatment of coronary artery disease mandates development of robust methods for assessing the efficacy of neovascular perfusion. Accordingly, we propose quantitative strategies based on cine MRI to detect improvements in wall motion defects in a pig model of chronic ischemia following stimulation of collateral development.

An ameroid occluder was surgically placed around the left circumflex coronary artery adjacent to a balloon occluder in seven pigs (25–50 kg). X-ray angiography documented that the ameroid occluder completely obstructed the artery after 4 weeks. MR imaging was performed at three time points; 1–2 weeks, 4 weeks, and 6–9 weeks after surgery. Additional control animals ($n = 9$) with only a balloon occluder were also studied. Short-axis cine imaging was performed at baseline, with the balloon inflated to occlude the artery (duration 30–60 seconds) and during recovery following release of the balloon. At the 6–9-week time point, dobutamine stress was administered (5→40 μg/kg/min) to test the functional reserve of the developed collateral circulation in the ameroid constrictor animals.

Image analysis consisted of delineation of the endocardial and epicardial borders to calculate wall thickening (%) over systole. The short-axis slice was divided into eight circumferential regions for comparison between imaging sessions and between animals.

Early after ameroid constrictor placement (1–2 weeks), the animals exhibited resting ischemia with a decrease in wall thickening from 40% to 30%. During balloon occlusion, wall thickening was absent. By 4 weeks, wall thickening both at rest and during occlusion remained normal, indicating development of protective collateral circulation subtending an occluded principal artery. However, during dobutamine stress, wall thickening diminished, indicating that the collateral circulation was not adequate to support inotropic stimulation. In contrast, the control animal (balloon occluder only) exhibited deficits in wall thickening during balloon occlusion in all sequential studies.

In conclusion, evidence of collateral circulation can be demonstrated by quantitative wall motion analysis by 4 weeks postameroid constrictor placement. However, the extent of collateralization is not sufficient by 6–9 weeks to sustain inotropic stimulation. Additional studies at later time periods are necessary to determine whether further evolution of the developed collaterals will allow tolerance of inotropic stimulation.

Intracoronary Stents Are Safe During MR Imaging of the Heart

M.G. Friedrich,[1] D. Kivelitz,[2] O. Strohm,[1] J. Schulz-Menger,[1] W. Gross,[3] D. Hamm,[2] and R. Dietz.[1] [1]*Franz-Volhard-Klinik, Charité, Humboldt University, Berlin;* [2]*Radiology Department, Charité, Humboldt University, Berlin;* [3]*Bayerisches Zentrum f. angewandte Energieforschung e.V., Erlangen, Germany*

The growing use of MR imaging of the heart and the wide application of intracoronary stents warrant extensive safety consideration. There is no evidence for movement of stents in the magnetic field. However, up to now it is not known whether the temperature of stents is increased during a routine cardiac MRI study. An increase of the temperature of more than 5° could lead to local thrombosis at the site of implantation.

We assessed 16 different stents currently used on or dedicated for the world market in conventional MR scanners at a field strength of 1.0 and 1.5 T, respectively (Siemens Magnetom Expert and Siemens Magnetom Vision). Using the body coil and surface coils we applied seven different sequences (15 sec to 4 min) with high-energy transfer rates, including EPI. Measurements at 1.5 T were repeated after implantation of the stents into coronary arteries of a pig heart. Temperature changes were assessed by an infrared camera system (ZAE Bayern, Erlangen, Germany) with a sensitivity of <0.1°. There was no movement of stents during the studies. Furthermore, we were not able to detect any changes of temperature more than 0.3°C in 224 measurements. A small copper coil showed an increase up to 48°C.

We conclude that intracoronary stents pose no problems to patients in cardiac studies.

Atherosclerotic Plaque Morphology of Human Carotid Artery: The Role of Magnetic Resonance Imaging (MRI)

Chun Yuan, Thomas S. Hatsukami. *Seattle, WA*

Introduction: Accurate measurement of atherosclerotic plaque burden and identification of plaque characteristics may provide the critical information needed to differentiate unstable plaques from stable ones. MR has shown great potential for characterizing atherosclerosis in both human and animal model studies. This study was carried out to evaluate the capability of high-resolution MRI with multiple contrast weightings to measure plaque volume and to identify the existence of a fibrous cap in human carotid arteries with advanced atherosclerosis.

Materials and Methods: Patients scheduled to undergo carotid endarterectomy at UW Medical Center and the VA Hospital in Seattle were recruited for the study. All MR scans were conducted on a 1.5-T Signa scanner using custom-made phased-array surface coils and a high-resolution multiple contrast imaging protocol. In this protocol, a flow-enhanced MOTSA technique was used along with two flow-suppressed spin echo (fast spin echo) techniques to obtain sequential cross-sec-

tional images centered at the carotid bifurcation. The excised plaque was scanned fresh ex vivo and processed for histologic evaluation. An IDL-based area measurement program was developed to calculate the vessel wall area following manual outlining of the lumen and outer wall boundaries. Ex vivo MR scans of plaque specimen were used as the reference standard and compared to the vessel wall area measured from in vivo T1 images. Blinded review of MR images to identify thick, thin, and ruptured fibrous cap were conducted and the results compared to histology findings.

Results and Conclusions: Based on paired measurements from 14 consecutive patients, the maximal wall area from in vivo and ex vivo images strongly agreed (both T1 and proton density weighted images). This result indicates that MRI is highly accurate for in vivo measurement of maximal wall area. Based on reviewing 22 cases of in vivo patient data, we found a strong agreement between MRI and histologic findings in identifying the three states of fibrous cap. Both findings indicate that the high-resolution MRI technique may allow for studies that examine the relationship between clinical outcome and changes in plaque volume and the fibrous cap.

Comparison of the Effects of Adaptive Ordering Techniques on Coronary Artery Imaging

P. Jhooti, J. Keegan, P. Gatehouse, D. Firmin. *Magnetic Resonance Unit, Royal Brompton Hospital, London, UK*

Introduction: It has previously been demonstrated that respiratory artifacts can be reduced by use of a variety of techniques, all of which involve altering the order of acquisition of phase encode lines depending on the position of the diaphragm (1,2). The aim of this study is to investigate the implications of the use of a variety of adaptive ordering techniques for coronary artery imaging.

Method: Simulations were carried out using data sets acquired of different-sized tubes (5, 3, and 1 mm), shifted by a series of 1-mm steps to generate motion data sets. The hybrid ordered phase encoding (HOPE) (Fig. 1) method identified two general ordering methods that could be used depending on the breathing pattern: symmetric (Fig. 1a) and asymmetric (Fig. 1b). Both ordering patterns were tested with a variety of single and dual acceptance windows to assess effects on scan efficiency and image quality. The effects of ordering only in the inner window was also tested along with the influence of phase encode direction with respect to motion. The curvature of the tube (Fig. 2) allowed more detailed analysis of the effects of the different parameters on its various sections.

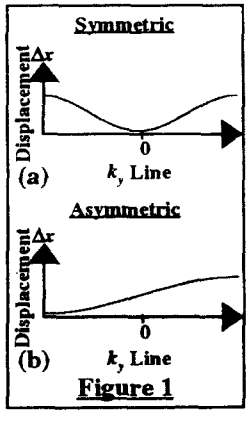

Figure 1

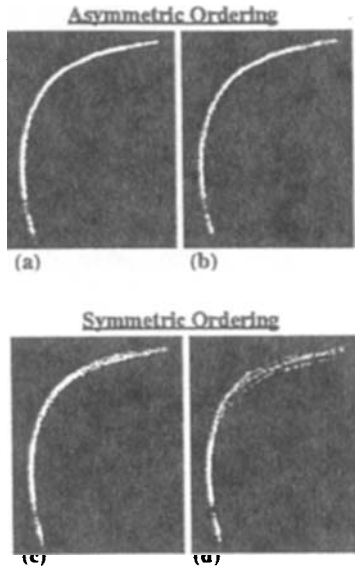

Figure 2. For every comparable windowing combination, where an asymmetrically weighted pattern was used rather than a symmetrically weighted pattern, the image quality was improved. In this example, a dual acceptance window, of 5 mm for the inner 75% (a, c) and 50% (b, d) of k-space and 10 mm for the outer regions, was used.

Results and Conclusion: Initial results have confirmed the importance of methods which use ordering to weight each segment of k-space. More importantly, however, a significant difference in image quality has been found depending on the ordering method used. For every comparable windowing combination, where an asymmetrically weighted pattern was used rather than a symmetrically weighted pattern, the image quality was improved. This was consistent for each vessel studied. These findings have important implications for techniques which use a symmetrically weighted scheme through k-space. Our studies suggest that it is better to order the central region of k-space using an asymmetric scheme and forsake ordering in up to 50% of the outer regions than to use a symmetrically weighted scheme.

References

1. Jhooti P, et al. JMRI, 1998; 8:968.
2. Sinkus R, et al. Proc. of ISMRM, 1997; 5:1894.

A Comparison of Flash Gradient Echo and Spiral MR Coronary Angiography Sequences at 0.5 T

A.M. Taylor, J. Keegan, P. Jhooti, P.D. Gatehouse, D.N. Firmin, D.J. Pennell. *London, UK*

Recently we implemented an interleaved spiral magnetic resonance coronary angiography (MRCA) imaging sequence at 0.5 T, establishing practical methods for dealing with main magnet inhomogeneities and attaining optimal epicardial fat saturation (1). In this current study, we use these techniques to compare 2D navigator echo (NE) gated MRCA images acquired with a segmented k-space, fast gradient echo sequence (Turbo-FLASH), and a spiral echo planar sequence (Spiral). MRCA images were acquired in 30 normal subjects and 15 patients with coronary artery disease. Images of the right coronary artery were acquired during free respiration using NE gating. Turbo-FLASH parameters: TE 6.7 ms; TR 12 ms; in-plane resolution 1.2 × 2.3 mm; read-out duration 105 ms; incremental flip angle 35–90°; acquired over 16 cardiac cycles. Spiral parameters: in-plane resolution 1.2 × 1.2 mm; read-out duration

18.6 ms; 20 interleaves; flip angle 90°. Image quality was scored by three independent blinded observers and image signal-to-noise ratio measured. There was a significant improvement in the image quality with the Spiral sequence (2.3 vs. 1.8, $p = 0.002$). This was associated with a twofold increase in the image signal-to-noise ratio (52.2 vs. 23.1, $p < 0.001$) and a twofold increase in the image resolution in the phase direction (intrinsic to the Spiral sequence) over the gradient echo sequence. However, there was a 25% increase in the total image acquisition time (20 vs. 16 accepted cardiac cycles) for the Spiral sequence. Spiral MRCA images were acquired during free respiration using navigator echo gating. Image quality, image signal to noise, and image resolution were superior to segmented k-space fast gradient echo images acquired in the same subjects. These improvements are secondary to the intrinsic characteristics of the Spiral sequence used and the short read-out period, which reduces the effects of both cardiac and respiratory motion on image quality.

Reference

1. Keegan J, et al. Coronary artery imaging in a 0.5 tesla scanner: implementation of real-time navigator echo controlled segmented k-space FLASH and interleaved spiral sequences. *Magn Reson Med* (in press).

A Fast 3D Approach for Coronary MRA

R.M. Botnar, M. Stuber, K.V. Kissinger, W.J. Manning. *Boston, MA*

Background: 2D-breathheld coronary magnetic resonance angiography (MRA) has been shown to be a fast and reliable method to depict portions of the proximal coronary arteries (1). Recent developments, however, allow for free-breathing navigator gated (2) and navigator corrected (3) 3D coronary MRA, which has an inherent better signal-to-noise ratio (SNR) and which allows for the acquisition of adjacent thin slices without the misregistration problems known from 2D approaches. The drawback of a 3D acquisition is the increased scan time.

Purpose: Implementation of a free-breathing 3D multishot EPI (TFE-EPI) sequence with a scan time is comparable to multislice 2D approaches but with the benefits of a 3D technique.

Methods: Eight healthy adult subjects were examined in supine position using a navigator gated and corrected ECG triggered 3D TFE-EPI (4) imaging sequence. All measurements were performed on a 1.5-Tesla Philips Gyroscan ACS-NT MR scanner (Philips Medical Systems, Best, NL) using a five-element cardiac synergy coil and an advanced coronary software package. The measured 3D volume consisted of 20 slices with a reconstructed slice thickness of 1.5 mm and an in-plane resolution of 1.0–1.3 × 1.4–1.8 mm. The diastolic TFE-EPI acquisition block was preceded by a T2 prep pre-pulse for muscle suppression (5), a 2D selective diaphragmatic navigator pulse for respiratory motion compensation, and a fat suppression prepulse. Each TFE-EPI shot consisted of two RF excitation pulses followed by seven EPI readouts. A complete *kz* plane was acquired in six TFE-EPI shots, resulting in a total scanning time of 2:34 min assuming a heart rate of 60 bpm and a navigator efficiency of 50%. With a TR of 19 ms and an effective TE of 5.4 ms, the duration of the acquisition window duration was 38 ms.

Results: All subjects were examined without any complications. In all cases, extensive portions of the left (LAD and LCX) and right coronary arteries (RCA) could be visualized (Fig. 1). Suppression of the myocardium was also excellent in all cases (Fig. 1). Scanning time varied between 2 and 3 minutes depending on the heart rate.

Conclusions: We presented a new approach for 3D coronary MRA, which allows for scan times comparable to 2D approaches but which takes advantage of the enhanced SNR of 3D acquisitions and the post-processing benefits of thin adjacent slices. The robust image quality and the short average scanning time suggest this approach may be useful for screening the major coronary arteries.

References

1. Manning WJ, Li W, Boyle NG, Edelman RR. *Circulation,* 1993; 87:94–104.
2. Li D, Kaushikkar S, Haacke EM, et al. *Radiology,* 1996; 201:857–863.
3. Botnar RM, Stuber M, Kissinger KV, Danias PG, Manning Wj. In Proc. ISMRM, Sydney, 1998, p. 23.
4. McKinnon GC. *Magn Reson Med,* 1993; 30:609–616.
5. Brittain JH, Hu BS, Wright GA, Meyer CH, Macovski A, Nishimura DG. *Magn Reson Med,* 1995; 33:689–696.

Accelerated Coronary MR Angiography in Volunteers and Patients Using Double-Oblique 3D Acquisitions Combined with SMASH

D.K. Sodickson, M. Stuber, R.M. Botnar, K.V. Kissinger, W.J. Manning. *Boston, MA*

Purpose: To reduce acquisition times for state-of-the-art coronary MR angiography sequences and to demonstrate the capabilities of SMASH image reconstructions in oblique image planes.

Methods: Four healthy adult volunteers and one patient with x-ray angiographically-confirmed coronary artery disease and a prior coronary stent placement were imaged as part of an ongoing study of MR coronary angiography using SMASH. To optimize coverage of the coronary artery tree and to take full advantage of high in-plane resolutions (0.7 × 1.0 mm), 3D volumetric acquisitions were planned in double oblique planes coinciding with the major axes of the coronary arteries (1), using a three-point planscan software tool on a Philips ACS-NT imaging system (Philips Medical Systems, Best, NL). The 3D acquisitions were obtained with reduced phase encoding for subsequent SMASH reconstruction (2), yielding two- to fourfold reductions in total acquisition time as compared with full acquisitions. Imaging was performed during free breathing with navigator gating and correction and a T2 prepulse for contrast enhancement (3,4). A six-element flexible linear coil array was used, with subjects in either a prone or a supine position.

Results: In all cases, SMASH image reconstructions were successful, and extensive portions of the coronary arteries could be visualized, even for slice angulations up to 30–40° from the coronal plane of the coil array. Some loss of SNR as compared with full-time acquisitions using the same coil array did not affect coronary visibility.

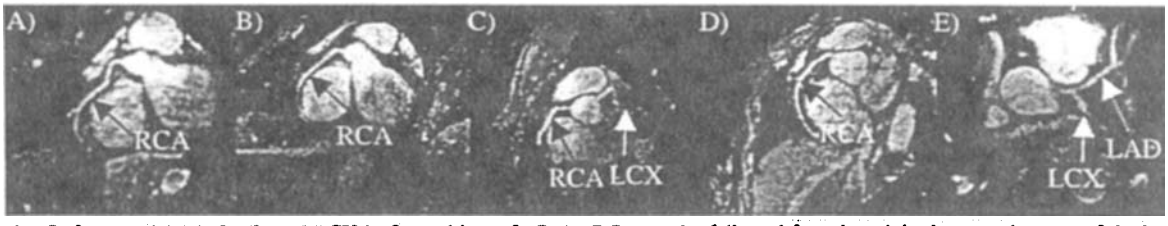

Figure 1. Reformatted RCA, LAD, and LCX in five subjects. In B the RCA can be followed from its origin down to the apex of the heart.

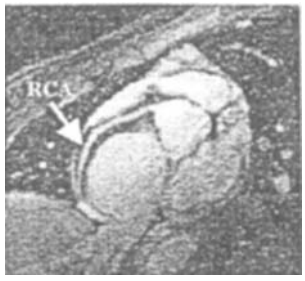

Figure 1. Single slice of a SMASH-reconstructed 3D volume in a healthy volunteer, showing a 7.5-cm length of the RCA (acceleration factor 2, total scan time 11 minutes).

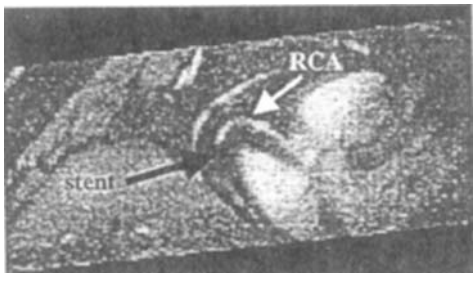

Figure 2. Local MIP of a SMASH-reconstructed 3D volume in a patient with coronary disease, showing the RCA interrupted by the signal void of a coronary stent (acceleration factor 2, total scan time 11 minutes as compared with 23 minutes for a full acquisition).

Conclusions: The SMASH technique has been succesfully combined with high-resolution double-oblique 3D acquisitions to yield high-quality coronary MR angiograms. Advantages of reduced scan times include increased patient comfort and compliance and reduced long-term navigator drift. This work has focused on the use of SMASH for acquisition time reduction in state-of-the-art coronary imaging sequences. Other sequence-dependent advantages of increased imaging speed, including increased spatial and/or temporal resolution and improved relaxation behavior, may also be achieved (5).

References

1. Stuber M, et al. Proc. SCMR (submitted).
2. Sodickson DK, et al. *Magn Reson Med,* 1997; 38:591–603.
3. Brittain JH, et al. *Magn Reson Med,* 1995; 33:689–696.
4. Botnar RM, et al. Proc. ISMRM 1998, Abstract 23.
5. Sodickson DK, et al. Proc. SCMR 1998, Abstract 27.

Noninvasive Detection of Significant Stenosis in the Coronary Artery Bypass Grafts Using Fast Velocity Encoded Cine MRI

N. Kawada, H. Sakuma, B.C. Cruz, T. Shimono, I. Yada, T. Hirano, K. Takeda. *Tsu, Mie, Japan*

Clinical usefulness of fast MR flow measurement in predicting significant stenosis in the internal mammary artery (IMA) to coronary artery bypass conduit was evaluated. Twenty-three patients who underwent IMA graft surgery were studied using a 1.5-T MR imager. On selective x-ray angiography, no significant stenosis was observed in 18 patients (group A) and significant stenosis (>75%) was found in 5 patients (group B). Breathhold velocity encoded cine (VEC) MR images of the IMA grafts were acquired before and after administration of dipyridamole. Volume flow rate and diastolic to systolic peak ratio (D/P ratio) were quantified by using Xphase software. Average blood flow rate in the IMA graft before stress in group B was 14.1 ± 11.0 ml/min, which was significantly lower than that in group A (76.4 ± 38.3 ml/min, $p < 0.01$). Sensitivity and specificity of MR flow measurement in predicting significant IMA stenosis were 100% and 89%. The D/P ratio in group B (0.98 ± 0.67) was significantly lower than that in group A (2.01 ± 1.37, $p < 0.01$). Evaluation of the IMA graft stenosis using the D/P ratio showed high sensitivity (100%) and specificity (89%). The pharmacologic flow reserve ratios in the IMA grafts were 2.01 ± 1.37 in group A and 0.99 ± 0.66 in group B ($p < 0.05$). However, substantial overlap between the two groups was observed in the flow reserve ratio. In conclusion, blood flow measurement in the basal state using fast VEC MRI is highly useful in predicting significant stenosis in the IMA graft and may replace x-ray angiographic study.

Coronary Artery Imaging with Breathhold and Retrospective Motion Correction

T.M. Munger, J. Zheng, J.P. Finn, D. Li. *Chicago, IL*

Introduction: Respiratory motion during image acquisition can cause substantial artifacts in cardiac magnetic resonance images. Breathholding can reduce or eliminate these effects (1). However, spatial coverage and resolution for a breathhold scan is limited by patients' ability to hold their breath with adequate duration and consistency. In this work, we attempt to improve the spatial coverage and resolution of coronary artery images by collecting data from multiple breathhold periods and correcting the spatial displacements between breathholds using phase shift (2).

Materials and Methods: All images were acquired in normal volunteers. Two coronary artery image data sets were collected using a 2D gradient-echo sequence from separate breathholds. A series of images were then reconstructed using the central half k-space of the first data set and the peripheral half k-space of the second data set. The k-space of the second data set was iteratively phase shifted based on the Fourier shift theorem within a spatial displacement range of −10 to 10 pixels in 0.5-pixel increments in the superior-inferior direction. The best phase correction was determined by using a linear least-squares fitting routine to find the greatest slope across the edge between the right ventricle and the interventricular septum in the phase encoding direction.

Results and Discussion: The images reconstructed with the best phase correction resemble closely the images of a single breathhold reconstructed with full k-space and are much better than those reconstructed with two data sets of separate breathholds without motion correction (artifacts eliminated, coronary artery boundary better defined). This method may provide a useful approach to improve spatial coverage and resolution with breathhold coronary artery imaging. Preliminary results using 2D imaging are encouraging, and further work is needed to extend this concept to 3D imaging.

References

1. Oshinski JN. Two-dimensional coronary MR angiography without breath holding. *Radiology,* 1996; 201:737–743.
2. Ehman RL, Felmlee JP. Adaptive technique for high-definition MR imaging of moving structures. *Radiology,* 1989; 173:255–263.

Coronary Artery Segmentation Using Connectivity

H.E. Cline,[1] S. Ludke,[1] D.R. Thedens,[2] C.H. Meyer,[2] D.G. Nishimura,[2] T.K.F. Foo.[3] [1]*Schenectady, NY;* [2]*Stanford, CA;* [3]*Milwaukee, WI*

Purpose: Segmentation of coronary arteries from the hyperintense blood pool is necessary to create projection angiograms from 3D cardiac magnetic resonance images.

Method: Three-dimensional images of the coronary arteries were acquired with a 1.5-T system using both the "3D stack of spirals method" (1) and the contrast-enhanced "3D segmented k-space navigator method" (2) with blood pool agent MS-325. Both nonlinear morphologic filters (3) and connectivity image processing were applied to segment the coronary arteries before applying a maximum intensity projection (MIP). The 3D data were filtered using mathematical morphology filters; gray scale erosion was followed by dilation to remove the blood vessels and noise from the blood pool. The difference between the original and filtered images gives the suppressed blood pool intensity relative to that of the coronary arteries. A seed is placed in a vessel of interest to connect voxels above a user-selected threshold. An MIP through the connected voxels removes the background noise. The segmentation method was applied to three 3D stack of spirals data sets and to four 3D navigator segmented k-space acquisitions. A program was written in the C++ computer language to process the images.

Results: The measured blood pool intensity is greater than the fine blood vessels. Hence, a maximum intensity projection shows only a portion of the vessel tree. In the 3D stack of spirals data, an MIP of the left coronary artery shows the proximal LAD and a diagonal branch. The nonlinear filter suppresses the blood pool to show the circumflex artery (LCX) and distal branches. Using connectivity further suppresses the background noise to improve the contrast. In contrast-enhanced acquisitions, the blood pool was suppressed to improve the coronary artery visualization, but the vessels appeared thicker and were not well separated from the blood pool.

Summary: Connectivity eliminates the confounding effect of blood in the cardiac chambers to improve the coronary artery conspicuity and allows the vessels to be viewed from different directions. More work is needed to extend connectivity to contrast enhanced navigator acquisition methods.

References

1. Meyer CH, Hu B, Nishimura DG, Macovski A. Fast spiral coronary imaging. *Magn Reson Med,* 1992; 28:203–213.
2. Ehman RL, Felmlee JP. Adaptive technique for high definition MR imaging of moving structures. *Radiology,* 1989; 173:255–263.
3. Cline HE, Thedens DR, Irarrazaval P, Meyer CH, Hu BS, Nishimura DG, Ludke S. 3D MR coronary artery segmentation. *Magn Reson Med,* 1998; 39:697–702.

Rotational Reconstructions of Three-Dimensional Magnetic Resonance Coronary Angiography Data Sets Improves Visualization of Coronary Anatomy

C.H. Lorenz, L.O.M. Johansson. *St. Louis, MO*

Three-dimensional magnetic resonance coronary angiography enables high through-plane resolution of the coronary arteries as compared to x-ray angiography, which is a two-dimensional projection technique. To detect asymmetric stenoses in x-ray angiography, multiple views are needed. The purpose of this work was to demonstrate a new method for visualizing coronary arteries using the three-dimensional information attained in magnetic resonance coronary angiography.

In this method the course of the coronary arteries is defined in the three-dimensional space using manual tracking of the artery using an EasyVision workstation (Philips Medical Systems). A plane is then reconstructed along the three-dimensional line. The plane is then rotated around the defined axis with a view created every 10 degrees for 180 degrees.

Figures 1 and 2 shows two resulting views from a pig with a constrictor placed around the left anterior descending coronary artery. Due to the asymmetric nature of this stenosis, the stenosis is only visualized in Figure 1, whereas in Figure 2 the vessel appears to have normal caliber. The plane is Figure 1 is reconstructed in the direction of the caliber change of the vessel, whereas Figure 2 is reconstructed perpendicular to that plane. Another benefit of the rotational reconstruction is that branch vessels can be detected. By rotating the view, the origin of the branch vessels can be visualized. This is also shown in Figure 1, where the origin of the left circumflex is visualized, whereas it is not seen in Figure 2.

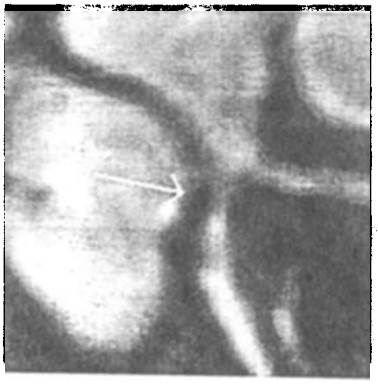

Figure 1

Figure 2

Early results with this method indicate that the detection of focal coronary artery stenoses and the visualization of branch vessels could potentially be improved by the use of rotational reconstructions of three-dimensional magnetic resonance coronary angiography datasets. Further evaluation in patient studies is warranted.

Zero Inter- and Intraobserver Variability Using the Automatic Multiple-Sectored Three-Dimensional Paraboloid Method for Determination of Lumen Vessel Area and Wall Shear Stress

S. Oyre, P. Bonvin, E.M. Pedersen. *Aarhus University Hospital, Skejby Sygehus, Denmark*

Methods are lacking for accurate, observer-independent, noninvasive, and invasive determination of the lumen vessel area and wall shear stress (WSS). The present study evaluates the previously introduced user-independent method (1) for determination of the above variables.

Method: **User input:** Identification (square ROI) of the vessel of interest. **Automatic initial vessel wall definition:** Initial data were selected according to a) 30% magnitude masking, b) pixels with 20–80% of the peak center velocity (2). Pixels within ±0.5 mm distance from the average radial distance from the center of the a) and b) selected

pixels were then used for the first circumferential 3DP fit (2). **Automatic multiple-sectored 3DP (AMS3DP) method:** We hypothesize that mean WSS cannot be overestimated (has a local maximum) and that the lumen area cannot be underestimated (has a local minimum) when using the multiple-sectored 3DP method (3). Therefore we propose a new index that reaches a local maximum when the "true" eliptic vessel wall is detected: $AMS3DP_{index} = 3DP_{mean\_WSS}/3DP_{area}$ (1). We changed the initial automatic edge detection radius 0.5 mm in both radial directions in steps of 50 μm, using 24 sectors with a 0.8-mm sector layer and 90-degree sector angle (3). The $3DP_{index}$ was calculated for each step, and the maximum index value was used as the "correct" value. **Data acquisition:** Measurements were performed in six young volunteers where through-plane blood velocity data in the common carotid artery 2 cm upstream of the carotid bifurcation were acquired using a 1.5-T Philips NT scanner with a standard phase contrast sequence and inplane resolution of 0.5 mm. **Evaluation:** The user input influence was examined by using two very different ROIs. A smaller square used would represent the closest possible ROI without eliminating any part of the vessel, whereas a second ROI would be made 50% larger in area (i.e., a much larger ROI than any person with a minimum amount of training would select). The hypothesis of a local maximum index was tested by reiterating the AMS3DP method four times (i.e., the true eliptic vessel wall was used as a new initial vessel wall position for applying the AMS3DP method).

Results: For all subjects, identical automatic initial vessel wall position was determined using both the small and large ROI. The mean adjusted R^2 (coefficient of determination) was 0.96 and the mean RMSE was 0.021 m/s² for the first iterated AMS3DP value. Using a paired *t*-test, no significant difference was found between any of the 5 AMS3DP results. The mean ± SD area for all subject iterations was 42.3 mm^2 ± 0.25 (range, 0.06–0.56).

Conclusion: The user input had zero "inter-" and intraobserver variability influence on the initial vessel wall position. The AMS3DP method is unique by having a local maximum at the "true" vessel wall. This was proven to hold true for in vivo data. The method has experimental and clinical potential for studying intraindividual and development over time of vascular disease and vascular responses to interventions (e.g., measuring accurate and user-independent endothelial function throughout the cardiovascular system).

References

1. Oyre S. Abstract, first meeting SCMR. JCMR, 1998; 1:90.
2. Oyre S. *JACC*, 1998; 32:128–134.
3. Oyre S. *MRM*, 1998; 40:645–655.

Improvements in Contrast-Agent Enhanced Navigator Gated and Corrected 3D Coronary MRA

M. Stuber, R.M. Botnar, P.G. Danias, M.V. McConnell, K.V. Kissinger, T. Nies, W.J. Manning. *Boston, MA*

Introduction: For free-breathing high-resolution 3D coronary MRA, scanning time is significantly increased with respect to 2D approaches. As a consequence, the application of contrast agents which are intravascular for long time periods is crucial for contrast enhancement between myocardial blood and muscle. Recent developments of intravascular contrast agents in concert with improvements in coronary MRA methodology have made it possible to take advantage of contrast enhanced free-breathing submillimeter 3D coronary MRA.

Materials and Methods: In six patients 0.1 mmol/kg of an intravascular contrast agent, AngioMARK (MS-325, EPIX Medical Inc., Cambridge, MA), was given followed by free-breathing 3D coronary MRA with real-time navigator gating and correction on a 1.5-T Philips Gyroscan ACS-NT system (Philips Medical Systems, Best, NL) equipped with an advanced coronary software package. In prone or supine position, image data of the left and right coronary system were acquired in double oblique imaging planes using the 2D selective navigator localized at the right hemidiaphragm. The navigator data were visualized in real time on the MR console. An ECG gated 3D TFE sequence (TE = 2.4 ms, TR = 8.8 ms, acquisition window = 70 ms) with an in-plane resolution of 0.7 × 1.0 mm was utilized for image acquisition. For contrast enhancement, a nonselective inversion prepulse precedes the 2D selective navigator and the 3D imaging part of the sequence.

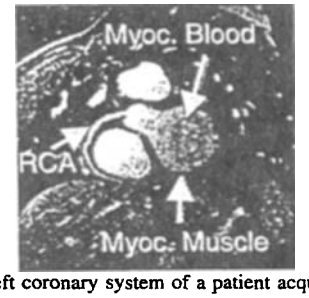

Figure 1. (a) Left coronary system of a patient acquired during free breathing using a double-dose injection of the intravascular contrast agent AngioMARK. A skin-line enhancement can be observed (arrow).

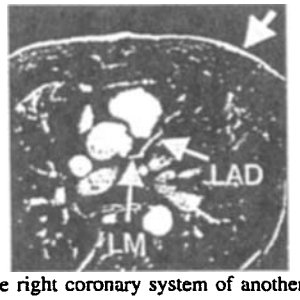

(b) Double oblique right coronary system of another patient acquired with the same contrast agent. Myocardial muscle is almost entirely suppressed by the inversion prepulse.

Results: A good vessel delineation (Fig. 1) was found in all cases for the left and right coronary system using the intravascular contrast agent AngioMARK. By the application of the inversion pulse, muscle signal was almost entirely suppressed (Fig. 1). Long portions of the left and right coronary system could be visualized with submillimeter resolution. Average scan time was 16 min per 3D acquisition. A high SNR of the navigator signal was also found as visualized on the navigator display tool in real time on the console. In all cases, an enhancement of the thoracic skin line adjacent to the surface coils could be observed (Fig. 1a, arrow). We hypothesize that due to phase shift in chest wall and diaphragmatic motion, skin-line enhancement resulted in artifacts overlaid to the image in phase-encoding direction. In the prone position, however, these artifacts were significantly reduced.

Discussion: The application of AngioMARK together with a navigator gated and corrected 3D inversion sequence allows for contrast-enhanced, high-resolution free-breathing coronary MRA. The presence of the agent in concert with a nonselective inversion pulse does not preclude the application of navigator technology. Due to the contrast agent-enhanced thoracic skin line, residual chest wall motion results in an increased artifact level in the images. In the prone position, however, breathing-induced chest wall motion can be reduced, which results in an improved image quality of the coronary MRA.

Isotropic Free-Breathing 3D Coronary MRA

R.M. Botnar, M. Stuber, K.V. Kissinger, W.J. Manning. *Boston, MA*

Background: In conventional x-ray angiography, multiple projections of the coronary artery tree are acquired to define coronary artery disease (CAD). Due to time constraints, coronary magnetic resonance angiography (MRA) usually only provides one or two views of the major coronary vessels.

Purpose: To develop a 3D coronary MRA technique with isotropic resolution and a short scanning time that allows for reconstruction of arbitrary views of the coronary arteries without constraints given by anisotropic voxel sizes.

Methods: Five healthy adult subjects were examined in supine position using a navigator gated and corrected ECG triggered free-breathing 3D multishot EPI (TFE-EPI) (1) coronary MRA sequence. All measurements were performed on a 1.5-T Philips Gyroscan ACS-NT MR scanner (Philips Medical Systems, Best, NL) equipped with a five-element cardiac synergy coil and an advanced coronary software package. Two 3D data sets with nonisotropic (1 × 1 × 3 mm) and isotropic (1 × 1 × 1 mm) image resolution were acquired in each subject. The 3D TFE-EPI imaging sequence (TR = 19 ms, TE = 5.4 ms, acquisition window duration = 38 ms) was preceded by a T2 prep prepulse (2,3), a 2D selective diaphragmatic real-time navigator, and a fat suppression prepulse. All imaging parameters except for image resolution were kept the same for both sequences.

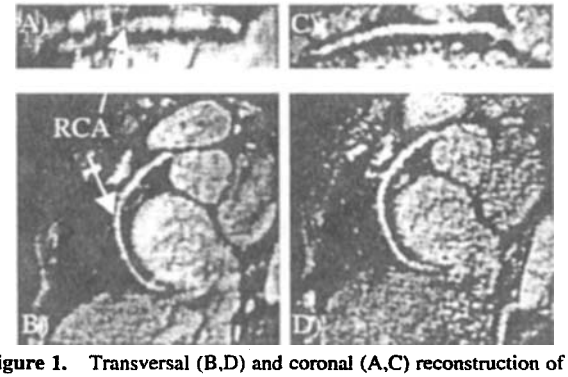

Figure 1. Transversal (B,D) and coronal (A,C) reconstruction of the LAD of one healthy subject. (A,B) Nonisotropic resolution (1 × 1 × 3 mm); (C,D) isotropic resolution (1 × 1 × 1 mm).

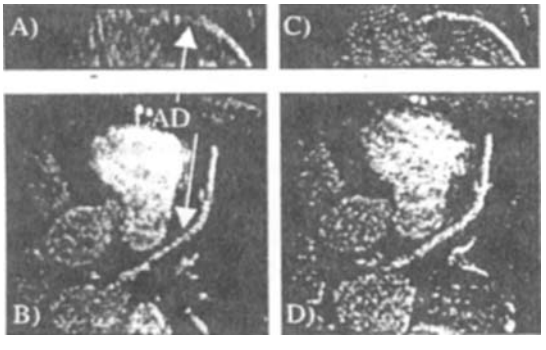

Figure 2. Double oblique views of the RCA in a healthy subject with nonisotropic (A,B) and isotropic (C,D) image resolution.

Results: All subjects were examined without any complications. Vessel delineation differed between views with nonisotropic voxel size (Fig. 1, A and B, and Fig. 2, A and B) and was similar between views with isotropic voxel size (Fig. 1, C and D, and Fig. 2, C and D). Especially views along the through-plane direction were less defined for nonisotropic when compared to isotropic images (Fig. 1, A and C, and Fig. 2, A and C). Average scanning time varied between 7 and 8 minutes.

Conclusions: We presented a new approach for isotropic 3D coronary artery imaging, which allows for reconstruction of arbitrary views of the coronary arteries. The good delineation of the coronary arteries in all views suggests that isotropic 3D coronary MRA might be a promising technique for the assessment of coronary disease. Comparative studies with conventional x-ray angiography are now needed to investigate the clinical impact of this approach.

References

1. McKinnon GC. *Magn Reson Med,* 1993; 30:609–616.
2. Brittain JH, Hu BS, Wright GA, Meyer CH, Macovski A, Nishimura DG. *Magn Reson Med,* 1995; 33:689–696.
3. Botnar RM, Stuber M, Kissinger KV, Danias PG, Manning WJ. Proc. ISMRM, Sydney, 1998, p. 23.

Efficacy of Slow Infusion of Gd-DTPA Contrast Agent in 3D MR Coronary Artery Imaging

Jie Zheng,[1,2] Debiao Li,[2] Kyongtae T. Bae,[3] Pamela Woodard,[3] E. Mark Haacke.[3] [1]*Bracco;* [2]*Northwestern University, Chicago, IL;* [3]*Washington University, St. Louis, MO*

Purpose: To investigate the efficacy of slow infusion of extravascular Gd-DTPA during 3D data acquisition for imaging coronary arteries.

Methods: Two slow infusion modes were studied in coronary artery imaging: 2-min relative constant rate and 2-min variable rate of infusion. The first infusion mode enhanced both peripheral and central k-space with relative smaller signal enhancement. The second one mainly enhanced central k-space with relatively larger signal intensity. Simulations and an animal study were performed to compare effects of two infusion modes on the coronary artery images. Six volunteers were examined by slow infusion of double-dose Gd-DTPA during data acquisition; three by constant rate and three by variable rate of infusion. The imaging technique was an IR prepared retrospective respiratory gated gradient echo sequence.

Results: Simulation demonstrated that 2-min constant infusion improved the signals from the small blood vessels by 20% in comparison with the variable rate of infusion. Two postcontrast coronary artery images were compared on one pig study. Volunteer studies also showed the significant improvement of signal-to-noise ratio by constant infusion mode.

Conclusion: Contrast enhancement on both central and peripheral k-space during data acquisition significantly improves the quality of MR coronary artery angiography.

Assessment of Myocardial Perfusion Reserve Before and After PTCA with MR First Pass Imaging

E. Nagel, N. Al-Saadi, M. Gross, C. Klein, S. Schalla, A. Bornstedt, B. Schnackenburg, H. Oswald, E. Fleck. *Berlin, Germany*

Myocardial perfusion reserve (MPR) can be determined with MR imaging by the assessment of the first pass kinetics of a gadolinium (Gd) bolus at rest and after dipyridamole (dipy) injection (1). Aim of this study was to define cutoff values for different parameters and assess MPR before and after PTCA.

Thirty-eight patients with angiographically significant coronary artery stenosis (≥75%) were examined with a 1.5-T MR tomograph (ACS NT, Philips, The Netherlands) using an inversion recovery turbogradient echo technique (spatial resolution 1.7 × 1.9 × 8 mm, acquisition time 360 ms). A short-axis image at the base of the papillary muscle

was acquired every heartbeat for 70 beats after the injection of 0.025 mmol Gd-DPTA/kg body weight into the superior caval vein before and after dipy infusion (0.56 mg/kg/min). The signal intensity curves of the left ventricle and six radial segments of the myocardium were obtained and fitted with a gamma variate function. From the fitted curves the steepness of the upslope was determined and corrected for the left ventricular curve. MPR was calculated as the value after dipy injection in comparison to the respective value at rest. Cutoff values were defined retrospectively in 20 patients with known single vessel coronary artery disease and prospectively applied to 18 patients before and 24 hours after successful PTCA.

A cutoff value of 1.2 was found for the steepness of the upslope. MPR was significantly reduced in those segments supplied by a stenotic coronary artery (S+) in comparison to the remaining segments (S−) (0.9 ± .05% vs. 1.8 ± 0.08%; mean ± SE, $p < 0.001$) before PTCA. After successful PTCA MPR in S+ increased significantly in comparison to pre-PTCA values ($p < 0.001$; paired t-test) and did no longer differ from S− (1.49 ± 0.27 vs. 1.15 ± 0.12, ns). For the detection of significant coronary artery disease, sensitivity was 91% and specificity 93% in the prospective cohort.

Myocardial perfusion reserve after dipy injection can be assessed with magnetic resonance imaging and allows the detection of myocardial ischemia with high diagnostic accuracy. After PTCA myocardial perfusion, reserve is normalized and might be useful for the assessment of the success of revascularisation and the noninvasive detection of restenosis.

Reference

1. Wilke N, et al. Myocardial perfusion reserve: assessment with multisection, quantitative, first-pass MR imaging. *Radiology*, 1997; 204: 373–384.

Do We Need Quantitative MR Perfusion Imaging? Grades Myocardial Perfusion Changes Assesssed with MR and Intravascular Contrast Agent

S. Gurchumelidze, J. Rodenwaldt, M. Jerosch-Herold, Y. Wang, G. R. Gong, J. Zhang, N. Wilke. *Minneapolis, MN*

Purpose: Controversy exists whether the use of intravascular contrast agents (CA) may discern mild to moderate perfusion defects. There is a threefold lower distribution volume of intravascular compared with interstitial CA (e.g., Gd-DTPA). The aim of the study was to determine the degree of relative myocardial blood flow changes that produces MR perfusion abnormalities.

Methods: Graded myocardial perfusion changes were induced in closed-chest instrumented dogs ($n = 22$) by a hydraulic occluder placed around the left anterior descending coronary artery (LAD). First-pass perfusion images were acquired with an ultrafast arrhythmia-insensitive Turbo-FLASH sequence using a bolus of intravascular CA (Polylysine-Gd-DTPA: 0.03 mmol/kg bw). Perfusion abnormalities were graded as mild ($n = 12$), moderate ($n = 10$), and severe ($n = 8$) at rest and stress (dobutamine 5–10 μg/kg/min) based on the myocardial blood flow (MBF) changes measured with radioactive-labeled microspheres. Quantitative relative perfusion ratios were derived for the anterior (LAD distribution) and posterior wall (LCX distribution) and compared to the microsphere ratios.

Results: Excellent correlations were found between the perfusion indices acquired with MR first-pass imaging and the microsphere measurements. Best results were calculated for maximal amplitude ($r = 0.93$) (Fig. 1) and up-slope ($r = 0.91$). Relative perfusion changes of 20–30% by microspheres can be detected with MR (Fig. 2). Visual qualitatively we were only able to discern mild to severe perfusion defects with a ratio <0.3, which was comparable to 70% MBF reduction.

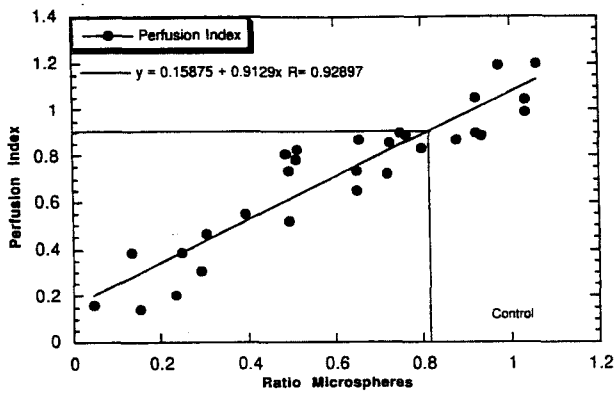

Figure 1. Correlation perfusion index/microspheres.

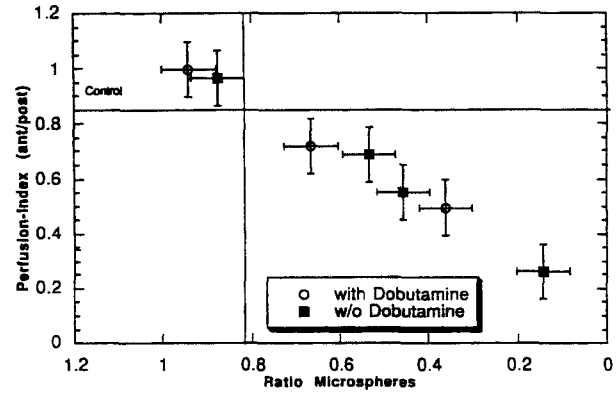

Figure 2. Perfusion quantification.

Conclusions: MR first-pass perfusion imaging allows the precise detection of mild to moderate to severe myocardial perfusion defects. To appreciate the diagnostic validity of first-pass images, quantification of perfusion is necessary. Novel revascularization strategies (gene therapy) would rely on quantitative graded myocardial perfusion assessment.

Reference

1. Tsekos N, et al. Fast anatomical imaging of the heart and assessment of myocardial perfusion with arrhythmia insensitive magnetization preparation. *Magn Reson Med*, 1995; 34:530–536.

Abnormal Transmural Blood Flow Gradient in Patients with Microvascular Dysfunction

M. Jerosch-Herold, R.K. Grewal, J. Cartland, N.M. Wilke, S. Gurchumelidze, B. Christensen, R.F. Wilson. *Minneapolis, MN*

MR perfusion imaging provides sufficient spatial resolution to investigate for the first time in patients with microvascular dysfunction the relation between the transmural blood flow gradient and the degree of impairment of the coronary flow reserve. This may help elucidate the pathophysiology of microvascular dysfunction. Patients ($n = 7$) with chest pain but without hemodynamically significant epicardial lesions and a decreased coronary flow reserve were selected for this study. The coronary flow reserve (CFR) was measured during catheterization with an intracoronary Doppler flow probe. T1-weighted Turbo-FLASH im-

ages (TR = 2.4 ms; TE = 1.2 ms; flip angle = 18°) were acquired on a Siemens Vision 1.5-T MRI scanner during the first pass of an injected bolus of Gd-DPTA (0.03 mmol/kg). Signal curves were generated for epi- and endocardial regions of interest and analyzed with a multicompartment, multi-path, tracer kinetic model to determine myocardial blood flow. At rest, myocardial blood flow averaged 1.03 ± 0.23 ml/min/g and did not drop below 0.85 ml/min/g in any myocardial segment, indicating the absence of ischemia at rest. The average ratio of endo- to epicardial MBF was 1.22 ± 0.1 at rest and showed a significant decrease during maximal hyperemia to 0.95 ± 0.1 for those patients with a CFR < 2.5 ($n = 4$; t-test; $p < 0.05$). The ratio of subendocardial to subepicardial MBF ratio during maximal hyperemia flow was found to correlate with the coronary flow reserve (linear regression statistics: $n = 7$; $R = 0.76$; slope = 0.45; $p < 0.05$; intercept = 0.156; n.s.). One possible hypothesis for patients with microvascular dysfunction has been that the symptoms reflect a true perfusion impairment that may be limited to the subendocardial layer. Using quantitative MR perfusion imaging, this study shows for the first time that during maximal hyperemia the transmural myocardial perfusion gradients are strongly reduced or even reversed in patients with microvascular dysfunction.

Supported by NIH RO1-HL58876 and The Whitaker Foundation.

Evaluation of the Precision of Magnetic Resonance Phase Velocity Mapping

G.P. Chatzimavroudis,[1] J.N. Oshinski,[1] P.G. Walker,[2] R.H. Franch,[1] A.P. Yoganathan,[1] R.I. Pettigrew.[1] [1]*Atlanta, GA;* [2]*Leeds, UK*

Purpose and Methods: The aim of this study was to systematically investigate the precision of magnetic resonance phase velocity mapping (MRPVM), both in vitro and in vivo. MRPVM is a technique that has been widely used clinically to measure blood flow. Despite the accuracy found in vitro, evaluation of MRPVM in humans is not straightforward, because of the absence of a validated clinical flow quantification technique, with which MRPVM could be compared. An alternative way to evaluate MRPVM clinically is to study its precision. Precision is the repeatability of MRPVM; in other words, whether different measurements taken at the same location agree with each other. This precision was first studied in vitro to obtain data the precision of which would serve as the reference for the in vivo situation. **In vitro measurements:** Steady and pulsatile flow experiments were conducted using a compliant aortic model (ID = 25 mm), under a variety of flow conditions (steady: 0.1–5.5 l/min; pulsatile: 10–75 ml/cycle) observed during diastole in the ascending aorta of patients with aortic regurgitation (AR). In steady flow, the true flow rate was known via a calibrated rotameter. In pulsatile flow, a computer-controlled piston pump was used to produce the desired flow waveform which was also measured with a flow probe. The flow loop was placed in a 1.5-T scanner. A coronal scout spin-echo image was acquired to locate the aortic model, and a transverse velocity-encoded gradient-echo image acquisition was performed (slice thickness [ST]: 5 mm; FOV: 200 mm; TR: 30 ms; TE: 6–9 ms; flip angle: 35°; matrix size: 128 × 128; VENC = 25–500 cm/s). In pulsatile flow, retrospective ECG gating was used to acquire 20 time phases per cycle. Each acquisition was performed twice. **In vivo measurements:** After a spin-echo scout image was acquired, MRPVM measurements were taken in the ascending aorta of 10 subjects, approximately 2 cm beyond the sinotubular junction (ST: 5 mm; FOV: 250 mm; TR: 14–30 ms; TE: 6–9 ms; flip angle: 35°; matrix size: 128 × 128). Seven of these subjects had AR (previously assessed by angiography and echocardiography). In those subjects without AR, measurements of the aortic flow waveform using a high VENC (300 cm/s) provided the left ventricular stroke volume. In those patients with AR, the regurgitant volume was calculated from measurements taken with a lower VENC (50 cm/s). Retrospective ECG gating was used to provide 13–18 phases during the cardiac cycle. The measurements were performed twice for each subject.

Results: Comparison between the measured and the true flow rates and volumes showed the high accuracy of MRPVM in mesuring flow in vitro. This accuracy was also confirmed by Mann-Whitney tests ($p > 0.85$). The in vitro repeatability of MRPVM was shown to be very high using regression analysis (steady: $y = 1.00x + 0.02$, $r = 0.999$, $p = 0.00$; pulsatile: $y = 0.98x + 0.72$, $r = 0.997$, $p = 0.00$; where x: measurement #1, y: measurement #2) and confirmed by Bland-Altman analysis (small means and standard deviations with small and random data scattering). Of great clinical significance was the high level of repeatability of the in vivo flow measurements, determined by regression analysis ($y = 1.01x - 0.04$, $r = 0.993$, $p = 0.00$) and confirmed with a Mann-Whitney test ($p = 1.00$).

Conclusion: MRPVM provided blood flow measurements of excellent precision. Although the in vivo accuracy of the technique cannot be reliably determined in the absence of a gold standard technique, the high accuracy and precision (repeatability) seen in vitro in combination with the same high levels of precision seen in vivo are key factors for the establishment of MRPVM as the gold standard for quantification of blood flow. In the case of AR, reliable blood flow information is very important to better monitor the progress of the disease and to quantitatively determine the effectiveness of vasodilators used for pharmacologic treatment.

"Virtual Transducer" Color Flow Magnetic Resonance Imaging

S.E. Fischer, S.A. Wickline, C.H. Lorenz. *St. Louis, MO*

Phase contrast magnetic resonance is an established method to measure time resolved blood flow and heart valve insufficiency. Different color schemes have been used to display the flow information obtained by MRI (1). Color Doppler ultrasound remains the standard clinical tool for robust assessment of valvular disease. We have developed a method to compare directly MRI phase contrast data with color Doppler data considering the fundamental physical differences of velocity measurement techniques. By acquiring three-dimensional phase contrast velocity MR data from each pixel at the location $\mathbf{p} = (x, y, z)$, within a slice a three-dimensional velocity vector, $\mathbf{v}(\mathbf{p}) = (v_x(\mathbf{p}), v_y(\mathbf{p}), v_z(\mathbf{p}))$, can be computed. By introducing retrospectively an omnidirectional "virtual transducer" at the position, $\mathbf{t} = [t_x, t_y, t_z]$ the flow information can be reduced to a scalar value, $v = (\mathbf{p} - \mathbf{t})/|\mathbf{p} - \mathbf{t}| \cdot \mathbf{v}$, which mimics the velocity information of the color Doppler ultrasound at the same location and direction.

Figure 1

In five patients with mild to severe mitral regurgitation, phase contrast images (32 frames throughout the cardiac cycle, four-chamber view) were acquired by a retrospectively gated scan in 2 minutes at 1.5

T (Gyroscan ACS-NT, Philips Medical Systems). To calculate the color MR flow images, a virtual transducer is positioned interactively (Figure 1) to match the setup of the color Doppler acquisition (Sequoia, Acuson) in the same four-chamber view.

The color Doppler ultrasound images provided superior contrast between myocardium and blood in the region outside the echo Doppler window. Identical flow patterns including the regurgitant jets, were depicted by the virtual transducer method. The advantage of the virtual transducer color flow MRI is the ability to freely position the virtual transducer also in regions not accessible by an ultrasound transducer. The proposed addition to MR velocity phase contrast imaging should be useful for rapid robust assessment of valve disease for clinicians trained in color Doppler ultrasound image evaluation.

Reference

1. Klipstein RH, Firmin DN, Underwood SR, Nayler GL, Rees RSO, Longmore DB. Color display of qualitative blood flow and cardiac anatomy in a single magnetic resonance cine loop. *Br J Radiol*, 1987; 60: 105–111.

Quantification of Mitral Regurgitation by Magnetic Resonance Imaging: Issues in Volume Analysis

M.W.S. Kon, J.M. Francis, S. Myerson, N.E. Moat, D.J. Pennell. *Royal Brompton Hospital, London, UK.*

Objective: To determine if magnetic resonance imaging can provide a quantitative assessment of mitral regurgitation using volumetric and velocity mapping techniques.

Methods: Twenty-eight patients with isolated mitral regurgitation underwent MR imaging at 1.5 T. A breathholding technique was used to enable cine-gradient echo imaging of the entire ventricular mass in a series of parallel slices in the short axis. End diastolic and end systolic volumes were obtained by manually tracing the endocardial borders of the left and right ventricles and regurgitant fraction calculated by expressing the difference between left and right stroke volume (LVSV and RVSV) as a fraction of left ventricular stroke volume. Aortic and pulmonary forward stroke volumes were obtained from flow curves generated by velocity mapping across the aorta and pulmonary trunk.

Results: Mean LVSV was 110 ml (range, 57–272 ml), RVSV 62 ml (range, 36–100 ml), regurgitant volume 47 ml (range, 11–159 ml), and regurgitant fraction 40% (range, 11–71%). There was good correlation of right and left forward stroke volumes measured by velocity mapping, slope 0.94, r^2 0.84. RVSV measured by volumetry was compared to aortic forward stroke volume by linear regression (slope = 0.80, r^2 = 0.60) and by generating a Bland-Altman plot (Fig. 1) (mean difference in stroke volume 3.5 ml, SD9.5 ml). Regurgitant fractions using RVSV derived by volumetry or aortic forward stroke volume were comparable (mean difference 2.1 ml, SD10.5 ml).

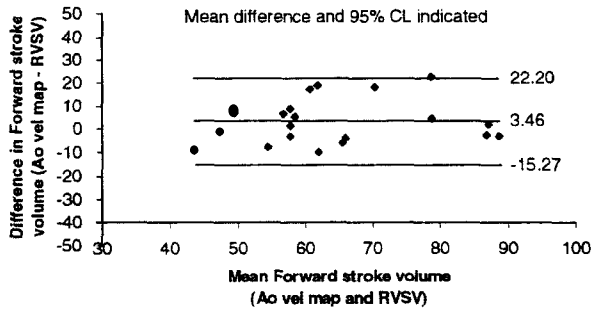

Figure 1

Conclusion: Mitral regurgitant volume and fraction may be obtained by subtraction from LVSV (by volumetry) of either RVSV derived from volumetry or aortic forward stroke volume by velocity mapping.

Recovery of Postischemic Myocardial Na^+/K^+ ATPase Function Does Not Depend on Glycolytic ATP

J.G. Van Emous, C.L.A.M. Lankamp, T.J.C. Ruigrok, C.J.A. Van Echteld. *Utrecht, The Netherlands*

Accumulation of intracellular sodium (Na^+_i) during myocardial ischemia is an important determinant of calcium overload upon reperfusion via Na^+-Ca^{2+} exchange. Postischemic reperfusion of ischemic myocardium surprisingly results in an immediate decrease of Na^+_i via (resumption) of Na^+-K^+ ATPase activity (1). Since energy from glycolysis has been suggested to be preferentially used to fuel membrane functions (2), in the present study the need for glycolytic ATP for the postischemic decline of Na^+_i was evaluated. Isolated rat hearts were subjected to 25 min of perfusion at constant pressure (76 mm Hg), 20 min of total ischemia, and 30 min of constant flow (70% of control) reperfusion, all at 37°C. Glucose hearts (n = 6) received 11 mM glucose as substrate before and after ischemia. Pyruvate hearts (n = 4) were reperfused with 5 mM pyruvate as sole substrate. In addition, the pyruvate hearts were treated with 500 μg/l glucagon for 20 min before ischemia to deplete glycogen. Na^+_i was measured with ^{23}Na NMR with a 5-s time resolution, using $TmDOTP^{5-}$ as shift reagent. Na^+_i in both glucose and pyruvate hearts increased during ischemia and amounted to 224 + 15 and 222 ± 25% of control after 20 min, respectively. Upon reperfusion, Na^+_i decreased immediately in glucose hearts and was 88 ± 5 and 62 ± 13% of the endischemic value after 60 s and 5 min of reperfusion, respectively. In pyruvate hearts, however, the decline of Na^+_i was retarded by approximately 15 s, although already after 60 s of reperfusion the decline of Na^+_i was similar to the glucose hearts (89 ± 7% of the endischemic value). This indicates that glycolytically derived ATP is not strongly coupled to Na^+-K^+ ATPase activity during postischemic reperfusion. The delayed activation of the ATPase in pyruvate hearts may reflect the longer and more complex pathway involved in oxidative phosphorylation compared to glycolysis. Postischemic recovery of the rate pressure product, as verified by an intraventricular balloon, was similar in glucose and pyruvate reperfused hearts (63 ± 12 and 76 ± 13% of control, respectively), which indicates that postischemic glycolytic activity is not a prerequisite for contractile recovery.

References

1. Van Emous JG, Schreur JHM, Ruigrok TJC, Van Echteld CJA. Both Na^+-K^+ ATPase and Na^+-H^+ exchanger are immediately active upon post-ischemic reperfusion in isolated rat hearts. *J Mol Cell Cardiol*, 1998; 30:337–348.

2. Weiss J, Hiltbrand B. Functional compartmentation of glycolytic versus oxidative metabolism in isolated rabbit heart. *J Clin Invest*, 1985, 75:436–447.

Contrast Enhancement and Contractile Function Following Reversible and Irreversible Ischemic Injury

R.J. Kim, D.S. Fieno, T.B. Parrish, K. Harris, O. Simonetti, J. Bundy, J.P. Finn, F.J. Klocke, R.M. Judd. *Chicago, IL*

Contrast MRI enhancement patterns in several pathophysiologies resulting from ischemic myocardial injury are controversial or have not been investigated. We compared contrast enhancement in nonreperfused acute infarction (NR-AI), following severe but reversible isch-

emic injury (RII), and in chronic infarction (CI). Dogs ($n = 13$) were chronically instrumented with a reversible hydraulic occluder and Doppler flowmeter on the distal left circumflex (for RII) and permanent ligation of the distal LAD (NR-AI). At 3 days post-op, cine MRI revealed reduced wall thickening in NR-AI (5 ± 6% vs. 33 ± 6% in normal, $p < 0.001$). In RII, wall thickening before, during, and after inflation of the occluder for 15 min was 35 ± 5, 1 ± 8, and 21 ± 10% and Doppler flow was 19.8 ± 5.3, 0.2 ± 0.5, and 56.3 ± 17.7 (peak hyperemia) cm/sec, respectively, confirming occlusion, transient ischemia, and reperfusion. Gd-DTPA enhanced MR images acquired 30 min postcontrast revealed hyperenhancement of NR-AI (294 ± 96% of normal, $p < 0.001$) but not of RII (98 ± 6% of normal, p = NS). Eight weeks later, the chronically infarcted region continued to hyperenhance (253 ± 54% of normal, $p < 0.001$). High-resolution (0.5 × 0.5 × 0.5 mm) ex vivo MRI demonstrated that the spatial extent of hyperenhancement was the same as the spatial extent of myocyte necrosis at 3 days ($R = 0.99$, $p < 0.001$) and collagenous scar at 8 weeks ($R = 0.97$, $p < 0.001$). In the pathophysiologies investigated, contrast MRI distinguishes between reversible and irreversible ischemic injury independent of wall motion and infarct age.

MRI Analysis of the Dor Left Ventricular Surgical Reconstruction for Nonischemic Dilated Cardiomyopathy

R.W.W. Biederman,[1] M. Doyle,[1] A.R. Fuisz,[1] E. Kortright,[1] C.L. Athanasuleas,[1] A.W.H. Stanley,[1] G.D. Buckberg,[2] G.M. Pohost.[1]
[1]*Birmingham, AL;* [2]*Los Angeles, CA*

Introduction: A vast supply and demand mismatch for donor hearts exists in cardiac transplantation. The results of the Batista LV surgical procedure, proposed as an alternative to transplantation, have been generally disappointing. Explanations include a failure to account for a priori regional wall function and disregard for cardiac fiber orientation. The Dor LV reconstruction approach attempts to address these issues by restoring the typically spherical heart to a prolate-ellipse, utilizing a single apical cut and Dacron patch insertion. We report MRI analysis of the first Dor procedure performed in the United States in a 68 YOWM with NYHA-IV symptoms with a nonischemic dilated cardiomyopathy.

Methods: The patient underwent MRI examination with respiratory compensation (ROPE) and cardiac gating to obtain conventional and orthogonal-tagged images in standard views (tag spacing 7 mm, interslice distance 10 mm, and matrix 256^2).

Results: Echocardiography found global LV dysfunction, whereas MRI qualitative RF tagging analysis revealed segmental abnormalities confirmed at surgery by palpation. Progressive favorable remodeling continued to occur at a time distant from surgery (Table 1).

Table 1

	EDV (ml)	ESV (ml)	SV (ml)	EF	r/h	RWT	Apex	Strain	NYHA
Surgery	303	238	65	21	3.9	0.25	Akinetic	Heterogeneous	IV
Week 4	242	189	52	22	3.1	0.32	Paradoxical	Improved	III
Week 12	215	166	50	23	2.4	0.43	Tardykinetic	Improving	I

r/h is radius/wall-thickness and RWT is relative wall-thickness.

Conclusions: MRI RF tagging analysis successfully identified functioning myocardium, as confirmed at surgery. Further, tag analysis allowed function to be followed postsurgery revealing beneficial remodeling which continued after surgery. This correlated well with marked clinical improvement despite reduced SV and stable EF. Restoration of a favorable LV geometry suggests that reconfiguration to a prolate-ellipse is advantageous as opposed to simple removal of myocardium (as in the Batista procedure). Qualitative apical strain analysis revealed that the initial paradoxical motion continues to decrease with time following surgery. MRI suggests that the Dor reconstruction technique for nonischemic cardiomyopathy may be a viable option for patients otherwise considered for cardiac transplantation.

Determination of the Acute Effects of Direct Ventricular Mechanical Actuation (DMVA) on the Beating Heart Using MRI

Sorin V. Pusca, James J. Pilla, Aaron S. Blom, Himanshu J. Patel, Qing Yuan, Victor A. Ferrari, Charles Prood, Leon Axel, Michael A. Acker. *University of Pennsylvania Medical Center, Philadelphia, PA*

DMVA is an experimental method of biventricular cardiac assist by intracorporeal pneumatic compression of the heart. The advantages of this technique are biventricular cardiac assist, no blood contact during cardiac assist eliminating thromboembolic and bleeding complications, pulsatile blood flow, and rapid and easy application. The hemodynamic effects and the mechanism of action of DMVA applied to a chronically failing heart are unknown. Instantaneous determination of cardiac volumes using cardiac echocardiography is difficult due to cuff air artifacts. The technique of dual-field conductance catheter is impractical due to continuous changes in parallel conductance resulting from the presence of a variable amount of air in the DMVA cuff surrounding the heart.

This study used MRI to assess the acute effects of DMVA in a model of chronic heart failure induced in four mongrel dogs by rapid ventricular pacing at 230 b/min for 4 weeks. Heart failure development was documented at 4 weeks by echo and by conductance catheter. A DMVA cuff was then placed via a median sternotomy. The closed-chested animals were imaged in a clinical 1.5-T MRI system. Left ventricular (LV) pressure-volume (PV) loops of the unassisted and DMVA-assisted beating heart were generated by combining MRI-calculated volumes and LV pressures recorded simultaneously by a Millar catheter. Synchronous cuff inflation produced a marked leftward shift of the LV PV loops (Fig. 1) and significant improvement of the LV contractility (Table 1) with no concomitant diastolic impairment. This opens the possibility for the use of the DMVA for long-term cardiac assistance in severe heart failure. MRI determination of cardiac function and volumes for assessment of cuff-heart dynamics will be crucial for the further development of DMVA.

Table 1

	Unassisted	Assisted
HR (b/min) − V-paced	110	110
LVPP (mm Hg)	62.79 ± 4.95	83.23 ± 3.64*
LVEDP (mm Hg)	5.17 ± 1.76	2.96 ± 1.54
dP/dt max (mm Hg/sec)	899.25 ± 194.9	1814.5 ± 62.7*
dP/dt min (mm Hg/sec)	−920.75 ± 184	−1324 ± 172
LVEDV (ml)	38.51 ± 8.61	24.41 ± 4.71
SV (ml)	16.29 ± 2.69	13.37 ± 1.62
EF (%)	45.56 ± 8.17	57.55 ± 4.5

LVPP = LV peak pressure, LVEDP = LV end diastolic pressure, LVEDV = LV end diastolic volume.
*$p < 0.05$.

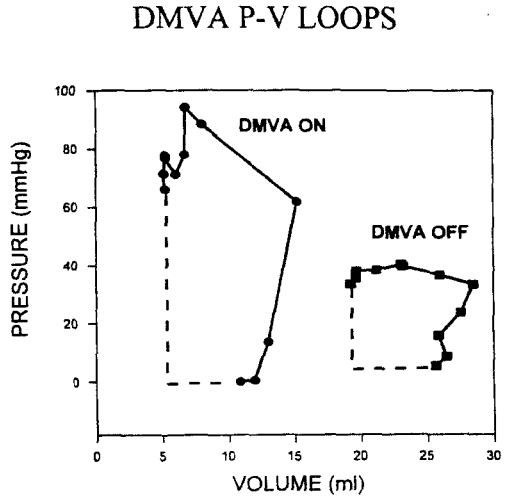

Figure 1

Perfusion Imaging of a Mouse Model of Hindlimb Ischemia by Dynamic Gd-DTPA Enhanced MRI

Shuichiro Kaji, Hoai-Ky V. Ho, Phillip Yang, Pedro Rivas, John P. Cooke, Bob S. Hu. *Division of Cardiovascular Medicine, Stanford University School of Medicine*

Background: There is no conventionally available imaging modality to display angiogenesis. The current dynamic contrast-enhanced magnetic resonance imaging (MRI) can reveal stress-induced angiogenesis of human cancer cells in nude mice. Mouse models of angiogenesis and perfusion are extremely important. However, the temporal and spatial resolution necessary to image mouse ischemia is difficult to achieve.

Purpose: To distinguish the perfusion of normal and ischemic mouse hindlimb by dynamic Gd-DTPA enhanced MRI.

Method: Dynamic Gd-DTPA enhanced MRI was performed in the normal and the ischemic hindlimb of eight mice using a 1.5-T MRI scanner (Signa, GE medical system) with a cardiac gradient enhancement. Signal enhancements (S(t)/S(0)) were evaluated after four dosages of Gd-DPTA injections. Custom-made surface coil was used to optimize the signal-to-noise ratio.

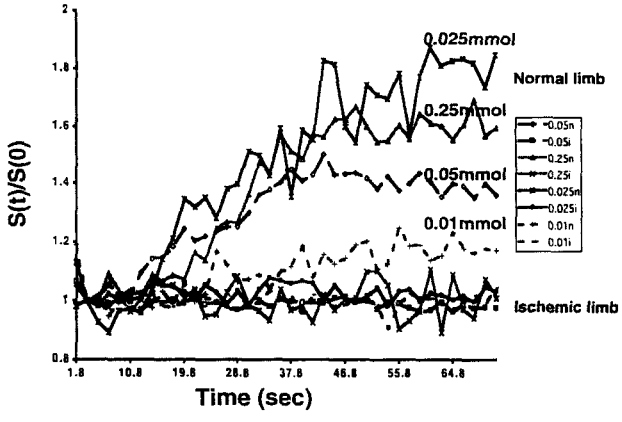

Figure 1

Results: With the new coil, spatial resolution of 80–160 μm and temporal resolution of 1.5 second were achieved. In the normal limb, signal enhancement after Gd injection was observed. In the ischemic limb, no signal enhancement was observed. We could observe differences of signal enhancements between four dosages of Gd-DTPA (Fig. 1).

Conclusions: The perfusion of normal and ischemic mouse hindlimb was visualized using dynamic Gd-DTPA enhanced MRI. This method may allow the evaluation of angiogenesis in the ischemic hindlimb mouse model.

MRI Assessment of Collateral Development in Porcine Model of Chronic Ischemia

M. Jerosch-Herold; Y. Huang, H. Huang, N.M. Wilke, A. Zenovich, F. Zhao, S. Gurchumelidze. *Minneapolis, MN*

There is an increasing clinical need to quantify the development of collaterals noninvasively and determine their functional capacity to deliver blood to collateral-dependent myocardium during rest and stress. This study was designed to demonstrate that MR perfusion imaging is sufficiently sensitive and accurate to quantify changes in the myocardial perfusion reserve that occur with the natural development of collaterals in porcine hearts with slowly-progressing occlusion.

Methods: In five pigs (17 ± 1.6 kg) the left circumflex coronary (LCx) artery was encased with an MRI compatible ameroid occluder (inner diameter < 2.5 mm). MRI follow-up studies were conducted at 10 days, 4 weeks, and 10 weeks after surgery to assess myocardial perfusion with T1-weighted Turbo-FLASH imaging and left ventricular (LV) function with gradient-echo cine MRI. Myocardial blood flow (MBF) was assessed during baseline conditions and during maximal vasodilation (0.2 mg/kg/min IV adenosine). Absolute myocardial blood flow was quantified from the measured signal curves.

Results: MBFs at rest in the LCx territory and other myocardial segments were not significantly different. During maximal hypermia, MBF in the LCx territory was significantly reduced compared with control regions (paired *t*-test: $p < 0.01$) in all studies. The perfusion reserve increased significantly with time after 10-day follow-up study and coronary occlusion. The improvement in MBF in collateral-dependent myocardium correlated with an improvement in global function. These findings were consistent with extensive retrograde collateral filling observed ex vivo with X-ray fluoroscopy and selective contrast agent injections into the right coronary artery.

Conclusion: This study demonstrates for the first time the ability to follow with MRI improvements in the functional capacity of collaterals that developed with a slow coronary occlusion and without boosting collateral development with gene therapy (Table 1).

Table 1

	10 days	4–5 weeks	10 weeks
LCx perfusion reserve	0.75 ± 0.21	1.26 ± 0.2	1.20 ± 0.1
EF (%)	46 ± 6%	49 ± 14%	57 ± 8%

Real-Time Cardiac MR Imaging at Echocardiographic Frame Rates Using SMASH

D.K. Sodickson, M. Stuber, R.M. Botnar, K. Kissinger, W.J. Manning. *Boston, MA*

Introduction: The high temporal resolution of 2D echocardiography (30 frames per second) makes it a valuable tool for dynamic assessment of cardiac function. Magnetic resonance imaging has the potential for

improved spatial resolution and contrast as compared with echocardiography, and MR is not limited by available acoustic windows, but presently achievable temporal resolution in MR lags behind that of echo. The purpose of this study was to investigate SMASH imaging (1) as a means to increase the temporal resolution of real-time cardiac MR images to frame rates typical of 2D echocardiography.

Methods: The SMASH imaging technique was combined with an ultrafast hybrid interleaved segmented EPI imaging sequence (2,3) (TR = 11.5 ms, TE = 3.3 ms, constant flip angle = 25°, matrix size = 103 × 128, FOV = 280 mm × 400 mm, in-plane resolution 2.7 mm × 3.1 mm, half-Fourier reconstruction in the phase-encode direction). Data were acquired simultaneously in the six elements of a linear array designed for SMASH imaging on a Philips ACS-NT scanner (Philips Medical Systems, Best, NL), in a free-running mode with continuous data acquisition over one to three cardiac cycles at a time. Partial acquisitions with reduced phase encoding were obtained and the full complement of phase-encoding lines was generated using the SMASH reconstruction procedure (1). For comparison, standard full acquisitions at a frame rate of 14 images per cardiac cycle were also obtained for reconstruction with a conventional sum of squares algorithm. A double oblique image plane, corresponding to a short-axis view of the heart, was used for both SMASH and reference scans (17.6°AP, 14.9° LR, −41.3° FH angulation from a sagittal plane).

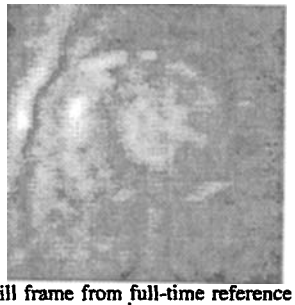

Figure 1. (a) Still frame from full-time reference image set (14 images per cardiac cycle).

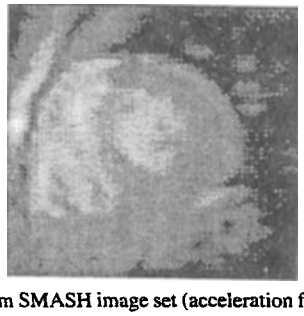

(b) Still frame from SMASH image set (acceleration factor 2, 28 images per cardiac cycle).

Results: Frame rates of 28 images per cardiac cycle (Tacq = 35 ms) were obtained using a SMASH acceleration factor of 2, while a SMASH acceleration factor of 3 yielded frame rates of 42 images per cardiac cycle (Tacq = 23 ms). Despite some loss of SNR compared with full acquisitions, cardiac borders were well defined in the SMASH reconstructed scans, with noticeable improvements in the fluidity of observed cardiac contraction.

Conclusions: SMASH has been used to achieve 2D echocardiographic frame rates in real-time cardiac MRI. At SMASH acceleration factors of 3 or more, some portion of the increased imaging speed may be used for increased spatial resolution rather than further increases in frame rate. A capability for real-time reconstruction and interactive scan plane manipulation will be an important next step in making real-time MR a clinically valuable tool. The SMASH technique is compatible with rapid inline reconstructions and may in some cases require less processing time than traditional sum of squares reconstructions on full data sets.

References

1. Sodickson DK, et al., *Magn Reson Med,* 1997; 38:591–603.
2. McKinnon GC. *Magn Reson Med,* 1993; 30:609–616.
3. Stuber M, et al. Proc. ISMRM 1997, Abstract 908.

Myocardial Contraction in Graded Coronary Stenoses: Tagging at Rest and at Dobutamine Loading

J. Rodenwaldt, M. Jerosch-Herold, Y. Wang, J. Zhang, G.R. Gong, N. Wilke. *Minneapolis, MN*

Purpose: The level at which degree of coronary stenoses MR tagging may allow for detecting early wall motion changes at rest and/or dobutamine is unknown. The aim of this study is to determine what degree of coronary blood flow reduction will produce myocardial wall motion abnormalities detected by MR tagging.

Methods: Instrumented closed-chest dogs (n = 18) were imaged of baseline control (n = 18), followed by mild (n = 6), moderate (n = 6), and severe (n = 6) coronary stenoses by partial hydraulic occlusion of the left anterior descending coronary artery (LAD) at rest and during dobutamine (5–10 μg/kg/min) loading. Short-axis images with spatial modulation of magnetization (SPAMM) were obtained at each level of stenosis, before and during pharmacologic stress. The images were analyzed using SPAMMVU (1). The MBF (ml/min/g) was measured with radioactive labeled microspheres.

Results: We found an excellent correlation between the principle strains λ1 and λ2 (Fig. 1). A relative MBF change of 20–30% results in a significant change in λ1 measured with MR Tagging (Fig. 1). At rest and stress λ2 correlated with MBF. Only λ1 demonstrated myocardial contractility reserve (Fig. 2).

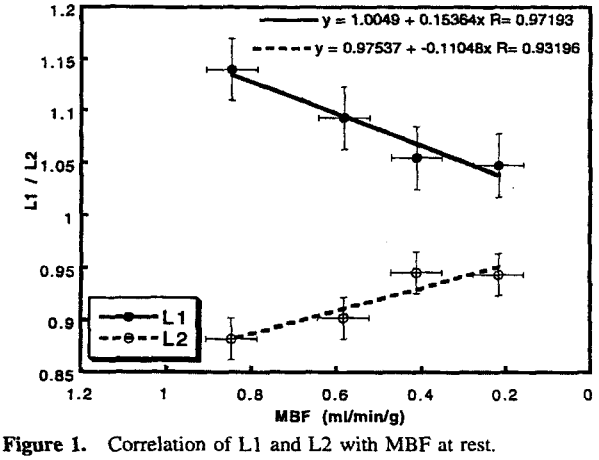

Figure 1. Correlation of L1 and L2 with MBF at rest.

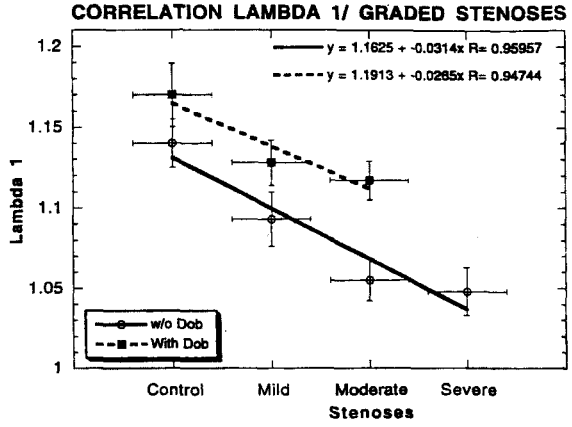

Figure 2. Lambda 1 at rest and stress.

Conclusions: Mild changes of myocardial blood flow (20–30%) produce wall motion abnormalities detected by MR tagging at rest. For dobutamine stress testing and MR tagging the myocardial contractility reserve is best assessed by using λ1 in this setting.

Reference

1. Axel L, Dougherty L. Heart wall motion: improved method of spatial modulation of magnetization for MR imaging. *Radiology*, 1989; 172:349–350.

Effect of Myocardial Infarction on Left Ventricular Torsion Rate in the Pig

R.M. Setser, R.E. Henson, S.E. Fischer, S.A. Wickline, C.H. Lorenz. *St. Louis, MO*

Introduction: Systolic contraction produces a twisting motion of the left ventricle (LV) about its own long axis. We have shown in healthy humans and pigs that the time course of ventricular twist exhibits three distinct phases and have proposed that each is optimized for a specific task (1,2). Changes in LV twist caused by acute myocardial infarction have yet to be defined. However, it is known that in the week following infarction, the LV begins a remodeling process inextricably related to patient prognosis. This early remodeling is manifest as chamber dilatation in an attempt to preserve cardiac output and is related to infarct size. Therefore, the purpose of this study was to define the time course of ventricular twist in pigs following acute myocardial infarction.

Methods: Seven young farm pigs were studied with MRI using a 1.5-T whole body scanner (Philips Gyroscan, ACS-NT) before and 1 week after ligation of the left circumflex artery. LV pressure was measured simultaneously using an MR-compatible catheter pressure transducer (Millar Instruments). Image acquisition included tagged cine MR images (5-mm grid) obtained from the atrioventricular valve plane to the apex in 5-mm-thick contiguous slices.

Results: Traditional measures of LV function remained statistically unchanged in the week following infarction, as shown in Table 1. Similarly, end systolic net torsion did not change following infarction. However, LV twist patterns were altered significantly postinfarction. Also, baseline animals exhibited a significant increase in net torsion rate in early systole, coinciding with the end of isovolumic contraction, as shown in Figure 1. This increase did not occur postinfarction. Velocity of fiber shortening (V_{cf}) showed a similar pattern to that of torsion rate, with a significant increase in early systole at baseline but with no such change postinfarct.

Table 1. Measures of LV function (mean ± SE)

	Baseline	Infarct	*p* value
ESV (ml)	16.2 ± 3.4	26.3 ± 5.5	NS
EF (%)	63.2 ± 2.0	58.7 ± 3.9	NS
SV (ml)	28.1 ± 6.2	37.1 ± 7.3	NS
CO (ml/min)	2815 ± 485	3563 ± 703	NS
dP/dt (mm Hg/sec)	1507 ± 269	1900 ± 466	NS
ES net torsion (deg/cm)	1.7 ± 0.7	1.3 ± 0.9	NS
	Early Systole	Late Systole	
Torsion rate (deg/cm/%sys)			
Baseline	0.5 ± 0.4	2.3 ± 0.3	<0.05
Postinfarct	1.1 ± 0.4	1.4 ± 0.4	NS
V_{cf} (mm/%sys)			
Baseline	2.8 ± 2.1	7.3 ± 1.1	<0.05
Postinfarct	4.9 ± 1.5	6.3 ± 1.3	NS

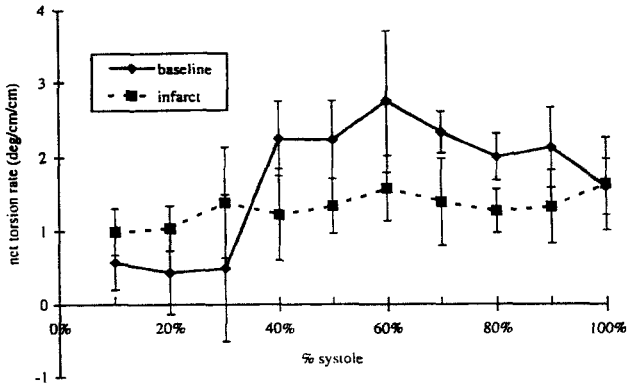

Figure 1. Net torsion rate baseline and postinfarct.

Conclusions: The rate of systolic torsion generation in normal pigs is biphasic, with a low constant rate during isovolumic contraction, followed by a significantly increased rate during systolic ejection. This pattern is altered in the week following myocardial infarction, yielding a single torsion rate throughout systole. Thus, even in the absence of significant alterations in traditional measures of LV function, and without a significant change in end systolic torsion, alterations in the pattern of systolic torsion rate might provide a sensitive indicator of early ventricular remodeling following myocardial infarction.

References

1. Lorenz CH, et al. In review.
2. Setser RM, et al. ISMRM 6th Scientific Mtg, 1998.

Effect of Skeletal Muscle Assistance on Cardiac Function as Assessed by Tissue-Tagged MRI

Aaron S. Blom, James J. Pilla, Sorin V. Pusca, Himanshu J. Patel, Lawrence Dougherty, Qing Yuan, Victor A. Ferrari, Michael A. Acker, Leon Axel. *University of Pennsylvania Medical Center, Philadelphia, PA*

The effects of dynamic cardiomyopathy (CMP) on global and regional left ventricular (LV) function in end-stage heart failure still remain unclear. MRI with tissue-tagging (1) is a novel tool for studying intramyo-

cardial motion and mechanics. This technique has previously been used to study regional short-axis strain variations in models of CMP (2), but no studies to date have attempted to use MRI to simultaneously study global and regional cardiac function in a model of CMP. In this study we used MRI with tissue tagging and a custom-designed MR pressure monitoring/recording system to assess long-axis regional strain and displacement variations and changes in global LV function in a model of cardiomyoplasty.

Three dogs underwent rapid ventricular pacing (RVP, 230 bpm) for 10 weeks; after 4 weeks of RVP, a left posterior CMP was performed. After 1 year of dynamic muscle stimulation, the dogs were imaged in a 1.5-T clinical MR system (GEMS). High-resolution images were acquired using the following parameters: TR/TE = 8.8/2.1 ms; FOV = 16–18 cm; tag spacing = 4–5 mm; 256 × 128 acquisition matrix interpolated to 256^2, four k-space lines acquired per heartbeat, two signal averages. Baseline and muscle stimulated tagged images were acquired. Quantitative 2-D regional image analysis was performed with a custom-written cardiac MR analysis program. The heart was divided into three regions: apical, septal, and lateral. Maximal and minimal principal strains (λ_1 and λ_2) and displacement (D) were determined and pooled for each region. Combining the pressure with the MR volume data, LV pressure volume (PV) loops were generated.

Muscle stimulation produced a leftward shift of the PV loops in two of three dogs and an increase in the peak LV pressure while stroke volume remained unchanged. Further, with stimulation λ_1 decreased significantly in the apical region, whereas values of λ_2 increased significantly in both the lateral and apical regions (Table 1), indicating a decrease in strain resulting from stimulation. D only increased significantly in the apical region.

The decrease in strain between unassisted and assisted states indicates the heart is performing less work, while maintaining stroke volume and increasing peak LV pressure. These findings demonstrate that the muscle wrap functions as an active assist, decreasing the workload of the heart, while preserving total pump performance.

Table 1

	Unassisted		Assisted	
Region	λ_1	λ_2	λ_1	λ_2
Apical	1.16 ± 0.011	0.847 ± 0.004	1.17 ± 0.011	0.867 ± 0.005*
Septal	1.18 ± 0.014	0.860 ± 0.005	1.16 ± 0.011	0.870 ± 0.005
Lateral	1.19 ± 0.014	0.883 ± 0.008	1.15 ± 0.011*	0.904 ± 0.004*

*$p < 0.050$

References

1. Axel L, Dougherty L. MR imaging of motion with spatial modulation of magnetization. *Radiology,* 1989; 171:841–845.
2. Blom AS, Pilla JJ, et al. Assessment of dynamic cardiomyoplasty mechanics using MRI with tissue tagging. *J Cardiovasc Magn Reson,* 1998; 1:65.

Fast-DENSE: High-Resolution Displacement Encoding of the Human Heart

A.H. Aletras, H. Wen. *Bethesda, MD*

Displacement encoding with stimulated echoes (DENSE) was recently presented for high-resolution myocardial displacement mapping (1,2). DENSE cardiac functional data combine desirable characteristics of both myocardial tagging and phase contrast (PC) velocity imaging. These include high spatial data resolution, black-blood contrast, and small first-order moments for the encoding gradients. With DENSE, pixel phase is directly proportional to the displacement incurred over the encoding period. DENSE data may be used to compute accurate strain maps of the heart. Fast-DENSE is used to sample the stimulated echo multiple times to speed up the acquisition process. This is accomplished via a low flip angle multishot segmented EPI sampling scheme. A modified centric k-space sampling scheme was implemented to increase SNR and reduce image artifacts. Planar functional data from the human heart were collected in 24 heartbeats within a single breath hold and strain maps were computed.

In vivo short-axis data from the human heart at 2.5 × 2.5 mm^2 in-plane resolution were collected at 1.5-T with the following parameters: encoding for 0.86 mm/180°, slice = 8 mm, TE = 4.2 ms, encoding interval TM = 105 ms. The position encoded magnetization was recalled via a segmented EPI imaging scheme (centric ordering, eight segments, six 30° RF pulses per segment, two gradient echoes per RF pulse, TR = 6.4 ms). Two-dimensional position-sensitive data were acquired in 24 seconds. Strain analysis was performed with in-house software. As expected, the principal direction of fiber shortening was along the circumference, whereas dilation was radial.

DENSE combines the high SNR of myocardial tagging with the high spatial resolution of PC velocity imaging. Displacement data along with "black blood" images are acquired due to the heavy intravoxel dephasing caused by the position encoding gradients. Encoding gradient moments are applied for a long period (TM) and the resulting phase maps possess a broader dynamic range of multiple π. Thus, instrument and physiologic noise have less effect on strain computations. Such high-resolution strain data may provide insight with respect to the functional heterogeneity of the heart. Further validation of this method has to be performed. Acquisition time has to be further reduced to accommodate patient requirements.

References

1. Aletras AH, Ding S, Balaban RS, Wen H. Displacement encoding in cardiac functional MRI. Proc ISMRM, 6th Scientific Meeting, Sydney, Australia, 1998.
2. Aletras AH, Ding S, Balaban RS, Wen H. DENSE: displacement encoding with stimulated echoes in cardiac functional MRI. *J Magn Reson* (in press).

Relation Between Intramural Mechanics and Change of Ejection Fraction 3 Months After First Myocardial Infarction.

M.J.W. Götte, J.T. Marcus, A.C. van Rossum, C.A. Visser. *Dept. of Cardiology, Dept. of Clinical Physics & Informatics, University Hospital VU, Amsterdam, The Netherlands*

Purpose: Left ventricular (LV) remodeling postmyocardial infraction is characterized by progressive LV dilatation and global LV dysfunction (decrease of ejection fraction [EF]). Regional differences in intramural function may contribute to the process of remodeling (1,2). We examined the relation between intramural mechanics (regional myocardial stretch and direction of stretch) and LV dysfunction in the 3 months after first MI, using MR tissue tagging and 2D strain analysis.

Methods: Fourteen patients (age 56 ± 11 yrs) were studied by MRI within 10 days (t_0) and at 3 months (t_1) after their first LAD-related MI. Intramural deformation was quantified using short-axis tagged images acquired at basal, mid and apical level. EF was obtained from cine-MRI images. Intramural deformation in patients with improved EF at 3 months was compared to patients with decreased EF.

Results: At t_1, seven patients showed an improvement of their EF (56–63%, $p < 0.005$, group A) and seven patients showed a reduction of EF (42–33%, $p < 0.010$, group B). The initial EF was significantly lower in group B ($p < 0.04$). Strain analysis revealed that at t_0, the mean systolic stretch was more circumferential oriented in group B compared to group A (21° vs. 14°, $p < 0.02$). At t_1, the difference in the orientation angle of systolic stretch had increased (24° vs. 14°, p

< 0.01). Additionally, at t_1 the systolic stretch became significantly different between both groups (13% vs. 20%, $p < 0.05$). At t_0, the difference in intramural function was mainly caused by differences in the remote area ($p < 0.02$). At t_1, both the infarct and remote area showed a progressive deterioration of intramural function in group B compared to A ($p < 0.02$, respectively).

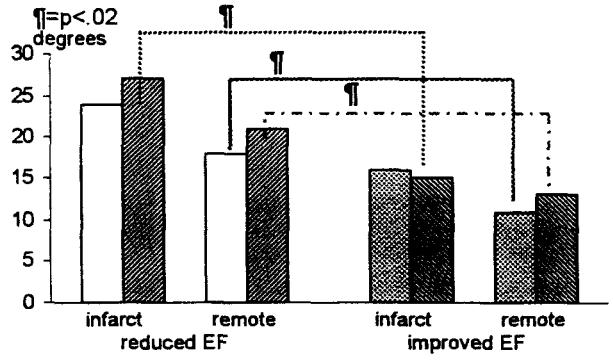

Figure 1. Direction of systolic stretch. Zero degrees indicate radial directed stretch, 30° indicate circumferential oriented stretch. Solid bars represent results at 1 week, dashed bars represent results at 3 months.

Conclusion: Circumferential oriented myocardial stretch in the infarct *and* remote area within 10 days post-MI is associated with deterioration of EF at 3 months post-MI. This intramural dysfunction is progressive, not only in the infarct but also in the remote area. These findings may reflect in a quantitative manner the mechanical aspects (slippage/rearrangement of bundles of myocytes) of the LV remodeling process.

References

1. Kramer et al. *Circulation*, 1997; 30:1625.
2. Marcus et al. *MRM*, 1997; 38:803.

Transmyocardial Laser Revascularization (TMLR) Preserves Left Ventricular Function in Acute Ischemia

J. Dutcher,[1] Y. Huang,[1] Y. Wang,[1] M. Jerosch-Herold,[1] M. Unress,[1] C. Classen,[1] N. Wilke,[1] M. Mirhoseini,[2] M. Cayton,[2] S. Wann.[2]
[1]*Minneapolis, MN;* [2]*Milwaukee, WI*

To date, long-term studies that demonstrated improvements in patients treated with TMLR have mostly relied on clinical exercise testing. A modality of high accuracy and precision is in need to detect early hemodynamic changes in ischemic hearts treated with TMLR. The purpose of this study was to demonstrate that Cardiac MRI can detect acute hemodynamic changes in ischemic swine hearts treated with TMLR.

Methods: Three groups ($n = 31$) of swine weighing 25–30 kg were studied. Group I ($n = 11$) was the Normal Control, group II ($n = 8$) underwent ligation of the left circumflex artery (LCx), and Group III ($n = 12$) underwent TMLR immediately followed by LCx ligation. A modified 850-W laser was used to create the myocardial channels. Quantitative assessment of left ventricular mass (LV mass), left ventricular ejection fraction (EF%), end systolic volume (ESV), end diastolic volume (EDV), left ventricular stroke volume (SV), and peak filling rate (PFR) were done by ultra-fast 3D cine MRI at 2 hours postligation at 1.5 T (Siemens). Left ventricular time volume curves were extracted to calculate PFR. Results are summarized in Table 1.

Table 1. Acute TMLR Cine Hemodynamics

Group	*n*	LV Mass (g)	EDV (mL)	ESV (mL)	EF (%)	SV (mL)	PFR (mL/sec)
Control	11	53 ± 17	39 ± 12	17 ± 6	58 ± 8	23 ± 8	205 ± 62
LCx ligation	8	50 ± 8	59 ± 11‡	40 ± 10‡	34 ± 8‡	19 ± 3	144 ± 31*
TMLR treated	12	53 ± 12	49 ± 10*¶	28 ± 9‡¶	45 ± 11‡¶	21 ± 4	201 ± 64¶

Values are means ± SEM.
*$p < 0.05$ vs. respective Normal Control, ‡$p < 0.01$ vs. respective Normal Control, ¶$p < 0.05$ vs. group II.

Conclusion: This study shows the first evidence that cardiac MRI can accurately detect early hemodynamic changes in acutely ischemic swine hearts treated with TMLR. These data also suggest that the laser created channels are functional early after TMLR treatment. Further, these results demonstrate that TMLR improves left ventricular diastolic function, and can now be applied in patients.

Longitudinal Evaluation of LV Remodeling with MRI After Myocardial Infarction in the Rat: Quantification of Efficacy of ACE inhibition

K.J. Lunn, J.S. Allen, R.M. Setser, D.L. Davis, M.J. Scott, S.A. Wickline, C.H. Lorenz. *St. Louis, MO*

Treatment with ACE inhibitors after myocardial infarction reduces morbidity and mortality in patients. However, the mechanism by which this is accomplished has not been fully elucidated. To facilitate development of novel approaches for prevention of ventricular remodeling after myocardial infarction, an inexpensive, reproducible, and accurate method of assessing *in vivo* longitudinal changes in ventricular size and function is needed. Therefore, the purpose of this study was to determine if ACE inhibitor-induced improvements in ventricular function and morphology after infarction could be demonstrated in an inexpensive and simple small animal model (rat) using MRI.

Three groups of rats were studied: control, infarct only, and infarct treated with ramipril (1 mg/kg/day). The rats were imaged at baseline, 1 week, and 4 weeks postinfarction (ligation of the LAD). Images were acquired on 26 Sprague-Dawley rats using a clinical 1.5-T whole body scanner (Philips Gyroscan ACS-NT, Best, the Netherlands) using a custom-designed 3.8-cm surface coil. Cine imaging was then performed in short-axis contiguous slices using a turbofield echo sequence with in-plane image resolution of 352 × 476 μm and a temporal resolution of 17 ms. Mean heart rate was 300–360 bpm.

At 4 weeks, treatment with ramipril prevented increase in LVEDV and LVESV and prevented LV hypertrophy as shown in Table 1. LV volume and ejection fraction in the ramipril treated animals were not significantly different from that of the controls (Fig. 1).

Table 1

	Control	Infarct Ramipril	Infarct Only	Significance
LV mass (g/g) ×10'	1.8 ± 0.2	1.5 ± 1.4	2.9 ± 0.5	$p < 0.05$ (C vs. I vs. IR)
EDV (ml/g) ×10'	1.5 ± 0.1	1.6 ± 0.2	3.5 ± 0.9	$p < 0.05$ (C vs. I, I vs. IR), p = ns (C vs. IR)
ESV (ml/g) ×10'	0.6 ± 0.2	0.6 ± 0.3	1.8 ± 0.7	$p < 0.05$ (C vs. I, I vs. IR), p = ns (C vs. IR)
EF (%)	61 ± 11	46 ± 11	49 ± 9	NS

Note: LV mass, and ESV normalized to rat body weight. No significant differences were found between groups at baseline and 1 week postinfarction.

Prevention by ACE inhibition of compensatory remodeling after infarction can be quantitated in vivo in the rat with MRI. The ability to discriminate small changes in ventricular size in the rat with MRI will permit cost-effective evaluation of new therapies as they emerge.

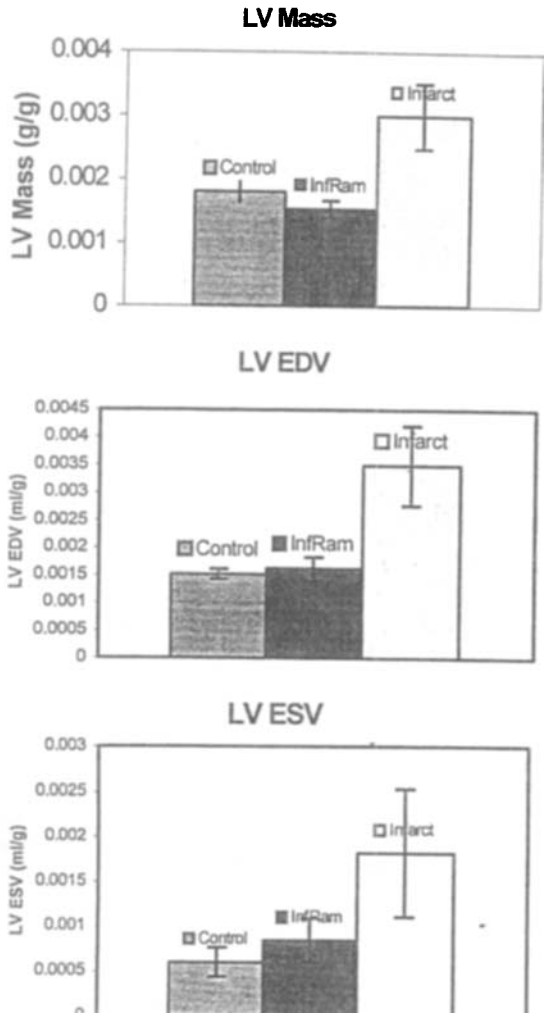

Figure 1

Comparison of Contrast Enhancement to Histology in Coronary Artery Disease-Related Myocardial Injury

D.S. Fieno, R.J. Kim, F.J. Klocke, R.M. Judd. *Chicago, IL*

The interpretation of MRI contrast enhancement patterns requires knowledge of their relationship to the underlying pathophysiology. Detailed comparisons between MRI and histology, however, are difficult due to methodologic limitations such as deformation of the heart during cutting. We developed a method to register MR images to contiguous 2-mm-thick histologic slices encompassing the entire vehicle and used this to study dogs (n = 7) subjected to infarction with and without reperfusion at 4 hours, 1 day, 3 days, and 8 weeks. After in vivo contrast MRI (0.3 mmol/kg Gd-DTPA), fluorescent microspheres were injected into the left atrium to identify the "risk" region. The hearts were then removed, immersed in 4°C saline, blotted dry, and balloons containing D_2O were placed in the cavities. Three markers were glued to the heart to define the imaging and cutting planes. After 500 × 500 × 500-μm T1-weighted ex vivo images were acquired, the hearts were cooled and sectioned on a commercial meat slicer. Slices (ca. 25 per heart) were then stained with TTC and photographed under room light for infarct size and ultraviolet light for the risk region. In 169 slices, the size and three-dimensional shape of hyperenhanced regions by ex vivo MRI matched those of infarcted regions ($y = 0.975x + 0.007$, $R = 0.992$, SEE = 2.37) while risk regions were of different shape and ranged from 20–400% larger ($y = 0.558x - 1.43$, $R = 0.802$, SEE = 5.20). These results indicate that when spatial resolution is adequate to represent the complex three-dimensional shape of the myocardial infarcts, MRI hyperenhancement occurs in nonviable myocardium but not in normal myocardium or reversibly injured but viable myocardium at 4 hours, 1 day, 3 days, and 8 weeks postinfarct.

Tissue Characterization and Intramural Mechanics in the Subacute Phase of Myocardial Infarction: Stir MR Imaging Versus Myocardial Tagging

A.M. Beek, M.J.W. Götte, J.T. Marcus, A.C. van Rossum, C.A. Visser. *Dept. of Cardiology, Dept. of Clinical Physics & Informatics, University Hospital VU, Amsterdam, The Netherlands*

Background: Short T1 inversion recovery (STIR) is a combination of T2-weighting, blood nulling, and fat suppression in a single breathhold sequence. It is presumed to be sensitive to regional edema in the early phase of acute myocardial infarction (AMI) (1). Regional intramural mechanics in AMI are accurately described by β, the deviation between regional systolic stretch and the radial direction. The aims of this study were to assess whether STIR applied in the subacute phase of AMI could accurately identify the infarcted area and further to establish a relationship between β and STIR signal intensity (SI).

Patients and Methods: Eleven patients (age 58 ± 9 yrs) with first AMI (8 anterior, 3 inferior) underwent an MRI study 5 days (4–14) after admission. The infarct-related coronary artery was determined by angiography. Basal, mid, and apical short axis of the left ventricle were determined by scout imaging. Myocardial tagging (7-mm grid) and STIR Turbo spin-echo imaging (turbofactor 23, TE 76 ms, breathhold duration 14 heartbeats) were subsequently applied. The midventricular slice was identified by the presence of both papillary muscles. The slice was divided into 12 equiangular regions, in a clockwise direction starting at the anterior insertion of the right ventricular wall. In each patient the region with highest signal intensity (SI) by STIR was identified. The opposite region was labeled as "remote." The infarct-versus-remote contrast ratio was calculated from the difference in SI as (SI-infarcted − SI-remote)/(SI-infarcted + SI-remote).

Results: In all patients the regions with highest SI by STIR corresponded well with the infarcted area derived from angiography. A significant correlation existed between β and the infarct-versus-remote contrast ratio (Fig. 1 and Table 1).

Table 1

IRV	Inf-rem Ratio	Beta (degrees)
LAD	0.62	55
LAD	0.46	28
RCA	0.32	19
LAD	0.35	28
RCA	0.44	7
RCA	0.28	9
LAD	0.40	33
LAD	0.53	20
LAD	0.54	40
RCA	0.18	14
LAD	0.42	24

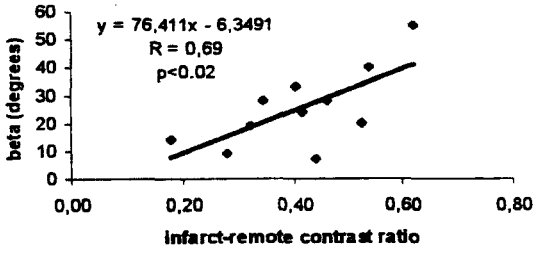

Figure 1

Conclusion: Regional infarct associated edema in the subacute phase of AMI is readily demonstrated by breathhold STIR MRI and correlates with the extent of mechanical dysfunction.

Reference

1. Simonetti et al. *Radiology,* 1996; 199:49–57.

Determination of Coronary Blood Flow Velocity After Stent Implantation

C. Klein, J. Hug, S. Bünger, A. Bornstedt, B. Schnackenburg, E. Wellnhofer, T. Thouet, S. Schalla, E. Nagel, E. Fleck. *Berlin, Germany*

The assessment of coronary artery stenoses by intracoronary Doppler flow measurements allows a functional assessment of the severity of a stenosis. With magnetic resonance (MR) tomography, the visualization of coronary artery stenoses becomes more and more feasible. However, after stent placement no direct visualization of the coronary arteries is possible, due to "black hole" artifacts (1). In these patients, a noninvasive assessment of the stents may be possible with MR flow measurements (2). The aim of this study was to evaluate MR phase contrast flow measurements for the noninvasive assessment of intracoronary blood flow after stent implantation.

Coronary blood flow velocities were measured in 64 patients 24 hours after stent implantation using a 1.5-T MR tomograph (ACS NT, Philips). Twenty-four patients were reexamined with MR and angiography after 3 months. Flow measurements were performed perpendicular to the vessel proximal and distal to the stent. A segmented k-space turbogradient echo technique with prospective navigator gating and adaptive motion correction was used. Spatial resolution was 1 × 0.9 × 4 mm, temporal resolution 45 ms, scan duration app. 150 sec with a gating window of 5 mm (TE: 6.9 ms, TR: 11.5 ms, flip angle: 60°, 4 k-lines per phase per heartbeat, velocity encoding: 50 cm/s). Regions of interest with an area of 2 × 2 pixels were drawn in the center of the vessel on the anatomic images for each cardiac phase and copied to the flow images. The average flow value (flow velocity [cm/s]) was determined for each phase and corrected for through plane motion. The highest diastolic value was used for the determination of peak flow velocity. The technique was previously validated in comparison to invasive measurements using a 0.014″ FloWire (FloMap system, Cardiometrics). Correlation between invasive and noninvasive measurements was good ($r = 0.86$). However, a systematic underestimation of coronary blood flow velocity in comparison to the invasive measurement was observed, which was mainly due to the relatively low spatial and temporal resolution (3).

An antegrade pulsatile flow signal could be obtained in 43 patients distal and in 39 patients proximal to the stent. Noninvasive determination of the maximal flow velocity yielded 19 ± 3 cm/s for the RCA, 23 ± 6 cm/s for the LAD, and 21 ± 9 cm/s in the RCX proximal of the stent (distal: 18 ± 8 cm/s, 21 ± 7 cm/s, 18 ± 9 cm/s). After 3 months a tendential decrease of maximal diastolic flow velocity could be observed proximal to the stent and a significant decrease distal to the stent ($p < 0.05$) which correlated with in-stent luminal diameter reduction.

In the present study it was possible to determine flow noninvasively in 67% of the patients. After 3 months a reduction of maximal diastolic flow velocity could be observed in patients with intraluminal diameter reduction. Thus, a noninvasive assessment and follow-up of patients after stent implantation is possible with MR. Further improvements and increased robustness of the technique are essential for routine clinical use.

References

1. Hug J, et al. Intracoronary stents: safety and artefacts during magnetic resonance imaging. *Circulation,* 1997; 96(Suppl):I-275.
2. Hundley WG, et al. Assessment of coronary arterial flow and flow reserve in humans with magnetic resonance imaging. *Circulation,* 1996; 93:1502–1508.
3. Nagel E, et al. Noninvasive determination of coronary blood flow velocity with magnetic resonance imaging: comparison of breath-hold and navigator techniques with intravascular ultrasound. *Magn Reson Med* (in press).

MR Measurement of Flow Reserve in Coronary Grafts

T. Voigtländer, K.-F. Kreitner, T. Wittlinger, J. Scharhag, N. Abegunewardene, J. Meyer. *Mainz, Germany*

Aim: MR angiography detects coronary graft patency with high sensitivity and specificity. But limited spatial resolution does not allow diagnosis of graft stenosis reliably. The aim of the study was to evaluate the feasibility of MR flow reserve measurement in coronary grafts (graft-CFR) to detect high-grade graft stenosis.

Methods: In 20 patients 27 coronary grafts (11/27 internal mammary grafts, 16/27 vein grafts) were investigated by conventional angiography (Siemens HICOR) and MR (Siemens Vision, 1.5 T). The course of the grafts was delineated using the HASTE sequence. Perpendicular to the course of the grafts a first measurement of mean velocity and mean flow was performed using MR phase change technique (TR 110 ms, breathholding, software Argus 2.3). The measurement was repeated during adenosin infusion. Two different graft-CFR were created. One consisted of a ratio of mean velocity during and before adenosin infusion, and the other of a ratio of mean flow during and before adenosin infusion. Values for grafts with stenosis > 75% ($n = 6$) were compared with grafts without stenosis ($n = 21$).

Results: The graft-CFR was reduced significantly in stenosed coronary grafts. Graft-CFR measurement based on mean velocity discriminates both graft types more significant compared to graft-CFR measurement based on mean flow:

	Mean Flow (ml/min)			Mean velocity (cm/sec)		
Angio.	No Adenosin	Adenosin	Graft-CFR	No Adenosin	Adenosin	Graft-CFR
No stenosis	33.0 ± 22.8	81.0 ± 54.6	2.9 ± 1.9	5.49 ± 4.4	12.1 ± 9.6	2.6 ± 1.5
>75%	95.3 ± 39.6	75.0 ± 62.4	1.2 ± 0.5	7.01 ± 1.8	5.1 ± 2.1	0.8 ± 0.4
p			<0.05			<0.005

Conclusion: The noninvasive evaluation of graft-CFR using MR identifies high-grade coronary graft lesions. By combining both MR coronary graft angiography and MR graft-CFR measurement, a comprehensive noninvasive coronary graft follow-up can be performed.

References

1. Sakuma H. Breath hold MR measurement of blood flow velocity in internal mammary arteries and coronary bypass grafts. *JMRI,* 1996; 1: 219–222.

2. Van Rossum. The role of MR in the evaluation of functional results after CABG/PTCA. *Int J Cardiac Imag,* 1993; 9:59–69.

Applications of Real-Time MRI with Color Flow Mapping: Fast and Slow Flow

K.S. Nayak, P.A. Rivas, A.B. Kerr, J.M. Pauly, B.S. Hu, D.G. Nishimura. *Stanford University, Stanford, CA*

We developed a real-time color flow imaging system by integrating rapid velocity mapping with our existing real-time interactive MR system (1,2). We are thereby able to acquire and display velocity maps superimposed (using color) on density images. Using MR, arbitrary scan planes can be quickly localized, and flow can be measured in any direction.

We use spiral trajectories for their good motion properties and efficient k-space coverage and phase contrast for computing velocity maps. Our current results were acquired on a GE Signa 1.5-T system, with gradients supporting $|G| < 4.0$ G/cm, and $|dG/dt| < 15.0$ G/cm/ms. When imaging slow flow (less than 1 m/s) our measurements use an 8-ms spectral-spatial excitation, 16-ms readouts, an imaging TR of 33 ms, and six interleave spirals. When imaging faster flow or high speed jets (up to 6 m/s) we incorporate a 3-ms conventional exicitation, 5-ms readouts, an imaging TR of 11 ms, and 18 interleave spirals. In flow mode, half as many interleaves are acquired to form each of two complete images, which are then used to infer density and velocity per pixel. We are able to achieve 2.24-mm isotropic resolution over a 20-cm FOV, and acquire 6 complete images per second, while reconstructing at a higher rate of 12 frames per second, using a sliding window.

We demonstrate real-time color flow mapping using MR, in a variety of application areas and particularly focus on fast versus slow flow issues.

References

1. Nayak K, et al. *Circulation,* 1998; 98:I-513.
2. Kerr A, et al. *MRM,* 1997; 38:355.

Velocity Profiles Beyond Mechanical Valves in an Aortic Arch Pulsatile Flow Model Recorded by Magnetic Resonance Velocity Mapping

M.W.S. Kon, K. McCormack, P.V. Lawford, P.J. Kilner, D.R. Hose, M.M. Black, N.E. Moat, D.J. Pennell, D.N. Firmin. *Royal Brompton Hospital, London, and Department of Clinical Engineering and Medical Physics, University of Sheffield*

Objective: A pulsatile flow model was designed and tested to explore the potential of magnetic resonance imaging techniques to map velocities through and around mechanical heart valves.

Methods: A geometrically correct aortic arch and pulsatile flow system compatible with MRI was developed and velocity-mapping techniques used to measure through-plane velocity in over 150 experiments. Stroke volume was calculated in a series of experiments to determine the stability, accuracy, and reliability of the model under a full range of cardiac outputs and in regions of complex flow geometry downstream of the mechanical valve. Vector maps were derived from measurements of velocity in two orthogonal directions.

Results: The model was found to be stable (<3% measurement error) and accurate (<5% measurement error) under a range of conditions. Stroke volume measurements downstream of a bileaflet valve were reliable (<9% measurement error) when compared with a series of known pump stroke volume. The longitudinal velocity profile of a bileaflet valve was examined in detail (Fig. 1), and peak velocity was correlated with changes in stroke volume. Vector mapping of flow patterns through a tilting disc valve indicated a highly skewed flow profile, with an area of recirculation distal to the smaller valve orifice (Fig. 2). Kinetic energy and shear distributions were graphically represented.

Figure 1

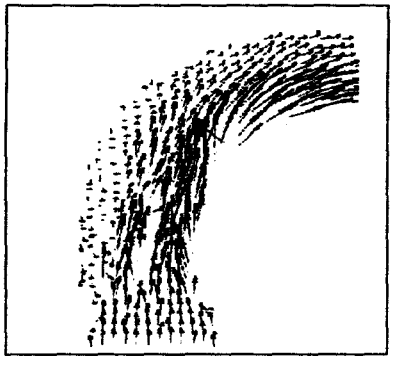

Figure 2

Conclusion: This validated model allowed unique visualization of velocity profiles around mechanical heart valves without significant artifact. The model can be used to assess prosthetic valve function in vitro, and similar techniques could be applied to patients to investigate flow patterns in vivo, which may be useful in defining the preferred orientation of different types of valve.

Noninvasive Assessment of Stenotic Valve Orifice Area by Magnetic Resonance Imaging: An In Vitro Study

O. Strohm, J. Schulz-Menger, R. Dietz, M.G. Friedrich. *Franz-Volhard-Klinik, Charité, Humboldt University, Berlin, Germany*

Exact and reliable determination of the remaining orifice area in stenotic valve disease is essential to guide therapy. With the currently used imaging methods such as echocardiography and cardiac catheterization, the orifice area is calculated by empirically derived formulas that may be susceptible to changes in the hemodynamic status of the patient, thus leading to wrong therapeutic decisions. Planimetry of the orifice by transesophageal echocardiography is difficult and semiinvasive. Gradient-echo MRI sequences visualize the transplanar flow, and the proximal jet at its minimal diameter (vena contracta) shows a very close correlation to the effective orifice area, which was confirmed by computer models.

We tested the ability of magnetic resonance imaging (MRI) to directly measure the effective orifice area by a planimetry of the proximal vena contracta in a physiologically shaped flow model using a simple post-processing technique and standard sequences. Results were com-

pared to those of a calculation with the Gorlin formula using the pressure gradient and to the true area as determined by a photographic method. There was a very close correlation of the vena contracta area in MRI and the true orifice area (r^2 = 0.985) and for the calculated area and the true orifice area (r^2 = 0.9997).

We conclude that MRI planimetry of the proximal vena contracta is a simple, fast, and reliable method to measure orifice areas. This should be evaluated in clinical studies of patients aortic and mitral valve stenosis.

Real-Time Imaging of Left Ventricular Function: Comparison to Conventional MR Imaging and Echocardiography

S. Schalla, U. Vogel, C. Klein, T. Ibrahim, H.B. Lehmkuhl, A. Bornstedt, B. Schnackenburg, E. Nagel, E. Fleck. *Berlin, Germany*

New ultrafast gradient systems and hybrid imaging sequences (1) make the acquisition of a complete image within minimal time possible. These new techniques allow functional cardiac images to be acquired in real time, without the need for breathholding or ECG triggering (2,3).

In 21 patients, left ventricular function was assessed using a turbo-gradient echo technique, an echo planar imaging technique, and a new real-time imaging technique (Table 1). End diastolic and end systolic volumes, left ventricular muscle mass, and ejection fraction of the new ultrafast techniques were compared to the turbo gradient echo technique. Twelve patients were also exmined with echocardiography.

Table 1

	TFE	EPI	RT
TE (ms)	2.1	5.6	6.8
TR (ms)	5.9	20	15.5
Flip angle (8)	25	30	20
k-lines per shot	4	7	36
EPI factor	—	7	9
Matrix	121 × 256*	96 × 128*	64 × 128*
Temporal resolution (ms)	50	20	62
Spatial resolution (mm)	1.3 × 2.6	2.6 × 3.4	2.2 × 4.4

* Raw data were filtered and zero-filled to 256 points.

Results of the new fast-imaging techniques are comparable to conventional ECG triggered turbogradient echo techniques. End diastolic volume was tendentially overestimated by 3.9 and 1.3 ml with EPI, respectively, real-time imaging, end systolic volume by 0.9 ml and 5.0 ml, left ventricular mass by 2.6 g and 23.8 g. Ejection fraction was tendentially overestimated by 1.1% with EPI and underestimated by 4.5% with real-time imaging. Inter- and intraobserver variability were low with all three MR techniques. Echocardiographic ejection fraction correlated well with MR results (r = 0.94 vs. turbo gradient echo, %error = 13%, r = 0.93 vs. real time, %error = 15%).

Scan time can be reduced significantly with this new technique. Further studies will have to assess the value of real-time imaging for the detection of wall motion abnormalities and the imaging of patients with atrial fibrillation.

References

1. McKinnon GC. Ultrafast interleaved gradient-echo-planar imaging on a standard scanner. *Magn Reson Med*, 1993; 30:609–616.
2. Yang P, Kerr A, Liu A, Liang DH, Hardy C, Meyer C, Macovski A, Pauly J, Hu B. New real-time interactive cardiac magnetic resonance imaging system. *J Am Coll Cardiol*, 1998; 31(Suppl A):3A (abstract).
3. Scheidegger MB, Spiegel M, Stuber M, Bonetti P, Dubach P, Boesiger P. Assessment of cardiac wall thickening and ejection fraction from real time cardiac MR images in patients with left ventricular dysfunction. Proceedings of the International Society of Magnetic Resonance in Medicine, Sydney, 1998:554 (abstract).

Zonal Fast Spin-Echo Imaging of the Heart Using Double-Inversion Preparation

C.L. Charrier, P.D. Gatehouse, D.N. Firmin. *Royal Brompton Hospital & Imperial College, London*

The aim of this study was to reduce the acquisition time and improve the blood-wall contrast in cardiac imaging by using a zonal fast spin-echo (FSE) sequence and a double-inversion (DI) preparation.

All images were acquired at 1.5 T. Contrast in the imaging slice was achieved by applying two inversion pulses, the first nonselective, the second slice selective (1). After an inversion time (TI), the inflowing blood in the imaging plane has a longitudinal magnetisation approaching zero, thereby giving a black blood image. In this study a novel FSE sequence was developed that utilised the zonal imaging technique (2), as an effective way of reducing overall imaging time by enabling a rectangular field of view (RFOV) acquisition without incurring phase wraparound. As in previous studies this was achieved by replacing the slice selective gradients applied during the 180° rf pulse with equivalent gradients applied in the phase encode direction, thereby creating an "inner volume" of tissue which will allow the RFOV acquisition.

Results show a reduction in imaging time, by a factor of 4 compared with nonzonal FSE, which can be used to either reduce the total acquisition time or the acquisition window in each cardiac cycle. The latter implementation enables acquisitions at any point of the cardiac cycle with minimal motion related blurring. The predicted drop of signal-to-noise ratio (SNR) is not sufficient to impede results due to the inherent high SNR of the FSE technique at 1.5 T. Furthermore, there is good blood-wall contrast which enables high contrast anatomic imaging and accurate automated volume measurements to be taken.

DI FSE zonal images achieve a significant reduction in imaging time and give good blood-wall contrast. Further work to be implemented with this method includes the use of respiratory navigators. This technique also has the potential of single shot imaging with reasonable temporal and spatial resolution.

References

1. Edelman RR, Chien D, Kim D. *Radiology*, 1991; 181:655–660.
2. Feinberg DA, Hoenninger J, Crooks L, Kaufman L, Watts JC, Arakawa M. *Radiology*, 1985; 156:743–747.

MR Assessment of Cardiac Structure and Function in Obesity

P.G. Danias, N.A. Tritos, K.V. Kissinger, W.J. Manning. *Boston, MA*

Background: Obesity is a common health problem, affects approximately one third of the adult U.S. population, and has significant associated cardiovascular morbidity. Conventional noninvasive cardiac imaging in obese individuals is frequently suboptimal, due to significant soft tissue attenuation. The role of cardiac MR imaging for evaluation of this population has not been explored.

Methods: We investigated the left ventricular (LV) structure and function of otherwise healthy obese (BMI > 30 kg/m^2) men and compared it to age-matched lean (BMI 19–25 kg/m^2) control volunteers. Fourteen men (8 obese, age 28.8 ± 7.8 yrs, and 6 lean, age 30 ± 3.9 yrs) underwent MR imaging using a 1.5-T whole body scanner (Gyroscan NT/ACS, Philips Medical Systems, Best, The Netherlands) with research software (cardiac patch CPR6) and standard gradient hardware

(21 mT/m, slew rate 100 mT/m/sec). Serial breathhold cine images were obtained for contiguous short axis slices (slice thickness 10 mm) to cover the whole LV, using a hybrid gradient echo–echo-planar (FFE-EPI) cine sequence (TR = RR interval, TE = 9 msec, matrix 128 × 256, FOV 320 mm). End-diastolic and end-systolic epicardial and endocardial LV borders were manually traced for determination of LV volumes, mass and calculation of ejection fraction.

Results: Scanning was successfully completed for all obese and lean subjects and image quality was excellent in all individuals. Our results (mean ± SD) are presented in the following table:

Subject Group	BMI (kg/m²)	LV mass (g)	LV mass index-BSA (g/m²)	LV mass index-ht (g/m)	LV EDV (ml)	LV EDV Index-BSA (ml/m²)	LV EDV Index-ht (ml/m)	LV EF (%)
Obese (n = 8)	36 ± 2	230 ± 13	97 ± 5	126 ± 6	185 ± 19	78 ± 6	101 ± 8	68 ± 5
Lean (n = 6)	22 ± 2	149 ± 6	83 ± 4	86 ± 4	145 ± 17	81 ± 8	84 ± 10	65 ± 5
p value	<0.001	<0.001	<0.001	<0.001	0.002	0.46	0.003	0.3

BMI, body mass index; LV, left ventricular; EDV, end-diastolic volume; ESV, end-systolic volume; EF, ejection fraction; BSA, body surface area; ht, height.

Conclusions: We conclude that obese males have increased LV mass and LV mass index (normalized for both body surface area and height) compared to lean controls. The LV end-diastolic volume (both absolute and height-adjusted values) were also significantly different between the two groups, while the LV ejection fraction was similar in lean and obese individuals. Cardiac MR imaging may be uniquely suited for evaluation of cardiovascular function in obese individuals.

In Vivo Magnetic Resonance Imaging of Aortic Atherosclerosis in a Healthy Population: Preliminary Observations

F.A. Jaffer, C.J. O'Donnell, K.V. Kissinger, R.M. Botnar, W.J. Manning. *Framingham and Boston, MA*

Introduction: Cardiovascular disease is a leading cause of morbidity and mortality in the United States. Risk stratification among asymptomatic subjects based on clinical variables may be suboptimal because of the lack of methods for direct visualization of atherosclerosis in vivo. Recently, MRI has been used to identify human atheroma in vivo among subjects referred for carotid endarterectomy (1). We postulated that similar methodology would allow detection and quantification of aortic atherosclerotic burden, and now report on our preliminary observations from aortic MR studies of healthy subjects followed in the Framingham Heart Study (FHS).

Methods: Twenty-five healthy FHS subjects (age 68 ± 14 yrs; 12M, 13F) were imaged using a 1.5-T Philips Gyroscan ACS-NT MR scanner (Philips Medical Systems, Best, NL) using a five-element cardiac synergy coil. Aortic imaging was performed using an ECG-gated T2-weighted turbo spin-echo sequence (TR = 3 RR, TE 45 ms, slice thickness 5 mm, NSA = 4, in-plane resolution 780 × 500 μ) extending from the aortic arch to the bifurcation of the abdominal aorta. Total imaging time was ≤20 min. Total descending thoracic and abdominal aortic volume along with atherosclerotic volume were recorded. Atherosclerotic burden was defined as the atherosclerotic volume expressed as a percent of aortic volume. Interobserver variability was assessed from aortic area data from a subset of 10 subjects that were individually analyzed by two observers. All determinations were made by individuals blinded to all clinical data.

Results: All subjects completed the study without complication. Aortic area data was well correlated between observers (r^2 = 0.974). A majority of subjects had evidence of aortic atherosclerosis by MRI (Fig. 1). Average total aortic atherosclerosis burden was 6.2 ± 4.9% (0.3–21.1%). Abdominal atherosclerosis burden was of much greater magnitude (10.3 ± 7.9%; 0.4–32.8%) than thoracic burden (0.5 ± 1.0%; 0–3.1%).

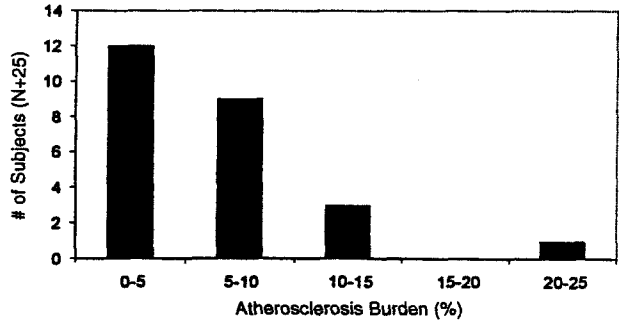

Figure 1

Conclusions: A majority of clinical healthy participants in the FHS Offspring Study had evidence of aortic atherosclerosis as visualized by MRI. MRI assessment of atherosclerotic burden may allow for the identification of individuals at increased risk for future cardiovascular events. A prospective study of a larger subset of the FHS population is in progress.

Reference

1. Toussaint JF, et al. Magnetic resonance images lipid, fibrous, calcified, hemorrhagic, and thrombolytic components of human atherosclerosis in vivo. *Circulation,* 1996; 94:932–938.

Design of New Receive Coils for Fast Cardiac Imaging

H.M.M. Creemers,[1] D.K. Sodickson.[2] [1]*Best, The Netherlands;* [2]*Boston, MA*

Two new coil array designs for cardiac MR imaging are described here, along with general coil design principles for improving image quality and accelerating acquisition.

The performance of radiofrequency (RF) surface coils is governed by a trade-off between signal-to-noise ratio (SNR) and field of view. Synergy or phased array coils (1) combine the SNR advantages of small coils with the advantages of large fields of view by simultaneously receiving with multiple small coils distributed over an extended area. Using simultaneous acquisition of spatial harmonics (SMASH) (2), imaging speed can also be increased with coil arrays by substituting coil-derived spatial information for time-consuming gradient steps.

The synergy principle was applied in the design of a dedicated five-element cardiac coil array for use on a Philips NT imaging system (Philips Medical Systems, Best, The Netherlands). The elements of this array surround the thorax so as to allow high-SNR imaging of the posterior and the anterior heart. When only the left or anterior heart is of interest, reconstruction time can be reduced by using appropriate subsets of the coil elements.

A linear six-element SMASH coil was also constructed covering roughly the same field the view as the posterior elements of the five-element synergy coil. In this case, some degree of volumetric coverage was sacrificed to maximize the number of independent spatial sensitivity profiles spanning typical cardiac fields of view, thereby maximizing the achievable SMASH acceleration factor. Six elements were used to take advantage of the full complement of six receivers on the NT system. Simulations and phantom experiments confirmed that the arrange-

ment of coil elements was compatible with accurate generation of sinusoidal spatial sensitivity profiles for the SMASH image reconstructions.

The performance of the five-element cardiac synergy array has been tested at several imaging centers and in a number of cardiac imaging applications. Use of the six-element SMASH coil has yielded as much as fourfold reductions in scan time for MR coronary angiography and cardiac functional imaging.

This work demonstrates that RF coil array designs can be optimized for cardiac geometries to yield improved image quality and enhanced imaging speed in practical cardiac imaging applications.

References

1. Roemer PB, et al. The NMR phased array. *Magn Reson Med,* 1990; 16:192–225.
2. Sodickson DK, et al. Simultaneous acquisition of spatial harmonics (SMASH): fast imaging with radiofrequency coil arrays. *Magn Reson Med,* 1997; 38:591–603.

Heavily T2-Weighted Breathhold MRI Visualizes Edema in Acute Myocarditis

M.G. Friedrich, P. Barckow, J. Schulz-Menger, O. Strohm, R. Dietz. *Franz-Volhard-Klinik, Charité, Humboldt University, Berlin, Germany*

Heavy T2-weighting leads to an almost selective imaging of water-bound protons. High signal therefore represents accumulation of water. We hypothesized that this technique would show edema in acute myocarditis.

We studied 13 patients with acute myocarditis as defined by symptoms like angina, dyspnea, malaise, or fatigue; a history of a flulike illness within the last 2 weeks; significant changes of the ECG; and an angiographic exclusion of coronary heart disease. The studies were performed on a conventional tomograph (Siemens Magnetom Expert 1.0 T) using a heavily T2-weighted breathhold sequence with short T1 inversion recovery (STIR, TE 64 ms, TR 800 to 2000 ms, slice thickness 20 mm) in a basal short-axis view. The results were compared to 13 healthy volunteers with no history of heart disease. The mean acquisition time was 16 seconds. Image quality was good to excellent in all cases. There was a strong patchy signal enhancement of the myocardial tissue in patients with acute myocarditis. The global myocardial signal intensity was related to that of the skeletal muscle within the same image. This ratio was significantly elevated on days 7 (2.05 ± 0.96; $p < 0.0001$) and 28 (1.85 ± 0.76; $p < 0.0001$) but not on day 2 (1.64 ± 0.76) and day 84 (1.66 ± 0.068) after the onset of symptoms, as compared to controls (1.58 ± 0.071).

We conclude that this MRI technique allows the visualization of myocardial edema from the second to the fourth week of the onset of disease in acute myocarditis. It may be a very fast, simple, and safe way to follow up those patients. In combination with contrast-enhanced studies the sensitivity in early phases may be increased. This issue should be addressed in further studies.

MRI Planimetry of Left Ventricular Outflow Tract Area in Patients with Hypertrophic Obstructive Cardiomyopathy

J. Schulz-Menger, O. Strohm, R. Dietz, M.G. Friedrich. *Franz-Volhard-Klinik, Charité, Humboldt University, Berlin, Germany*

The degree of left ventricular outflow tract (LVOT) obstruction is essential in the evaluation of hypertrophic obstructive cardiomyopathy (HOCM). But the pressure gradient is susceptible on hemodynamic variations and the correlation to the clinical outcome is poor. Furthermore, the echocardiographic follow-up of diameter and LVOT pressure gradient strongly depends on the "ultrasound window" and on the investigator's experience. The area of LVOT as the key parameter can only be estimated. Magnetic resonance imaging (MRI) enables the accurate visualization of the myocardium and of the blood flow with free choice of plane orientation.

We investigated 15 patients with a conventional MRI scanner (Siemens Expert 1.0 T; Siemens AG, Erlangen, Germany). Using gradient-echo sequences we measured minimal orifice area of LVOT during maximal systolic blood flow and quantified myocardial muscle mass, ventricular volumes, and end systolic wall stress. Measurements were compared to echocardiographic results obtained within 2 days. We found a very good correlation ($R = 0.8$, $p < 0.0001$) between LVOT orifice area and the present NYHA class and a good correlation between echocardiographic pressure gradient and NYHA class ($R = 0.7$, $p < 0.002$). Furthermore, our experience in follow-up measurements after embolization of septal artery shows a good correlation between improvement of symptoms and increase of LVOT orifice area.

In conclusion, systolic LVOT orifice area seems to be a reliable and reproducible noninvasive parameter in quantifying LVOT obstruction in HOCM.

Virtual Reality Techniques for Evaluation of Pediatric Aortic Malformations

G. Wesley Vick, III,[1] Roxann Rokey.[2] [1]*Baylor College of Medicine, Houston, TX;* [2]*Marshfield Clinic, Marshfield, WI*

Background: Pediatric aortic malformations typically have complex structures. Projective x-ray angiography (PXRA) and standard tomographic methods (STM), such as x-ray computed tomography, two-dimensional echocardiography, and magnetic resonance imaging, have substantial limitations in these disorders. Structure overlap, nonuniform magnification, and contrast dosage limit PXRA. Curvilinear structures of interest and the consequent necessity to review large arrays of tomographic images limit STM.

Purpose: To assess virtual reality computer display techniques for evaluation of pediatric aortic malformations.

Methods: A variety of virtual reality computer techniques was used in pediatric aortic MRI examinations for coarctation, aneurysm, and vascular ring. (1) Variable phase trip through the body. Successive images at different phases of the cardiac cycle (typical spin echo acquisition). Images electronically stacked and displayed in an oscillating loop digital movie. (2) Uniphasic trip through the body. Successive images of the same cardiac phase. (3) Three-dimensional multiplanar reformatting. Clipping planes arbitrarily repositioned, and multiple parallel slice sections created. (4) Multiphasic multilevel montage. Images acquired at multiple levels during a single cardiac phase and placed side by side on an electronic sheet. Electronic sheets stacked and played in a continuous loop. (5) Multiphasic trip through the body. Images electronically stacked, multiphasic loop played at each anatomic level. (6) Three-/four-dimensional wireframe and point modeler displays. File size is extremely small, facilitating real-time rotation. (6) Three-dimensional uniphasic rendered surface/volume displays. Maximal intensity and ray-traced surface rendered projective techniques used. (7) Four-dimensional display—an extension of the three-dimensional uniphasic surface/volume display to multiple cardiac phases. (8) Three- and four-dimensional stereo displays.

Results: Precise volumetric location of aortic segments was easily performed from the MRI data sets with the virtual reality methods, facilitating efficient display of pathologic anatomy for review.

Conclusion: Advanced computer virtual reality techniques can abrogate many of the limitations of traditional methods of pediatric aortic evaluation.

MRI-Derived Left Ventricular Function Parameters and Mass in Healthy Young Adults: Relation with Gender and Body Size

J.T. Marcus,[1] L.K. DeWaal,[1] M.J.W. Götte,[2] R.J. van der Geest,[3] R.M. Heethaar,[1] A.C. Van Rossum.[2] [1]*Dept. of Clinical Physics and Informatics,* [2]*Dept. of Cardiology, Institute for Cardiovascular Research ICaR-VU, Vrije Universiteit Amsterdam, The Netherlands;* [3]*Dept. of Radiology, Leiden University Medical Centre, Leiden, The Netherlands*

Purpose: To obtain normal values of left ventricular (LV) end-diastolic volume (EDV), stroke volume (SV), cardiac output (CO), and LV mass, in relation to gender, weight (W), length (L), and body surface area (BSA).

Methods: Sixty-one healthy volunteers (32 male, 22.4 ± 2.2 years) were examined, weight was 70.9 ± 12.1 kg, length was 1.78 ± 0.09 m, BSA was 1.88 ± 0.19 m^2. Segmented k-space breathhold cine MRI was used to obtain a stack of parallel short-axis images, from which LV volumes and end-diastolic mass were derived by slice summation.

Results: After indexing for W, L, or BSA, the gender differences were still significant. Thus, separate regression analyses for males and females were performed. EDV, SV, CO, and EDM correlated significantly with W, L, and BSA, both in males and in females. Length or BSA was a better predictor for LV parameters than weight. Linear regression equations of EDV(ml) vs. L(m) were for males: EDV = 278 × L − 357 and for females: EDV = 219 × L − 263 (Fig. 1). Equations of SV(ml) vs. L were for males: SV = 182 × L − 224 and for females: SV = 128 × L − 136. Equations of LV mass(g) vs. L were for males: mass = 162 × L − 161 and for females: mass = 95.1 × L − 68.

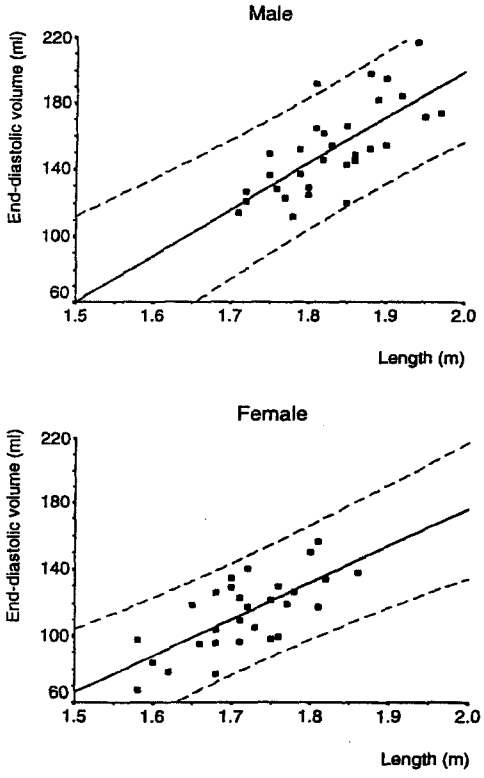

Figure 1. Scatter plots with regression lines of EDV vs. length, separately for males and females. The dashed lines denote the 95% prediction intervals.

Conclusion: Normal values for LV parameters are given in relation to weight, length, and BSA. Separate regression coefficients for males and females have been calculated by regression analysis. These normal values serve to obtain more accurate reference values for a patient with given weight and length and thus to improve the differentiation between normal and abnormal LV parameters.

MRI-Compatible Gating System for Cardiac Imaging

James J. Pilla, Aaron S. Blom, Lawrence Dougherty, Qing Yuan, Himanshu J. Patel, Michael A. Acker, Leon Axel. *University of Pennsylvania Medical Center, Philadelphia, PA*

A development allowing cardiac MR imaging under various conditions such as skeletal myoplasty and cardiac pacing, for example, would prove invaluable in helping to elucidate the ways in which these conditions alter cardiac function. Such a development has previously been unattainable due to the intense static and gradient magnet fields and RF interference associated with today's clinical MR systems. We present a system that we designed and tested, which allowed us to perform cardiac MR studies in a canine model of cardiomyoplasty (CMP) in a clinical MR system at 1.5 T.

Cardiomyoplasty is a surgical therapy for end-stage heart failure in which the patient's lattissimus dorsi muscle is wrapped around the heart and electrically stimulated to provide contractile assistance. The MR-compatible system designed to allow the study of CMP consists of a central control unit which provides the cardiac pacing, muscle stimulation, and timing control for the system. It also controls the ventilator and MR gating trigger. To minimize the blurring effect of respiration on cardiac imaging, the system triggers the scanner to acquire images only during the interval from end expiration to preinspiration. The cardiac pacing and muscle stimulation signals are optically isolated, and the outputs to the ventilator and MR trigger are RF filtered.

The system can provide muscle stimulation without the need for cardiac packing. This is accomplished by taking the signal from the scanner's physiologic acquisition computer, bandpass filtering to minimize noise and T-wave amplitude, and porting it into the control unit. The ECG trigger system also has a blanking circuit which senses the QRS and eliminates erroneous triggering which could occur while imaging during muscle stimulation.

The MR-compatible pressure system consists of an RF-shielded transducer control unit connected to the scanner's penetration panel with shielded wire. The transducer signal is RF filtered and connected to an amplifier. The pressure signal is monitored and stored using custom-written data acquisition software. Pressure-volume loops can be generated by combining the acquired pressure with the volumes obtained from the MR images.

The development of this system has afforded us the ability to use MR imaging to study a promising new therapy for end-stage heart failure. Further, this system can be utilized to assess the effect of other surgical therapies for heart failure such as ventricular reduction and mechanical assistance on cardiac function.

Subendo- and Subepicardial Gadophrin-2 and Blood Flow Distribution in Acute Infarctions

A. Zenovich,[1] A.M. Mansoor,[1] S.P. Gurchumelidze,[1] Y. Huang,[1] M. Jerosch-Herold,[1] J.R. Dutcher,[1] H.J. Weinmann,[2] A.E. Stillman,[1] N.M. Wilke.[1] [1]*Minneapolis, MN;* [2]*Berlin, Germany*

Novel necrosis-avid MR contrast agent bis-gadolinium mesoporphyrin (gadophrin-2) exhibited uniform enhancement at 10–24 hours after acute myocardial infarction (1). However, the signal effects to delineate

areas of acute myocardial infarction in its early distribution phase are unknown.

Methods: Obtuse branches of the left circumflex coronary artery were ligated in pigs (n = 5). Myocardial blood flow (MBF, ml/min/g) was measured with microspheres. Gadophrin-2 was injected (0.04 mmol/kg) and cine MR images and in vivo T1 measurements were performed at 3 hours postligation and contrast agent injection. T1 values were calculated as ratio R1 (infarcted)/R1 (normal myocardium). The infarcted areas enhanced with gadophrin-2 were compared with regional wall motion, MBF, and histochemical analysis with triphenyltetrazolium chloride (TTC).

Results: The infarcted areas revealed patchy TTC patterns with a residual MBF of 0.33 ± 0.14 ml/min/g. Cine MR showed hypokinesis of all infarcted segments. Infarcted areas displayed two distinct zones of contrast enhancement. A significant ($p < 0.01$) subepicardial enhancement (R1 ratio = 0.98 ± 0.1) with a residual MBF of 0.44 ± 0.2 ml/min/g was compared with a nonenhanced subendocardium (R1 ratio = 0.85 ± 0.03, $p < 0.01$) with MBF of 0.28 ± 0.2 ml/min/g. TTC-unstained areas were twice the size of the nonenhanced infarction core.

Conclusions: In the early distribution phase, gadophrin-2 shows a nonenhanced subendocardial infarction zone and a subepicardial hypoenhanced zone, stained red with TTC. This distribution pattern depends mainly on the different residual MBF in these two layers 3 hours postcontrast agent injection. For the first time, by contrast to any MR agent to date, the delineation of nonviable myocardium using gadophrin-2 suggests a specific flow- and time-dependent mechanism.

Reference

1. Marchal G, Ni Y, Herijers P, et al. Paramagnetic metalloporphyrins: infarct-avid contrast agents for diagnosis of acute myocardial infarctions. *Eur Radiol*, 1996; 6:2–6.

Detection of Mild and Moderate Coronary Stenoses: MRI Perfusion Reserve vs. Wall Thickening at Rest

N.M. Wilke, R.K. Grewal, S.P. Gurchumelidze, M. Jerosch-Herold, R. Wilson, A. Zenovich, A.E. Stillman. *Minneapolis, MN*

We hypothesized the possibility of detection of mild to moderate coronary stenoses using myocardial perfusion reserve and wall thickening as measured with MR.

Methods: We studied patients (n = 5) with angiographically proven 50–70% coronary artery stenoses. Two patients had lesions within the left anterior descending artery (LAD), two had lesions in left circumflex artery (LCx), and one had lesions of both LAD and LCx. Segmental myocardial function was quantitatively assessed by using modified centerline method (MASS 1.0). Myocardial perfusion at rest and stress (adenosine, 140 µg/kg/min) was quantitatively analyzed using MR first-pass imaging (gadolinium-DTPA, 0.025 mmol/kg). Perfusion reserve was defined as rest/stress flow. Twenty segments were studied corresponding to anterior, lateral, inferior, and septal walls of the heart. All target regions were supplied by vessels 50–70% stenosed, and the remote region had <50% stenoses.

Results: Wall thickening (%) at rest in remote regions appeared significantly higher than in ischemic zones (73.2 ± 15.0 vs. 34.8 ± 14.7, $p < 0.002$). The perfusion reserve was significantly lower in target zone than in the remote zones (1.32 ± 0.38 vs. 2.8 ± 0.39, $p < 0.005$). The decrease of wall thickening at rest in target region matched the decreased myocardial blood flow reserve at maximal hyperaemia in the same region ($p < 0.007$). Only segments with 60–70% stenoses were hypokinetic on cine MRI (Figure).

Conclusion: Myocardial perfusion reserve and cine MR appear sensitive to detect moderate stenoses while only the perfusion reserve demonstrates mild coronary stenoses. Therefore, MR perfusion may distinguish varying degrees of myocardial stunning and hibernation in patients with subcritical coronary artery stenoses.

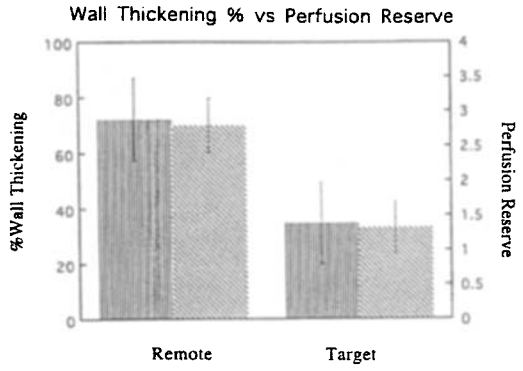

Noninvasive Estimation of Global and Regional Wall Stress in Aortic Insufficiency Before Aortic Valve Replacement

Pavlos Moustakidis, Giridhar Vedala, Randall Scheri, Brian Cupps, Michael Moulton, Douglas Fishman, Nicholas Kouchoukos, Victor Dávila-Román, Michael Pasque. *St. Louis, MO*

Sensitive indices of left ventricular (LV) systolic performance are necessary for optimal clinical management of asymptomatic patients with aortic insufficiency (AI). Myocardial wall stress determines cardiac remodeling under abnormal loading conditions. An accurate description of its global and regional distribution can improve our understanding of LV function in these patients.

Objectives: (1) Define sensitive noninvasive indices of ventricular systolic performance to assist the clinician in the evaluation of patients with AI and (2) quantify differences in instantaneous global and regional end-systolic LV stress (ESS) distribution between normal controls and patients.

Methods: Resting MRI was performed on 10 normal volunteers (age 32 ± 17) and 8 patients (age 40 ± 11, EF 58 ± 7%) with chronic AI and normal systolic function (determined by echocardiography and cardiac catheterization) who underwent aortic valve replacement within a month of the MRI. Finite element analysis (FEA) was employed to estimate global and regional ESS. Nonaxisymmetric models of the heart were constructed from MRI images and were loaded with pressures derived from linear interpolation of noninvasively obtained Millar carotid artery tracings calibrated using the brachial artery blood pressure cuff measurements (acquired during the MRI). Measurements were performed in four segments encompassing one midventricular short-axis slice.

Results: ESS was significantly higher in the AI patients globally (155,418 ± 27,956 dynes/cm^2 vs. 102,595 ± 24,774, $p < 0.001$) and regionally ($p < 0.001$ in all segments).

Conclusion: Global and regional ESS as determined by MRI and FEA may have considerable potential as a noninvasive clinically applicable index of LV function in AI patients.

Clinical Assessment of Hybrid Ordered Phase Encoding (HOPE) for Cine Imaging

J.M. Francis, P. Jhooti, D.J. Pennell. *London, UK*

Background: Cardiac imaging is prone to motion artifact, especially from respiration. Phase reordering methods have been developed to combat this and improve diagnostic image quality. HOPE has shown

to be a robust method in normal subjects. This study attempts to assess the clinical value of this method for cine imaging.

Method: Twelve patients were studied using gradient echo cines in the long axis with and without HOPE. Mean signal values in the myocardium and blood and mean noise signal inside and outside the phase encode artifact areas were obtained. Images were also scored for diagnostic quality from 1 (uninterpretable) to 9 (excellent).

Results:

		Phase Encode Noise		Nonphase Encode Noise	
	Score	CNR-ED	CNR-ES	CNR-ED	CNR-ES
Non-HOPE	4.9	2.0	1.7	4.2	3.1
HOPE	5.9	3.9	3.1	6.0	4.4
p	0.04	0.004	0.008	0.03	0.03

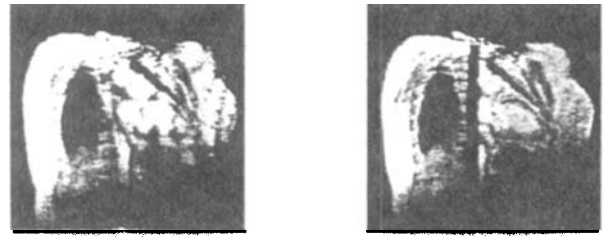

Diastolic frames from a gradient echo cine acquisition. Note the improvement over the conventional image (1) when HOPE is applied (2). The artifact from the navigator echo is clearly seen.

Conclusion: HOPE is a robust method of reducing respiration artifact and improving the diagnostic image quality in patients referred for cardiac imaging. It has been demonstrated to be most useful in the vertical long-axis projection which is particularly susceptible to respiratory artifact.

Reference

1. Jhooti P, et al. Hybrid ordered phase encoding (HOPE): an improved approach for respiratory artefact reduction. *JMRI*, 1998; 8:968–980.

Severity of Mitral Regurgitation Is Correlated with Left Atrial Size and Function, not Regurgitant Fraction

D. Gopalakrishnan, T.P. Kerwin, V. Dávila-Román, S.A. Wickline, C.H. Lorenz. *St. Louis, MO*

Few quantitative indices exist for grading severity of chronic mitral regurgitation. Our objective was to develop and evaluate MRI parameters of atrial function in addition to regurgitant fraction as measures of mitral regurgitation severity compared to qualitative grading by echocardiography.

Nineteen patients with chronic mitral regurgitation and nine healthy volunteers were studied. Doppler and 2D echocardiography were performed, and mitral regurgitation was graded by two blinded observers on a scale of 0–3: none, mild, moderate, severe. 3D MRI measurements of the left atrium were made throughout the cardiac cycle. Left atrial (LA) cyclic volume change was determined as the difference between the maximal and minimal left atrial volumes in the cardiac cycle, normalized to body surface area. Regurgitant fraction (RF) was determined as the difference between the mitral annular inflow volume and the forward stroke volume exiting the aorta using velocity encoded cine MRI and expressed as a fraction of the mitral inflow.

MRI-determined RF was higher in mitral regurgitation patients than in normals but did not discriminate among severity levels (p = n.s.). Both maximal LA volume and the LA cyclic volume change discriminated among severity levels ($p < 0.05$) (Figure).

Parameters of left atrial size and function provide better discrimination among levels of severity of mitral regurgitation than does regurgitant fraction.

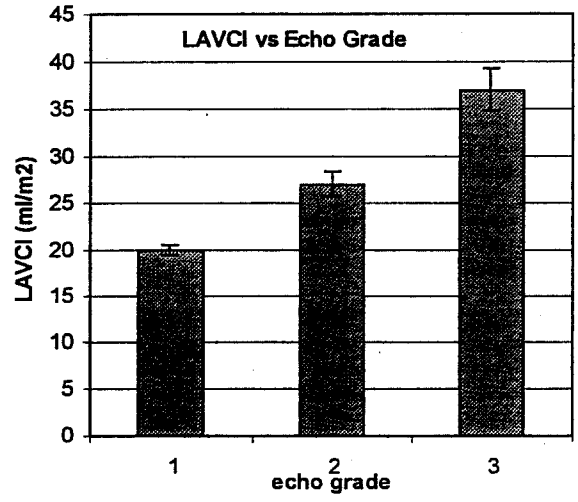

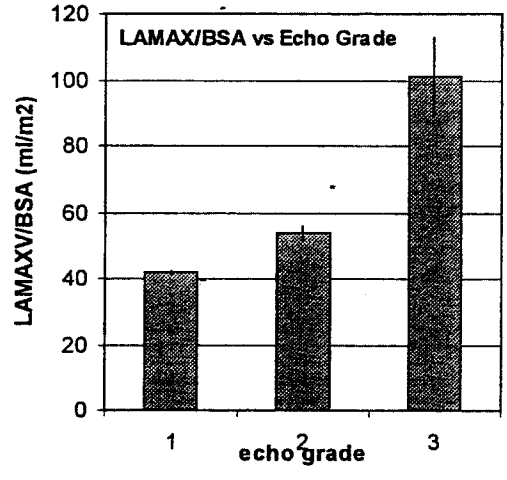

Double-Oblique Free-Breathing High-Resolution 3D Coronary MRA

M. Stuber, R.M. Botnar, D.K. Sodickson, P.G. Danias, K.V. Kissinger, W.J. Manning. *Boston, MA*

Objectives: To develop a new strategy for high-resolution 3D coronary magnetic resonance angiography (MRA) that takes advantage of the "natural" coordinate system defined by the anatomy of the native coronary arteries.

Background: For high-resolution 3D free-breathing coronary MRA, coverage of the coronary artery tree may be limited due to excessive measurement times associated with large volume acquisitions. The problems associated with nonisotropic voxel sizes also remain to be resolved. Planning the 3D volume along the major axis of the coronary vessels may help to overcome such limitations (1).

Figure 1. (a) Right coronary artery (RCA) of a healthy subject. In-plane resolution = 500 × 500 μm. (b) Coronary MRA of a patient with a 50% proximal RCA stenosis (arrow). (c) X-ray angiogram of the RCA of the same patient as displayed in b.

Methods: Fifteen healthy adult volunteers and seven patients with x-ray angiographically confirmed coronary artery disease underwent coronary MRA on a 1.5-T Philips Gyroscan ACS-NT system (Philips, Best, NL) equipped with a five-element cardiac synergy coil and an advanced coronary software package. Scout scanning was performed using an ultrafast navigator gated and corrected free-breathing 3D imaging sequence. For an accurate volume targeting of the high-resolution scans, a three-point planscan software tool (2) was applied to define the imaging plane of the left and right coronary arteries. For high-resolution 3D coronary MRA, a T2Prep (3,4), free-breathing navigator gated and corrected 3D imaging sequence was utilized (TR = 8.8 ms, TE = 2.4 ms, acquisition window = 70 ms) for the left and right coronary system (Fig. 1a). In-plane resolution was in the range of 0.5 × 0.5 to 0.7 × 1.0 mm with a reconstructed slice thickness of 1.5 mm.

Results: The average length of contiguously visualized left main coronary artery and left anterior descending coronary artery was 81.8 ± 13.9 mm in the healthy volunteers and 76.2 ± 16.5 mm in the patients (p = NS). For the right coronary artery, a total length of 111.7 ± 27.7 mm was found in the healthy volunteers and 79.3 ± 4.6 mm in the patients (p = NS). A good agreement of anatomy and pathology was found in all patients between x-ray angiography and coronary MRA as displayed in Fig. 1, b and c. Imaging planes for the left and right coronary systems were patient specific.

Conclusions: Double oblique submillimeter free-breathing coronary MRA allows depiction of extensive portions of the native coronary arteries with a high blood-muscle contrast while disadvantageous effects of anisotropic voxel size are minimized. The results obtained in patients suggest that the method has the potential to be applied in broader prospective multicenter studies where coronary MRA is compared with x-ray angiography.

References

1. Wielopolski PA, van Geuns RJ, de Feyter PJ, Oudkerk M. *Radiology,* 1998; 209:209–219.
2. Stuber M, Danias PG, de Becker J, Botnar RM, Kissinger KV, Manning WJ. (abstract) Proc. ISMRM, 1998; 3:1953.
3. Brittain JH, Hu BS, Wright GA, Meyer CH, Macovski A, Nishiimura DG. *Magn Reson Med,* 1995; 33:689–696.
4. Botnar RM, Stuber M, Kissinger KV, Danias PG, Manning WJ. (abstract) Proc ISMRM, 1998; 1:23.

Free-Breathing 3D Coronary MRA: The Impact of Navigator Position

M. Stuber, R.M. Botnar, P.G. Danias, K.V. Kissinger, W.J. Manning. *Boston, MA*

Purpose: In this study, we describe free-breathing submillimeter 3D coronary MRA in which we utilize a prospective real-time navigator correction. While many investigators have utilized a right hemidiaphragm navigator position, a location in close proximity to the major coronary arteries may have advantages. We objectively compare free-breathing coronary MRA data acquired from using different navigator locations.

Materials and Methods: Free-breathing 3D coronary MRA with real-time navigator gating and correction was implemented on a 1.5-T Philips Gyroscan ACS-NT system (Philips, Best, NL) equipped with an advanced coronary software package. Image data of the left (transverse) and right (sagittal oblique) coronary system were acquired in eight healthy subjects using a 2D selective navigator localized at the right hemidiaphragm (RHD) and at the anterior basal free wall of the left ventricle (LV) (Fig. 1a). An ECG gated T2Prep (1,2) fat-suppressed 3D TFE sequence (TE = 2.4 ms, TR = 7.4 ms, acquisition window = 60 ms) with an in-plane resolution of 0.7 × 1.0 mm was utilized for image acquisition. Contrast to noise and the delineation (vessel sharpness) of the left and right coronary arteries was quantified using a DeRiche algorithm implemented on a LINUX PC (3). The results from both navigator locations were objectively compared.

Results: Excellent contrast to noise and vessel delineation (Fig. 1b) was found in all cases for the left and right coronary arteries for both navigator locations. Contrast to noise in the images was independent of the utilized navigator position (p = NS). For mid- to distal portions of the coronary arteries, a RHD navigator results in a more distinct improvement of vessel delineation (54% vs. 60%, $p < 0.05$). There was a trend for vessel sharpness of the proximal native coronary arteries to be slightly enhanced utilizing a RHD navigator (53% vs. 58%, p = NS). Average scan efficiency was 55% and was not found to be navigator position dependent (p = NS).

Conclusions: Free-breathing submillimeter 3D coronary MRA has been successfully implemented together with real-time navigator technology. The present computer-assisted image analysis procedure allows for objective comparisons of coronary MRA data. Considering locally improved vessel definition and the easier setup for the localized navigator at the right hemidiaphragm, we conclude that the use of a diaphragmatic navigator is currently preferred.

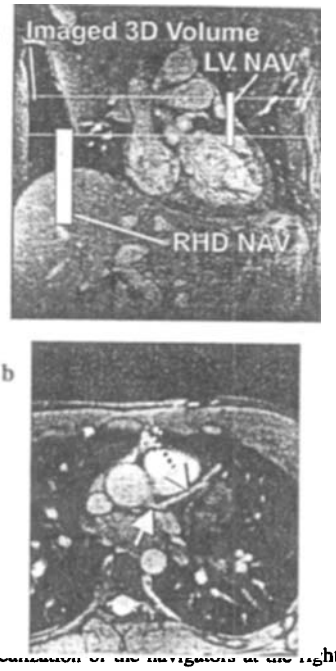

Figure 1. (a) [illegible] hemidiaphragm (RHD NAV) and at the anterior basal free wall of the left ventricle (LV NAV). (b) LM (solid arrow) and LAD (dotted arrow) of a healthy volunteer acquired with an LV navigator.

References

1. Brittain JH, Hu BS, Wright GA, Meyer CH, Macovski A, Nishimsura DG. Coronary angiography with magnetization-prepared T2 contrast. *Magn Reson Med,* 1995; 33:689–696.
2. Botnar RM, Stuber M, Kissinger KV, Danias PG, Manning WJ. T2 preparation prepulses for contrast enhancement in 3D-coronary MRA: implementation with real-time left ventricular navigator tracking. In: Proceedings of the 6th Annual Meeting of the International Society for Magnetic Resonance in Medicine. Sydney: International Society for Magnetic Resonance in Medicine, 1998; 1:23.
3. Deriche R. Fast algorithms for low-level vision. IEEE Trans., PAMI, 1990; 12:78–87.

Short- and Long-Term Safety of Magnetic Resonance Imaging Soon After Stenting for Acute Myocardial Infarction

Christopher M. Kramer, Walter J. Rogers, Sunil V. Mankad, Diana L. Pakstis, Diane Vido, Nathaniel Reichek. *Allegheny General Hospital, Pittsburgh, PA*

Purpose: The goal of our study was to evaluate the safety of magnetic resonance imaging in patients who undergo stent placement for treatment of acute myocardial infarction (AMI).

Methods: We studied 13 patients (12 male, ages 50 ± 13, peak creatine kinase, 2,685 ± 1,573 U/L) on day 3 ± 1 after stenting for AMI. Patients were studied in a Siemens Vision 1.5-T scanner as part of a study of post-AMI myocardial viability. Four stent types had been placed: multilink (ACS, $n = 8$), crown (Cordis, $n = 2$), GFX (AVE, $n = 2$), and Nirvana (Scimed, $n = 1$). The involved arteries were left anterior descending ($n = 6$), right coronary ($n = 5$), left circumflex ($n = 1$), and ramus intermedius ($n = 1$). Imaging included gradient echo cine, breathhold gradient echo tagging at baseline and after 5 and 10 μg/kg/min dobutamine, contrast enhanced inversion recovery, and breathhold fat-suppressed coronary angiography.

Results: There were no adverse events during the MRI. All patients tolerated the procedure well. Patients have been followed clinically for a mean of 5 ± 2 months. Three patients underwent repeat angiography for clinical indications at an average of 3 months post-MI. One patient with stent placement to the left circumflex had in-stent restenosis at 6 months and had repeat PTCA and stenting. The stents from the remaining two patients were widely patent.

Conclusion: MR imaging of patients early after stenting for acute MI is safe. Recent stent placement, even in the setting of acute MI, should not be considered a contraindication to MRI. Further experience and long-term follow-up will be necessary to exclude any effect on the rate of restenosis.

Differences Between Normal Subjects and Patients with Coronary Artery Disease for MR Coronary Angiography Respiratory Suppression Techniques

A.M. Taylor, J. Keegan, P. Jhooti, P.D. Gatehouse, D.N. Firmin, D.J. Pennell. *London, UK*

A comparison between three magnetic resonance coronary angiography (MRCA) respiratory motion suppression techniques was performed for both normal subjects and patients with coronary artery disease (CAD). MRCA images of the right coronary artery were acquired in 17 normal subjects and 15 patients with CAD, using conventional breathhold MRCA, navigator echo (NE)-guided breathhold MRCA (LED feedback), and NE-gated MRCA during free respiration. Image quality, diaphragm registration, and the total acquisition time were assessed. Overall, there was poor diaphragm registration for conventional breathholding compared with free respiration ($p < 0.001$). CAD patients found it significantly more difficult to attain the same diaphragm position over multiple breathholds than normal subjects ($p = 0.02$). All normal subjects but only 3 of the 15 CAD patients were able to perform the LED feedback technique ($p < 0.001$). For normal subjects, image quality was similar between the three respiratory suppression techniques ($p = 0.3$), whereas for CAD patients there was an improvement in image quality for images acquired during free respiration (breathhold vs. free respiration, $p < 0.01$). There was no significant difference in the total acquisition times between the breathhold and free respiration techniques ($p = 0.2$). There are substantial differences in the effectiveness of MRCA respiratory suppression techniques between normal subjects and CAD patients. In patients, only NE-gated MRCA performed well, requiring minimal cooperation with no increase in total acquisition time. Validation of NE-MRCA techniques should always be performed in patients and normal subjects to ensure correct evaluation of the technique for the target population.

Coronary Artery Imaging in Congenital Heart Disease: Complementary Role of Magnetic Resonance and X-Ray Coronary Angiography

A.M. Taylor, S.A. Thorne, M.B. Rubens, P. Jhooti, J. Keegan, P.D. Gatehouse, F. Wiesmann, J. Somerville, D.J. Pennell. *London, UK*

There is a high incidence of anomalous coronary arteries in subjects with congenital heart disease. These abnormalities may be responsible for myocardial ischemia and sudden death and may also be damaged during surgical intervention. It can be difficult to define the proximal course of anomalous coronary arteries with conventional x-ray coronary angiography (1,2). MRCA has been shown to be useful for assessing the 3D relationship between the coronary arteries and the great vessels

in subjects with normal cardiac morphology (3–5) but has not been performed in patients with congenital heart disease. Twenty-five adults with a variety of congenital heart abnormalities were studied. X-ray coronary angiography and respiratory-gated MRCA were performed in all subjects. Coronary artery origin and proximal course were assessed for each imaging modality by separate blinded investigators. Images were then compared and a consensus diagnosis reached. With the consensus reading of both MR and x-ray coronary angiography, it was possible to identify the origin and course of the proximal coronary arteries in all 25 subjects, 18 with coronary anomalies and 9 with normal coronaries. Respiratory-gated MRCA had a sensitivity of 92% and specificity of 100% for detecting abnormal coronary arteries. MRCA was superior to conventional x-ray angiography for defining the proximal course of the coronary arteries ($p < 0.02$), identifying six clinically significant coronary anomalies. For assessing coronary artery anatomy in subjects with congenital heart disease, x-ray coronary angiography should be combined with MRCA. MRCA provides correct spatial relationships, whereas x-ray angiography provides an overall view of coronary tree dynamic flow. Furthermore, respiratory-gated MRCA can be performed without breathholding and only limited subject cooperation.

References
1. Ishikawa T, et al. *Am J Cardiol,* 1985; 55:770–776.
2. Serota H, et al. *Am J Cardiol,* 1990; 65:891–898.
3. McConnell MV, et al. *Circulation,* 1995; 92:3158–162.
4. Post JC, et al. *Circulation,* 1995; 92:3163–171.
5. Vliegen HW, et al. *Am J Cardiol,* 1997; 79:773–776.

High-Resolution Ex Vivo MR Imaging of In Situ Coronary Wall Components in a Porcine Model of Atherosclerosis

S.G. Worthley, G. Helft, Z.A. Fayad, J.I. Osende, J.T. Fallon, G. Aguinaldo, M. Roque, M. Shinnar, V. Fuster, J.J. Badimon. *New York, NY*

Atherosclerotic plaque composition plays a critical role in plaque rupture and subsequent acute thrombosis. Thus, the identification of atherosclerotic plaque composition will have significant clinical implications. MR imaging has been shown to be effective in identifying plaque components. Our aim has been the MR characterization of in situ coronary artery plaques in an experimental model of coronary atherosclerosis.

Yucatan miniswine ($n = 4$) underwent balloon angioplasty to the LAD and LCx arteries (the RCA was used as a control) and fed an atherogenic diet for 6 months. At sacrifice the hearts were perfusion fixed and removed from the thoracic cavity. MR imaging of the coronary arteries was acquired from the intact heart with a 3-inch surface coil in a 1.5-T magnet (GE). Gradient echo sequences were used to locate the coronary arteries, and then high-resolution fast spin echo imaging was performed. T1 (TR/TE 600/13 msec), T2 (TR/TE 2300/55 msec), and proton density weighted (PDW) (TR/TE 2300/19 msec) images were obtained. In-plane resolution was 156 × 156 microns; slice thickness was 2 mm with four signal averages. The MR images of coronary arteries were matched with histology ($n = 54$) and computer-assisted morphometry performed. Atherosclerotic plaque was easily discernable from the nonatherosclerotic vessel wall and mean wall thickness on MR imaging was highly correlated ($p < 0.0001$) with histology ($r = 0.94$, slope 0.81). Fibrocellular plaques were accurately characterized by MRI.

Thus, we are able to accurately identify atherosclerotic plaque and quantify coronary artery wall measurements, despite the curved nature of the vessels. With cardiac gating and respiratory motion suppression, it should be possible to extend these techniques to in vivo coronary wall imaging and plaque characterization.

Does Curvature Predict Differential Septal Function by MRI Tagging Strain Analysis in Patients with Left Ventricular Hypertrophy?

R.W.W. Biederman,[1] E. Kortright,[1] M. Doyle,[1] A.A. Young,[2] S. Thrupp,[2] G.M. Pohost for the LIFE Study Investigators.[1]
[1]*Birmingham, AL;* [2]*Auckland, New Zealand*

Introduction: We previously showed in patients with left ventricular hypertrophy (LVH) and preserved ejection performance that the septal wall has decreased circumferential and radial strain (ε) by MRI tagging techniques. This occurred in a setting where, despite similar shortening fraction (SF), end-systolic stress (ESS), and wall thickness, the posterior wall, taken as a reference point, had 2.5-fold greater circumferential strain ε than the septum. We postulated that depressed septal wall function may result from a flatter geometric curvature. Theoretically, low (flatter) curvature would predict large Laplacian stress, implying decreased myocardial function.

Methods: Nineteen patients with ECG criteria for LVH from the LIFE study and eight normals underwent conventional and tagged MRI to measure circumferential and radial ε. Respiratory and cardiac gating with orthogonal imaging with tag spacing: 7 mm, interslice distance: 10 mm, and matrix: 256 × 256 were performed. Curvature was calculated from short axis (SA) and long axis (LA) (tagged), defined as the inverse of the radius of a circular arc fitted manually to each region of interest. An index of dynamic myocardial geometry, fractional change in curvature from diastole to systole (ΔC), was defined as $(C_d - C_s)/C_d$, expressed as a percentage.

Results: LV mass ($g/m^{2.7}$) in patients vs. normals was 66 ± 23 vs. 28 ± 6 ($p \leq 0.001$), while SF was comparable between groups (30 ± 5% vs. 33 ± 3%). ESS was similar (175 ± 22 vs. 146 ± 28 g/cm^2).

SA mean curvatures were uniformly lower in patients than in controls for both septum and free wall, although only the septum at end systole reached statistical significance ($p < 0.031$). In patients, ΔC was significantly lower in the septum than the free wall in both SA (21%, $p = 0.024$) and LA (−54%, $p = 0.006$). This suggests a functional importance to initial diastolic curvature as it predicts altered end-systolic curvature, LA preferentially over SA. However, despite both a flatter septum and altered ΔC, there was no significant correlation between either depressed circumferential and radial strain ε and the curvature.

In the controls, ΔC was not significantly different between septum and the posterior wall. Despite a trend toward a rounder septum, again there was no strong correlation between normal circumferential and radial strains ε and the curvature.

Conclusions: In patients with LVH, MRI tagging analysis yields nearly 2.5-fold depressed septal circumferential strain and also a tendency for septal radial strain ε to be depressed compared to the posterior wall. Although in patients mean septal curvature was uniformly less than the posterior wall and dynamic myocardial geometry would suggest reduced septal strain, curvature does not appear to discriminate regional myocardial function by MRI strain analysis.

Variability and Reproducibility of 2D and 3D Calculations of Regional Left Ventricle Wall Thickness and Wall Motion in Short Axis MR Images

T. Ibrahim,[1] S. Nekolla,[1] F. Roder,[1] R.J. van der Geest,[2] J.H.C. Reiber,[2] M. Schwaiger.[1] [1]*Nuklearmedizinische Klinik, Klinikum Rechts der Isar, TU München, München, Germany;* [2]*Department of Radiology, Leiden University Medical Center, Leiden, The Netherlands*

Introduction: Quantitative assessment of regional left ventricular wall parameters is important in the evaluation of various heart diseases such as coronary artery disease or cardiomyopathy. The purpose of this study

was to investigate the variability and reproducibility of left ventricular wall thickness and wall motion analysis by MR.

Methods: Short-axis, breathhold, ECG-gated, ultrafast gradient-echo-cine-images (Philips Gyroscan ACS NT, 1.5 T) were obtained in 24 healthy volunteers (9 females, 15 males) with 12 heart phases and five to eight slices (depending on heart size) excluding apex and valve plane. Images were acquired continuously with a slice thickness of 8 mm, TE 11 ms, 30° flip angle, and with a matrix size of 256 × 256. MR data were transferred to UNIX workstations. Endo- and epicardial contours were manually traced using MASS software (University Leiden) (1,2). Papillary muscles were carefully excluded. Based on these contours, end-diastolic and end-systolic wall thickness and wall motion were calculated in 4 (anterior, septal, inferior, lateral) and in 12 segments (6 basal and 6 mid) with a conventional 2D and a modified 3D centerline method, including information from slices above and below to correct for non perpendicular slicing.

Results: We obtained very homogenous results of wall thickness and wall motion parameters within the different regions of the heart, independent of size and location of the segments (Table 1). Calculations of smaller segments did not show significantly different values. The coefficient of variation was 14% in end-diastolic and end-systolic wall thickness and 22% in wall motion measurements. 3D calculation resulted in systematically and significantly smaller values of regional wall thickness than 2D methods ($p < 0.05$, t-test), but the absolute difference was small (less than 1.5 mm). Intraobserver variability analysis for wall thickness ($r > 0.999$, slope = 0.92) and wall motion ($r > 0.999$, slope = 0.96) yielded excellent results.

Table 1. Wall Thickness and Wall Motion in Four Different Segments (coefficient of variance).

	Anterior	Septal	Inferior	Lateral	Mean
ED-2D (mm)	8.1 (13.7%)	8.5 (14.1%)	8.1 (12.5%)	8.1 (12.9%)	8.2 (13.3%)
ED-3D (mm)	7.6 (14.8%)	8.2 (15.4%)	7.8 (12.8%)	7.6 (13.2%)	7.8 (14.1%)
ES-2D (mm)	12.6 (13.1%)	12.5 (13.0%)	12.4 (13.7%)	12.8 (13.6%)	12.6 (13.4%)
ES-3D (mm)	12.0 (13.4%)	12.1 (13.8%)	12.0 (13.7%)	12.2 (14.3%)	12.1 (13.8%)
Wall motion (mm)	7.9 (21.9%)	7.1 (22.5%)	7.7 (20.1%)	7.8 (21.5%)	7.6 (21.5%)

Conclusion: Assessment of global and regional wall thickness and wall motion from short axis MR studies can be realized with high reproducibility and low intraobserver variability and fluctuation in healthy volunteers by using 2D and 3D calculation. 2D calculation results in a slight overestimation of the apparent wall thickness compared to 3D. Reducing the size of the segments within reasonable limits did not increase the fluctuation; thus, a comparison to normal databases can be applied to detect small abnormal regions.

References

1. Buller VGM, van der Geest RJ, Kool MD, et al. Assessment of regional left ventricular wall parameters from short-axis MR imaging using a 3D extension to the improved centerline method. *Invest Radiol,* 1997; 32:529–539.

2. van der Geest RJ, de Roos A, van der Wall EE, Reiber JHC. Quantitative analysis of cardiovascular MR images. *Int J Card Imag,* 1997; 13:247–258.

Transmyocardial Laser Revascularization (TMLR) Prevents the Onset of Ischemia Demonstrated by Quantitative Segmental Wall Motion Analysis

J. Dutcher,[1] Y. Huang,[1] Y. Wang,[1] M. Jerosch-Herold,[1] M. Unress,[1] C. Classen,[1] N. Wilke,[1] M. Mirhoseini,[2] M. Cayton,[2] S. Wann.[2]
[1]*Minneapolis, MN;* [2]*Milwaukee, WI*

This study evaluated the hypotheses that TMLR may improve the segmental function of acutely ischemic myocardium and that cardiac MRI can accurately assess myocardial wall thickening.

Methods: Regional wall thickening (RWT) was assessed with MRI in three groups of pigs (n = 23, 27–30 kg). Group I was a normal control (n = 6). Group II had proximal left circumflex (LCx) ligation (n = 7). Group III received channels with an 850-W laser to the left ventricular (LV) lateral wall (LT) followed, 10 minutes later, by LCx ligation (n = 10). Closed-chest Cine MRI was obtained 2 hours after LCx ligation at 1.5 T (Siemens). RWT analysis was conducted by two blinded observers using the centerline method. The myocardium was divided into three segments (anterior, lateral, and septal). Normalized RWT was calculated by dividing LT percent thickening by the septal wall percent thickening.

Results: LT thickening in group III (19 ± 11%) was significantly greater than group II (−5 ± 11%, $p < 0.001$) but less than the control group (79 ± 17%, $p < 0.001$). Anterior wall thickening in group III (52 ± 23%) was not significantly different than group II (35 ± 11%, $p > 0.05$) or the control (68 ± 20%, $p > 0.05$), but group II was significantly worse than the control group ($p < 0.05$). There was no significant difference in RWT for any groups in the septal wall ($p > 0.05$). Normalized RWT in group III (0.8 ± 0.9) was significantly greater than group II (−0.1 ± 0.3, $p < 0.05$) but not significantly different than the control group (1.4 ± 0.3, $p > 0.05$).

Conclusion: For the first time, cardiac MRI was used to demonstrate a cardioprotective role of TMLR before LCx ligation. In summary, TMLR preserves regional LV contractile function after acute myocardial damage.

MRI and TT-99M Sestamibi Gated SPECT for Detection of Myocardial Viability

D.L. Kraitchman, I.I. Oznur, E.R. McVeigh, B.B. Chin. *Baltimore, MD*

Differentiating subendocardial infarction from myocardial stunning is important for determining prognosis after revascularization. Thus, the purpose of this study was to examine myocardial function and perfusion determined from MRI and SPECT in canine models of myocardial infarction (MI) and stunning.

Ten animals were studied with 50% as normal controls. The remaining dogs were subjected to a closed-chest LAD occlusion of either 20-minutes or 90-minutes duration followed by reperfusion to cause myocardial stunning or nontransmural MI, respectively. Tagged MRI (1,2) was performed on a 1.5-T scanner (General Electric) at rest and during stress (5 μg/kg/min dobutamine) using a fast breathhold, segmented k-space, ECG gated gradient echo acquisition. Contrast-enhanced MRI was performed after either intracoronary injection of gadophrin-2 (Schering AG) in MI dogs or intraventricular injection of Gd-DTPA (Berlex) in stunned dogs. After MRI, 0.75–1.0 mCi/kg sestamibi was injected. Rest and stress gated SPECT was performed on a three-detector system (Trionix). Regional myocardial blood flow was determined using standard microsphere techniques. TTC staining delineated viable myocardium. Radial strain (i.e., wall thickening) was determined from tagged MRI and compared to systolic wall thickening ([ES thickness − ED thickness]/ES thickness) determined from SPECT. Perfusion abnormalities were determined based on hyperenhancing regions in MI dogs or signal intensity time curves in stunned dogs. Defect severity on SPECT was quantified from bull's-eye plots.

Anterior apical wall thickening at rest in MI and stunned dogs was reduced relative to normal dogs as determined from both MRI and SPECT (ANOVA, $p < 0.001$). In addition, the region of wall motion abnormalities was larger than the infarct area based on TTC. Both MRI and SPECT showed improved wall thickening in the anterior apex with stress in both stunned and MI dogs. However, anterior apical endocardial and midwall radial strain determined by MRI, while improved in the infarct dogs, was still abnormal ($p < 0.05$). Only one MI dog was hypokinetic with stress by SPECT; all stunned animals showed greater improvement in wall thickening than MI dogs (11% vs. 33% improve-

ment). Mild to moderate defects were present in the anterior apex of both MI and stunned dogs by SPECT. No perfusion defect was present in the stunned dogs based on contrast-enhanced MRI; myocardial enhancement in MI dogs at MRI was in agreement with TTC nonstaining regions ($y = 1.028x + 0.272$, $r = 0.983$).

Nontransmural infarctions and myocardial stunning, which produce similar defects at SPECT, can be differentiated by greater improvements in wall thickening in stunned tissue with stress. Transmural evaluation of radial strain using tagged MRI demonstrates abnormal wall thickening during stress in infarcted tissue but normal thickening in stunned tissue. Contrast-enhanced MRI clearly delineates infarcted from stunned. Thus, MRI shows promise for differentiating subendocardial infarction from stunned myocardium with a higher spatial accuracy.

References

1. Zerhouni EA, Parrish DM, Rogers WL, et al. Human heart: tagging with MR imaging—a method for noninvasive assessment of myocardial motion. *Radiology,* 1988; 169:59–63.
2. Axel L, Dougherty L. MR imaging of motion with spatial modulation of magnetization. *Radiology,* 1989; 171:841–845.

Reproducibility of Fast Acquisition CMR Sequences for Left Ventricular Function in Patients

N.G. Bellenger, J.M. Francis, L.C. Davies, D.J. Pennell. *London, UK*

Background: The assessment of volume, mass, and function is the cornerstone of noninvasive cardiac imaging. CMR is now considered to be the gold standard, but its use has been limited by long acquisition times. Faster segmented k-space gradient-echo cine techniques have now made CMR more clinically acceptable, but there have been few studies other than in the normal population. We assessed the reproducibility of a fast low-angle shot sequence (FLASH) in the normal population and in patients with dilated cardiomyopathy and concentric hypertrophy.

Method: Twenty patients with normal hearts, dilated cardiomyopathy, and concentric hypertrophy following cardiac transplantation underwent FLASH CMR to generate a stack of short-axis breathhold cine slices encompassing the entire left ventricle. Volumes, mass, and ejection fraction was derived from endocardial and epicardial tracings. Images were analyzed, in a blinded manner, twice by one observer and once by a second observer. The normal volunteers underwent two separate scans. The intraobserver, interobserver, and interstudy reproducibility was assessed (Table 1).

Results: CMR was well tolerated and total imaging time was 16 minutes.

Table 1

	Intraobserver			Interobserver			Interstudy
	N	DCM	Tx	*N*	DCM	Tx	*N*
Absolute mean difference ± SD							
EF (%)	−2.0 ± 2.4	−0.2 ± 2.3	−2.0 ± 3.0	−1.3 ± 2.9	−2.1 × 4.3	−2.5 ± 1.7	−0.9 ± 2.9
Mass (g)	1.1 ± 3.9	2.7 ± 5.2	−6.6 ± 9.0	1.3 ± 8.5	−4.0 ± 9.0	6.9 ± 11	−2.1 ± 7.7
% Variability							
EF (%)	3.3	5.6	4.1	3.9	13	2.4	6.1
Mass (%)	2.4	2.5	4.6	5.4	4.8	5.1	4.7

Conclusion: Faster more clinically acceptable imaging sequences retain good reproducibility in patients with abnormal hearts compared with normals.

Detection of Regions of Myocardial Infarction in Pigs: Higher Sensitivity and Specificity Using 3D Velocity-Encoded Cine MR Imaging Compared to Wall Thickening

R.J. van der Geest, L.J.M. Kroft, H.W.M. Kayser, E.E. van der Wall, A. de Roos, J.H.C. Reiber. *Leiden, The Netherlands*

Myocardial infarction is associated with systolic and diastolic function abnormalities. MR velocity mapping techniques may be used to assess the three-dimensional myocardial velocity throughout the complete cardiac cycle at high temporal and spatial resolution. The purpose of this study was to assess the value of three-dimensional velocity encoded cine MRI (3D-VEC-MRI) for the detection of regions of myocardial infarction.

In six pigs with surgically induced myocardial infarction, 3D-VEC-MRI was performed in a midventricular short-axis slice using velocity encoding in three orthogonal directions with a VENC of 30 cm/s. Endocardial and epicardial contours were traced at end diastole, end systole, and the time point of peak filling rate (TPFR). Using the centerline method, 100 wall thickness centerline chords were constructed perpendicular to the myocardium to obtain wall thickness measurements and a division of the myocardium into 100 segments. At TPFR, for each chord the average radial velocity was obtained. In addition, end-systolic wall thickening was calculated. As an independent gold standard, pathologic examination was performed to assess for each individual chord whether it corresponded to a region of normal or infarcted myocardium.

The size of myocardial infarction was 19 ± 20 chords. The figure shows an example of in-plane velocity vectors at TPFR demonstrating lower velocities in the anterior region, corresponding to the region of myocardial infarction in the PA image. Radial myocardial velocity at TPFR was 5.0 ± 3.2 cm/s in normal versus 0.88 ± 1.7 cm/s in regions of myocardial infarction ($p < 0.001$). Wall thickening was 34 ± 19% in normal versus 17 ± 19% in infarcted areas ($p < 0.001$). Only a poor correlation was found between radial myocardial velocity at TPFR and end-systolic wall thickening ($r = 0.33$). Radial velocity at TPFR showed a higher sensitivity (84%) and specificity (85%) than end-systolic wall thickening (sens 73%, spec 70%) for the detection of infarcted regions.

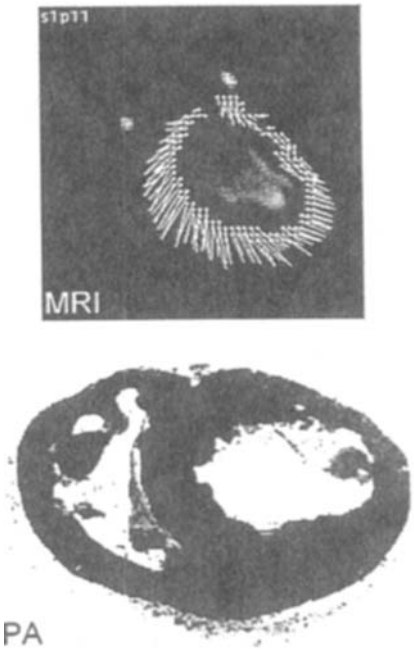

Figure 1

In conclusion, 3D-VEC-MRI allows detection of regions of myocardial infarction in pigs. The sensitivity and specificity of this new technique are higher than for end-systolic wall thickening. Further study is required to assess the value of this technique in humans.

Visual and Parametric Map Analysis of Adenosine Stress Echo Planar Spin Echo Myocardial Perfusion Imaging at 0.5 T: A Comparison with Radionuclide SPECT and Coronary Angiography

J.R. Panting,[1] P.D. Gatehouse,[1] G.Z. Yang,[1] D.N. Firmin,[1] M. Jerosch-Herold,[2] N. Wilke,[2] D.J. Pennell.[1] [1]*London, UK;* [2]*Minneapolis, MN*

Purpose: We describe the results of qualitative visual and semiquantitative parametric map analysis of single-slice myocardial perfusion studies in patients with ischemic heart disease to test the feasibility of using echo planar spin echo imaging (EPI) for detecting ischemia.

Methods: We studied 26 patients with coronary artery disease within a mean of 2 months of abnormal adenosine stress thallium scans. Of these, 21 also had conventional x-ray angiography within a mean of 7 months of the MR scan. Scanning was performed on a mobile in-house designed 0.5-T scanner. Single-shot, inversion recovery, spin echo EPI was used to study the first pass of gadolinium-DTPA at rest and during 140 μg/kg/min adenosine. The images were analyzed by visual assessment of the contrast wash-in and by parametric maps of time to peak, peak intensity, and slope of contrast wash-in.

Results: At rest, there were significantly more abnormal MR segments detected by visual, peak, and slope parametric analysis than thallium ($p < 0.02$). During stress, there was no significant difference (Tables 1 and 2). Time to peak maps showed significantly fewer abnormal segments during stress ($p < 0.003$) but no significant difference at rest. In 12 patients the parametric maps were easier to interpret than the visual analysis ($p < 0.04$). Only in three cases were the parametric maps less easy to interpret.

Table 1. Sensitivity and Specificity of MR Analysis Methods to Thallium by Coronary Territory

	Rest				Stress			
	Visual	Time	Peak	Slope	Visual	Time	Peak	Slope
Sensitivity	80	53	87	80	82	49	77	79
Specificity	65	70	59	59	92	69	85	85

Table 2. Sensitivity and Specificity to Coronary Angiography by Coronary Territory

		Magnetic Resonance			
	Thallium	Visual	Time	Peak	Slope
Sensitivity	91	83	60	74	71
Specificity	43	57	43	57	57

Conclusions: The overall diagnostic performance of MR and thallium is similar. Perfusion abnormalities at rest by MR are larger than with thallium, but this difference is less marked with stress. Parametric mapping is useful but can be limited by artifacts which can be more easily discounted on the visual analysis of the cines, suggesting both need to be reviewed for diagnosis.

Automated Magnetic Resonance Imaging Tag Tracking Algorithm for Regional Wall Motion Analysis

N.J. Corron,[1] H.E. Schonrock,[1] J.R. Amos,[1] R.W.W. Biederman,[2] A. Fuisz,[2] M. Doyle,[2] E. Kortright,[2] S.M. Gilbert,[1] G.M. Pohost.[2] [1]*Huntsville, AL;* [2]*Birmingham, AL*

Background: Quantification of regional wall motion is possible with cardiac MRI (CMRI) by means of a grid pattern produced by RF tagging and has numerous potential clinical applications. However, such tagging analysis is currently cumbersome and time-consuming, requiring considerable manual intervention. We have developed an automated tag-tracking algorithm, that we have named DynaTag, to enhance the clinical utility of tagging.

Method: DynaTag uses correlative image processing techniques to fully automate tag identification and location. The anticipated nearest neighbor algorithm (ANNA) is implemented to track tags in successive MRI frames using a relaxed grid and quantify motion within images. This novel tracking algorithm eliminates the cumbersome manual approach that has limited the utility of the technique in previous applications. Using cluster analysis, grid intersections are used to intelligently segment the image and highlight regions which are identified with essentially no user intervention. Localized heart muscle evaluation is performed quickly and automatically and the results are effectively generated in nearly real time. The approach output can then be supplemented with quantitative muscle stress and deformation estimates. Such estimates would be an advancement in our ability to assess regional and transmural LV performance. A software implementation has been developed using MATLAB for both PC and UNIX workstations.

Conclusions: DynaTag requires minimal user intervention and provides an automated method for the analysis of regional wall dynamics with tagging, thus enhancing the clinical utility of CMRI.

Multishot (Segmented) EPI for Evaluating Cardiac Function in Patients with Severe Coronary Artery Disease: Experience in 50 Exams

J.N. Oshinski, G.P. Chatimavroudis, R. Muthupillai, R.I. Pettigrew. *Atlanta, GA*

Purpose: For MRI to become a modality of choice for evaluating patients with ischemic heart disease, a rapid and robust method of assessing ventricular function must be developed. The aim of this study was to qualitatively and quantitatively examine the reliability and image quality of multishot EPI for evaluation of left ventricular function in 50 exams.

Methods: All patients had severe CAD as determined by coronary angiography. All patients had undergone a previous intervention (either bypass graft surgery or angioplasty) and were not candidates for further surgical treatment. The EPI sequence collected 16 cardiac phases with an image resolution of 1.4 × 1.4 × 8 mm (9 k-lines per excitation, α = 40–60°, Teff = 11, TR = 24). A five-element phased-array coil was employed. The breathhold length varied from 10–14 seconds per slice, depending on heart rate. In each patient, single-slice images were obtained in the vertical long axis and the horizontal long axis. Eight to ten slices were obtained in the short-axis view for calculation of ejection fraction. Images were qualitatively evaluated by rating them on a scale of 1–5 (1 = poor, 5 = excellent) for image quality and artifacts by an experienced reviewer. Images were quantitatively evaluated by determined contrast-to-noise ratio (CNR) between the blood pool and the myocardium at end systole and end diastole. A "successful" image had a rating of at least 3 on the 1–5 scale and had a CNR of at least 7.0. Reliability was defined as the percentage of "successful" images divided by the total number of images.

Results: Ejection fraction was determined, and regional wall motion was evaluated successfully in all patients. Reliability of the segmented

multishot EPI technique was 92%. Average rating of the qualitative review was 3.6. Average CNR was 11.3.

Conclusion: Multishot EPI is a rapid and robust method of evaluating ventricular function in patients with CAD. The method has a reliability of 92% in patients with severe CAD.

Establishment and Performance of Magnetic Resonance Cardiac Function Clinic

N.G. Bellenger, J.M. Francis, L.C. Davies, A.J.S. Coats, D.J. Pennell. *London, UK*

Background: The accuracy and reproducibility of ventricular volume, mass, and function by cardiac magnetic resonance (CMR) is well established in the normal population. We assessed the reproducibility of a rapid acquisition technique in heart failure patients attending a same day cardiology outpatient clinic.

Methods: Fifty-eight patients attended the CMR function clinic on the same day as their cardiology outpatient appointment. A stack of short-axis cines encompassing the entire left ventricles were acquired on a 1.5-T scanner by a fast low-angle shot (FLASH) breathhold technique. The total imaging time was 17 minutes. The images were analyzed immediately and the results sent to the outpatient clinic.

Results: Scanning was well tolerated by all patients. The reproducibility was as follows:

	Intraobserver	Interobserver	Interstudy
Absolute mean difference in EF ± SD	−0.2 ± 2.3	2.1 ± 4.3	1.0 ± 2.9
% Variability	5.6	13	6.1

Many patients had already undergone a MUGA (47%), echo (50%), or both (40%). MUGA EF was closer to the CMR gold standard than echo but still significantly different. Echo EF was highly significantly different from MUGA. The mean CMR EF was 36%:

	CMR–MUGA	CMR–Echo	MUGA–Echo
Mean diff ± SD	4.6 ± 9.0	−6.6 ± 12.0	−12.6 ± 14.0
Limits (range)	−13.8 to 23 (37)	−29.9 to 16.7 (47)	−40.1 to 14.9 (55)
p	<0.02	<0.009	<0.001
% Variability	25	33	39

Mean difference in ejection fraction (absolute EF% units), limits of agreement.

Conclusion: CMR can provide a rapid, accurate, and reproducible assessment of cardiac function in heart failure patients, and other methods appear to have wide variance. CMR is ideal for baseline assessment and follow-up of clinical progression and the effect of treatment in patients with heart failure.

High-Resolution Ex Vivo MR Imaging of the Aorta: A Swine Model of Complex Atherosclerotic Plaque

G. Helft, S.G. Worthley, Z.A. Fayad, J.I. Osende, J.T. Fallon, M. Roque, M. Shinnar, V. Fuster, J.J. Badimon. *New York, NY*

The accurate identification of the components of atherosclerotic plaques will potentially lead to the risk stratification and help direct therapeutic approaches in patients with atherosclerotic disease. MR imaging has been shown to accurately characterize plaque components. We investigated the ability of high-resolution MR imaging to identify all plaque components in a 1.5-T system in a swine model of complex aortic atherosclerosis.

Atherosclerotic plaques were induced in the Yucatan minipigs (n = 4) by a combination of atherosclerotic feeding and double-balloon injury of the abdominal aorta with a 4 Fr Fogarty embolectomy catheter (at diet initiation and 3 months). At sacrifice the aortas were perfusion fixed and ex vivo MR imaging performed with a 3-inch surface coil. Fast spin echo sequences were performed with an in-plane resolution of 234 × 234 microns, slice thickness of 3 mm, and signal averaging of 4. Images with T1 (TR/TE 600/14 msec), T2 (TR/TE 2300/80 msec), and proton density weighting (PDW) (TR/TE 2300/16 msec) were acquired. MR images and histologic sections (n = 43) were matched and analyzed with computer-assisted morphometry. Extensive complex atherosclerosis was noted. Measurements from the MR images of mean plaque area were highly correlated ($p < 0.0001$) with histology (r = 0.97, slope = 0.90). Accurate identification of plaque hemorrhage, calcification, fibrous cap, and lipid-rich regions was observed. As previously reported, T2-weighted images exhibited good contrast between the plaque components. Interestingly, the PDW images also accurately depicted all of the above. T1-weighted images accurately identified calcification.

Thus, PDW and T2-weighted images should be considered when atherosclerotic plaque characterization is required. This model of cholesterol feeding and double-balloon injury produces complex plaque and is potentially a useful model for future in vivo MRI studies of atherosclerotic plaque characterization.

Preliminary Observations of Flow in the Total Cavopulmonary Connection Assessed by Magnetic Resonance Phase Velocity Mapping

Ann E. Ensley, Shiva Sharma, Timothy M. Healy, Katharine Hopkins, George Chatzimavroudis, Ajit P. Yoganathan. *Atlanta, GA*

To understand factors involved in conservation of energy within the total cavopulmonary connection in the single ventricle supported circulations, we initially performed in vitro flow experiments. These included glass models of the total cavopulmonary connection (TCPC) and study of the flow dynamics within them. Having gained valuable insight from in vitro experiments, we proceeded with in vivo flow assessment of the TCPC in patients using magnetic resonance phase velocity mapping.

Nine patient volunteers with the TCPC performed by two surgeons in our institution underwent sedated magnetic resonance phase velocity mapping. The MR images were acquired using a 1.5-T whole-body clinical scanner (GE Medical Systems, Milwaukee, WI). Coronal and axial scout images were used to localize the total cavopulmonary connection site. Once slice locations were determined, velocity data were acquired using a standard gradient-echo pulse sequence with flow quantification enabled. Three adjacent 5-mm-thick coronal slices were acquired. Velocity was encoded in each slice along three principal directions: superior-inferior, right-left, and anterior-posterior. Respiratory and retrospective ECG gating were employed to acquire 16 phases during the cardiac cycle. Imaging parameters were as follows: FOV: 20 cm, TR: 23 ms, TE: 6.2 ms, matrix: 256 × 256, flip angle: 35°, and velocity encoding value: 70 cm/s. The total examination time was approximately 75 minutes. The raw binary scanner data were reconstructed and visualized using commercial computational fluid dynamics visualization software. Animations of spatial and time varying data were used to elucidate the flow within the TCPC and adjoining vessels.

Analysis of data reveals that flow within the inferior vena cava (IVC) was random and chaotic in seven of the nine patients, while two patients had a more organized flow. In contrast, superior vena cava

(SVC) flow was more streamlined. The chaotic flow in the IVC persisted in all acquired slices and throughout most of the cardiac cycle. Figure 1 is an example of one patient's reconstruction. The possible explanations for this phenomenon are many, including the relative dilation of IVC conduit compared to SVC, the difference in materials used for the IVC conduit compared to the patient's native SVC, or the introduction of "noise" into a sluggish area of flow. Further work is needed to elucidate the cause of this important finding.

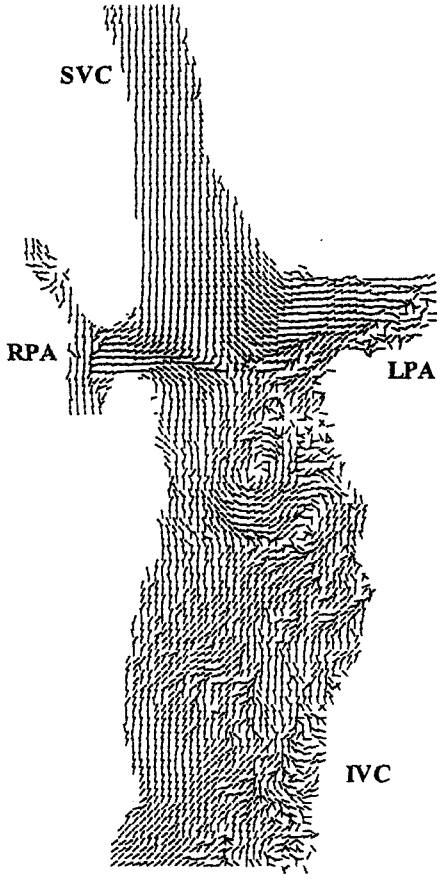

Figure 1. Example reconstruction of TCPC flow.

Evaluation of Hemodynamic Data in Patients with Dilated Cardiomyopathies: Comparison of Magnetic Resonance Imaging and 2- and 3-D Echocardiography

Th. Wittlinger,[1] T. Voigtländer,[1] K.F. Kreitner,[2] J. Scharhag,[1] P. Kalden,[2] K. Grauvogel,[1] M. Thelen,[2] J. Meyer.[1] [1]*2nd Medical Clinic and* [2]*Department for Radiology, University Hospital, Mainz, Germany*

It was the purpose of the study to evaluate hemodynamic data of patients with dilated cardiomyopathy (DCM) and to show the correlation between magnetic resonance imaging (MRI) and 2- and 3-D echocardiography.

Methods: We investigated 28 patients (22 men, 6 women) with a clinical manifested DCM. MR cineventriculography (1.5 T, Vision, Siemens AG) was performed with an ECG-gated, breathhold, multislice FLASH 2-D sequence with a thickness of 8 mm. A 2-D echocardiography (Sonos 2500, Hewlett Packard) was performed in all patients and a 3-D echocardiography in 12 patients. We determined the left ventricular muscle mass (MM), the ejection fraction (EF), the end diastolic (EDVI) and end systolic (ESVI) volumes, and the systolic thickness of the posterior wall (inf. w.s.) and of the septum (Ss).

Results:

	EF	EDVI	ESVI	inf.w. s.	S.s.	MM/g	MM/g
MR	21.84%	102.1 ml	79.72 ml	1.3 mm	1.24 mm	219.6	219.6
Echo	27.89%	113.4 ml	84.46 ml	1.34 mm	1.08 mm	290.5 2-D	182.0 3-D
p Value	0.0005	0.0005	0.005	n.s.	0.005	n.s.	0.035

Conclusions: Concerning the EF, EDVI, ESVI, and the systolic septum thickness, a significant statistical correlation could be found. No correlation could be determined with regard to the thickness of the posterior wall and the muscle mass between MRI and 2-D echocardiography. There is a trend to statistical correlation between 3-D echocardiography and MRI concerning the muscle mass determination. At present, MRI is the gold standard in the evaluation of the muscle mass of the left ventricle, since 2-D echocardiography supplies to high muscle mass data.

References

1. Kondo C. Right and left ventricular stroke volume measurements with velocity-encoded cine MR imaging. *AJR*, 1991; 157:9–16.
2. Hundley WG. Quantification of cardiac output with velocity-encoded, phase-difference magnetic resonance imaging. *Am J Cardiol*, 1995; 75:1250–1255.

Calculation of Relative Cardiac Pressure Along Streamlines Using Time-Resolved 3D Phase Contrast MRI

T. Ebbers,[1] A. Fyrenius,[1] L. Wigström,[1] A.F. Bolger,[2] M. Karlsson.[1] [1]*Linköping University, Sweden;* [2]*University of California at Riverside, CA*

Introduction: Noninvasive cardiac pressure registration has potential to become an important diagnostic tool for assessing cardiac function. However, calculation of the relative pressure field from a phase contrast data set using the Navier-Stokes equations (1), is time consuming for time-resolved 3D data. Furthermore, the method requests an accurate segmentation. A fast calculation of the cardiac pressures can be performed based on instantaneous streamlines calculated from 3D phase contrast data.

Methods: A time-resolved 256 × 96 × 16 velocity data set was obtained from a healthy volunteer using a GE Signa Horizon Echospeed scanner and a 3D cine phase contrast sequence (TR = 18 ms, TE = 6 ms, and VENC = ±60 cm/s). The velocity data were corrected for eddy current and concomitant field effects. Instantaneous streamlines were obtained by integrating the velocity starting at a specific location and time. Based on the Euler equation, spatial pressure gradients were calculated along these streamlines from the spatial and temporal gradients. The relative pressure was obtained by integrating the pressure gradients along the streamline.

Results: During diastole, streamlines were constructed starting in the left atrium for early and late ventricular filling. The pressure at the starting point of the streamline is taken as reference pressure ($p = 0$ mm Hg). The vena contracta (VC) and following pressure recovery could be easily recognized.

Discussion: Relative cardiac pressure calculation along streamlines provides a noninvasive quantitative parameter to assess diastolic function. This three-dimensional method obtains the important relative pressures, without necessity of an accurate segmentation or time-consuming calculation.

Reference

1. Yang GZ, Kilner PJ, Wood NB, Underwood SR, Firmin DN. Computation of flow pressure fields from magnetic resonance velocity mapping. *MRM*, 1996; 36:520–526.

Calculation of Left Ventricular (LV) Parameters—A Faster Method

Paulo R. Schvartzman, Scott D. Flamm, Jeffrey M. Bundy, Michael L. Lieber, Richard D. White. *Cleveland Clinic Foundation, Cleveland, OH and Siemens Medical Systems*

Introduction: Magnetic resonance imaging (MRI) of the heart is performed routinely to evaluate LV mass, volumes, and function, but the required postprocessing is time consuming. A faster but accurate and reproducible method is desirable.

Methods: Thirty patients with symmetric LV morphology (normal; dilated cardiomyopathy; and aortic valve disease) were studied. Contiguous 8–10-mm-thick cine gradient echo slices were acquired in the short-axis (SA) plane from the base of the heart to the apex using a 1.5-T Siemens Vision scanner. A surface coil was used for improved S/N and breathholding to minimize respiratory artifacts. LV mass (LVM), end-diastolic volume (EDV), end-systolic volume (ESV), stroke volume (SV), and ejection fraction (EF) were measured using the Siemens Argus software platform after endocardial and epicardial contours were drawn ("every slice") [ES]). Beginning with the basal slice as 1, all even numbered slices were then deleted. Parameters were then recalculated on the remaining slices using the same software, which accounts for missing slices by interpolation between adjacent slices ("every other slice" [EOS]).

Results: Linear regression (ES = b + m(EOS)) was performed relating ES and EOS for each parameter (Table). Observed EOS values for all parameters showed good agreement with ES over a broad range of LV dimensions:

	LVM	EDV	ESV	SV	EF
Every slice	7.39 + 0.99 (EOS)	0.81 ± 1.02 (EOS)	−0.12 + 1.02 (EOS)	1.75 + 1.02 (EOS)	0.69 + 0.99 (EOS)
95% CI	+2%, −9%	+1%, −6%	+7%, −10%	+7%, −18%	+9%, −14%

Conclusions: Calculation of LV mass, volumes, and ejection fraction with EOS method correlates well and demonstrates good agreement with ES and can be used routinely to shorten the required acquisition and postprocessing time.

Is Enhancement with Gadophrin-2 Related to Matrix Metalloproteinase Expression Postmyocardial Infarction?

A. Zenovich, N. Wilke, M. Jerosch-Herold, A.M. Mansoor, H. Huang, J.R. Dutcher. *Minneapolis, MN*

Novel MR contrast agent bis-gadolinium mesophorphyrin (gadophrin-2) demonstrated itself as necrosis-avid in acute ischemic models (1). The ability of postcontrast MR imaging with gadophrin-2 to differentiate the severity of myocardial necrosis has been recently demonstrated (2). Specificity toward necrosis, absence of enhancement of the normal myocardium, prolonged retention at the site of enhancement, consistent hyperenhancement in chronic and transient ischemia 6 hours postinjection in pigs (n = 17) at 1 wk, and the hypoenhancement at 6 and 27 hours 4–6 wks (n = 5) post-left circumflex coronary artery ligation indicate a potential specific association mechanism of gadophrin-2 within myocardial tissue at the early (3–8 days) stages postinfarction. Myocardial injury results in increased expression of matrix metalloproteinase (MMP) via two major pathways: protein kinase C− and apoptosis-induced transcription of MMP mRNA. Elevation of protein kinase C is a direct consequence of the increase in circumferential wall stress with concomitant increase in local expression of catecholamines, angiotensin II, and endothelin (3). Apoptosis-induced MMP mRNA transcription is mediated by TNF-alpha, IL-1, and IL-6 (4). The maximum MMP transcription occurs at day 7 postinfarction (5), the time of neutrophilic and macrophage infiltration, nuclear loss, and sarcoplasmic coagulation but absence of ongoing scar formation with increase in collagen production, which begins at 2 weeks and is completed at 4–6 weeks postinfarction. Interestingly, the enhancement with gadophrin-2 is observed at 1 week postinfarction and is not seen at 4–6 weeks, even though sufficient time (27 hours) was allowed for possible diffusion of the agent into the area of myocardial damage. Enhancement distribution pattern of gadophrin-2 suggests absence of interaction with the components of the scar (collagen, elastin) and the existence of possible noncovalent interations between gadophrin-2 and MMP, which may account for specificity of the agent, prolonged retention in the damaged area, and differentiation of severity of myocardial necrosis. The insights into possible interactions of gadophrin-2 and MMP merit further research.

References

1. Marchal G, Ni Y, Herijers P, et al. *Eur Radiol*, 1996.
2. Wilke N, Zenovich A, et al. *Circulation*, 1998.
3. Mann D, Spinale F. *Circulation*, 1998.
4. Ono H, et al. *Circulation*, 1998.
5. Kai H, Ikeda H, et al. *JACC*, 1998.

Sodium Delivery Determines the Increased MR Signal Intensity of Acute Reperfused Myocardial Infarction

H.B. Hillenbrand,[1] L.C. Becker,[1] C.E. Rochitte,[1] R.J. Kim,[2] E.L. Chen,[2] J.A.C. Lima.[1] [1]*Johns Hopkins Hospital, Baltimore, MD;* [2]*Northwestern University, Chicago, IL*

Fast, 3D, 23Na MR imaging (Na MRI) has been used to detect and monitor reperfused MI in vivo. Delayed signal intensity (SI) increase in the areas of microvascular obstruction (MO) has suggested that sodium delivery is an important mechanism to explain the increased SI in reperfused MI. However, the relationship between sodium delivery and the SI in infarcted areas without MO has not been explored.

To address this question, eight dogs were submitted to a closed-chest model of coronary occlusion (90 min, ballon angioplasty, left anterior descending coronary artery) and reperfusion. Coronary occlusion and reflow were verified by angiography, MI by postmortem TTC stain. Absolute flow was determined using radioactive microspheres at baseline, during occlusion, and after 20 min of reperfusion. In vivo Na MR images were obtained between 130 and 210 min after reperfusion in seven dogs using a segmented k-space, fast, 3D GRASS sequence at 4.7 T (TR = 12.6 ms, TE = 4.3 ms, nvp = 32, NEX = 32, FOV = 384 mm, slab thickness = 96 mm, matrix = 128 × 128 × 32, voxel size = 3 × 3 × 3 mm). One animal died before MR imaging could be performed. The sodium SI in the infarcted tissue (excluding MO), expressed as the ratio of infarcted versus remote tissue (MI/R), was correlated to either absolute flow in ml/g/min or the cumulative absolute flow over time (in ml/g), taking into account the varying time delays between the onset of reperfusion and MR imaging.

Mean absolute flow to the TTC-negative tissue (excluding areas of MO) during reperfusion was 2.89 ml/g/min and 348 ml/g until the first

Na MR image in all dogs. MI/R was highly correlated to absolute flow (r = 0.85) and cumulative absolute flow (r = 0.93, see Fig.).

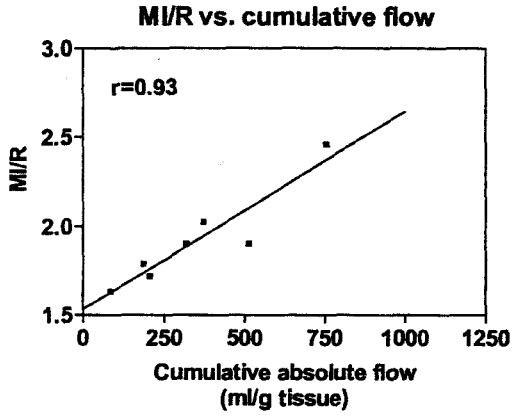

Figure 1

We conclude that in acute reperfused MI, sodium delivery is a predominant mechanism for the increased sodium signal intensity.

Analysis of the First-Pass Myocardial Perfusion in Patients with Acute or Subacute Infarction Using Ultrafast MRI

J. Scharhag,[1] T. Voigtländer,[1] T. Wittlinger,[1] K.-F. Kreitner,[2] W. Schreiber,[1] P. Kalden,[2] M. Thelen,[2] J. Meyer.[1] [1]*2nd Medical Clinic,* [2]*Clinic for Radiology, University Clinic, Mainz, Germany*

The aim of the study was to compare perfusion parameters in infarcted and noninfarcted myocardium after successful revascularization using ultrafast magnetic resonance imaging (MRI).

Methods: Nineteen patients (55 ± 10 years) with acute or subacute myocardial infarction and angiographic TIMI flow 0 were included into the study. Successful revascularization with TIMI flow 3 was obtained by PTCA or stenting within 7.5 ± 6.8 hours in 16 patients. MRI was performed within 5.8 ± 1.7 days (Siemens Magnetom Vision 1.5 T, single slice, turbo-FLASH, breathhold, ECG-gated, Gd-DTPA). The left myocardium was divided clockwise into 16 segments. In each segment following parameters were determined: 1. normalized signal intensity (NSI) = SI − baseline SI; 2. time to peak; 3. slope.

Results: In all cases central dark zones with significant diminished NSI at the perfusion beds of the infarct-related artery were obvious. Also time to peak and slope were significantly different:

	Infarcted	Noninfarcted	Difference (%)	p Value
NSI	22.5 ± 13.4	41.2 ± 16.4	−45%	<0.0001
Time to peak (sec)	25.4 ± 10.76	19.9 ± 11.31	+128%	0.0012
Slope (NSI * 10^{-3}/sec)	0.99 ± 0.69	2.59 ± 1.71	−62%	<0.0001

Conclusion: Infarcted myocardium can be distinguished exactly from noninfarcted myocardium. In the infarcted segments the perfusion is represented by the diminished SI, the prolonged time to peak, and the reduced slope, at which the slope shows the biggest difference. These data support the concept of the retarded wash-in of the infarcted region.

References

1. Lima et al. Regional heterogeneity of human infarcts demonstrated by contrast enhanced MRI—potential mechanisms. *Circulation,* 1995; 92:1117–1125.

2. Kim et al. Myocardial Gd-DTPA kinetics determine MRI contrast enhancement and reflect the extent and severity of myocardial injury after acute reperfused infarction. *Circulation,* 1996; 94:3318–3326.

Stunned Myocardium—Detection of the Infarcted Region and Improved Contraction After 3 Months by MRI After Successful Interventional Revascularization

J. Scharhag,[1] T. Voigländer,[1] T. Wittlinger,[1] K.-F. Kreitner,[2] W. Schreiber,[1] S. Möbus,[1] P. Kalden,[2] M. Thelen,[2] J. Meyer.[1] [1]*2nd Medical Clinic,* [2]*Clinic for Radiology, University Clinic, Mainz, Germany*

In cardiothoracic MRI, the fast short inversion recovery sequence (STIR) allows the illustration of the intra- and extracellular edema in the early period of the myocardial infarction and the cine-MRI allows the analysis of myocardial contraction. The aim of the study was to study the effects of interventional revascularization (PTCA, stenting) on the myocardium by STIR and cine-MRI.

Methods: In 12 patients with acute myocardial infarction and successful interventional revascularization, after 2–7 days and after 3 months STIR and cine-MRI were performed (Siemens Magnetom Vision 1.5 T, short-axis view, single slice, slice thickness 10 mm, breathhold, ECG-gated). After automatic division of the left myocardium into 40 segments, in each segment following parameters were determined: the relative signal intensity (RSI): $(SI_{max} - SI_{min})/SI_{abs} * 100$ [%] and the diastolic-systolic thickening of the myocardial wall.

Results: After myocardial infarction in the acute period 11.7 ± 3.4 segments of the perfusion bed of the infarct related artery showed an increased RSI > 50%. In these segments a significant improvement of the myocardial wall thickening was obvious after 3 months:

	Thickening (mm)		
	Acute	3 Month Follow-Up	p Value
RSI > 50%	4.34 ± 2.6	6.04 ± 3.9	0.038
RSI < 50%	5.57 ± 2.7	6.30 ± 3.0	n.s.

Conclusion: In segments of myocardial infarction detected by STIR with an increased RSI > 50% in the early period of the myocardial infarction, 3 months after successful interventional revascularization a significant improvement of the wall thickening could be obtained. This observation supports the concept of the retarded recovery and improvement of the regional contraction of the myocardium. The benefit of a interventional revascularization can be demonstrated and controlled by MRI.

Evidence of Low and High Coronary Disease Groups by Magnetic Resonance Perfusion Parameters

M. Doyle,[1] E. Kortright,[1] A. Fuisz,[1] R.W.W. Biederman,[1] E. Walsh,[1] V.N. Miele,[2] B.L. Sharaf,[2] V. Bittner,[1] W. Rogers,[1] G.M. Pohost.[1] [1]*Birmingham, AL;* [2]*Providence, RI*

Introduction: Magnetic resonance perfusion imaging has shown great promise for detection of coronary artery disease (CAD). However, in our experience with the Women's Ischemia Syndrome Evaluation (WISE) study, the modality still lacks adequate diagnostic sensitivity. In part, this is attributable to highly variable appearance of perfusion defects between patients. Therefore, we examined the characteristics of MR first-pass perfusion data to determine if certain image characteristics differentiated between low and high disease groups. Knowledge of disease probability (derived from the test) would aid in data interpreta-

tion and serve to increase sensitivity. This is analogous to use of pretest probabilities to interpret data.

Methods: For 92 patients the relative slope of myocardial signal increase compared to the left ventricular blood pool was calculated in six myocardial regions for two slices and averaged. The extent of coronary artery disease was determined by a computer-assisted reading of the catheterization angiograms at the WISE core laboratory and a severity score calculated for three cardiac territories: anterior, inferior, and lateral.

Results: A plot of the maximal regional disease severity against the slope index (Figure) shows a trend for probability of disease occurrence and severity to increase as the slope index decreases. Selecting a threshold of 0.22 to differentiate high and low relative slopes and selecting a regional disease severity threshold of 15 produces the following grouping: low slope: 45 patients with 31% (14) diseased patients, and high slope: 47 patients with 6% (3) diseased patients ($p < 0.01$). Probability of disease occurrence can be calculated for any slope index.

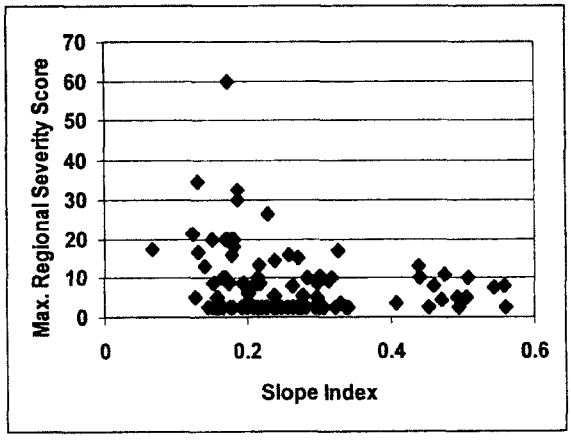

Figure 1

Conclusions: It appears that image characteristics in MR perfusion imaging are associated with differences in likelihood of coronary artery disease, perhaps due to underlying differences in blood flow. Knowledge of coronary disease probability may allow more sensitive reading of perfusion images by adjustment of interpretation parameters. The relative slope index, which is unique to MR perfusion images, provides such a discriminator of disease probability.

Discrimination Between the Flow Patterns of the Great Cardiac Vein and LAD with MR Phase Contrast Velocity Mapping

W.L.F. Bedaux, M.B.M. Hofman, A.C. van Rossum, C.A. Visser. *Dept. of Cardiology, Clinical Physics & Informatics, University Hospital Vrije Universiteit, Amsterdam, The Netherlands*

Purpose: With MR flow mapping it is possible to quantify flow velocity and volume flow in the coronary arteries. Because of the close anatomic relationship of the left anterior descending coronary artery (LAD) with the great cardiac vein (GCV), they are easily misinterpreted. We examined a method to discriminate between these two structures.

Methods: Six patients, mean age 53 yrs, all male, underwent MR imaging to quantify the flow in the LAD. [One vessel disease (5), LAD stenosis 90% (3), LAD no stenosis (3), after anterior myocardial infarction (2) treated with thrombolysis (1) or primary PTCA (1)]. From series of angiographic MR images using connectivity to the aortic root, differentiation between LAD and GCV was made. Perpendicular to the LAD MR phase contrast velocity mapping was performed within a breathhold. A region of interest (ROI) was drawn around the LAD, GCV, and nearby located myocardial tissue to analyze the flow data.

Results: After correction for cardiac motion of the vessel, we could differentiate between the LAD and the GCV by the direction of the cross-sectional averaged mean velocity: LAD 5.0 ± 1.0 cm/s vs. GCV −3.3 ± 2.5 cm/s. The arterial flow pattern is mainly diastolic in contrast with the venous flow pattern, which is mainly systolic (Figure). The absolute flow velocity values were lower in this group than one would expect in healthy individuals.

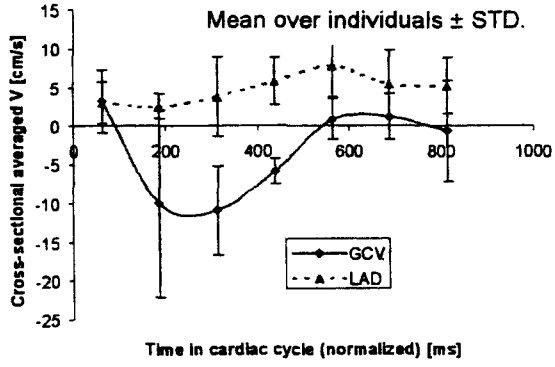

Figure 1

Conclusion: Differentiation can be made between the GCV and the LAD using the flow pattern. The flow in the GCV is mainly systolic and points in the inverse direction as the flow in the LAD. These differentiation criteria appeared valid even in cases with highly stenotic arteries. The phasic flow pattern in the GCV in humans has not been described before. Our findings are in agreement with flow patterns described in animal studies (1).

Reference

1. Canty JM Jr, et al. *Am J Physiol,* 1990; 258:H1457–H1463.

Perfusion Processing: Correcting Phased-Array Coils Intensity Modulations

J.E. Siebert, M.C. DeLano, J.D. Eisenberg, J.A. Gift. *East Lansing, MI*

Derived parametric images can portray the dynamics information contained in the cardiac perfusion image set to aid exam interpretation and to summarize exam results. Calculation of perfusion-dependent parameters requires a correction of the spatial SI modulations arising from cardiac phased-array surface coil reception. We present a correction method based on the perfusion image set itself that requires no additional scan time (1–3), introduces no additional noise sources (1,2), and avoids the edge effects and attenuation of anatomic low spatial frequencies of corrections based on low-pass filtering (1,2).

Methods: The baseline images of the perfusion acquisition—those images acquired prior to the Gd arrival into the LV—serve as the basis for the intensity correction estimate. The correlation procedure: (1) detect the first-pass event in LV blood pool. The arrival time of the Gd bolus in the LV is the end of the baseline period. (2) Average all baseline images at each slice location—provides the basis for the estimated intensity correction. (3) Identify myocardium voxels to serve as a sparse 2D sampling of the smoothly varying coil sensitivity (x,y); spatial filter to reduce noise errors. (4) Fit a minimum curvature surface to this sampling—serves as the estimate of coil sensitivity (x,y) across entire image area. If the curved surface fit quality is inadequate, a plane is then

fitted. (5) Compute an intensity correction factor (x,y) as a scaled reciprocal, multiplied pixel-wise with all the original images at that slice location. Scaling is set to maintain the same average value of myocardium voxels for constant display window level.

Results: The performance of the intensity correction method is demonstrated by scanning a body-sized doped-water phantom using the cardiac phased array coil set and the retrospectively gated FastCard with echo-planar readout perfusion pulse sequence (4). The resulting intensity-corrected image shows that the minimum curvature estimation performs satisfactorily across the image field while ensuring a high quality correction in the region of the sampling contour (LV myocardium in actual perfusion images).

Discussion: The actual surface coil sensitivity across any image FOV will be always smoothly varying and will contain one inflection at most across the LV. Analytical solution is hampered by undetermined coil shapes (flexible devices), undetermined spatial orientations, variable relative positions for every slice position, and impracticality of additional calibration acquisitions. Thus we attempt this approach to correction estimation based on minimum curvature surface fitting. In the resulting images, SI scaling is flattened assuredly across LV myocardium, while estimation errors can worsen with extrapolation into distant image regions (irrelevant to perfusion postprocessing). In low SI regions distant from coils, lower SNR can become very apparent in intensity-corrected images. The presented method of correcting spatial SI modulation by surface coil sensitivity variations enables the calculation of the first-pass leading SI-increase slope (time rate) image, any parameter dependent on slope measure, and tracer kinetic modeling. Intensity correction also facilitates visual interpretation and enables more effective filming (windowing).

References

1. Murakami JW, Hayes CE, Weinberger E. Intensity correction of phased-array surface coil images. *Magn Reson Med,* 1996; 35:585–590.
2. Grant PE, Vigneron DB, Barkovich AJ. High-resolution imaging of the brain. *MRI Clin N Am,* 1998; 6:1:139–154.
3. Thulborn KR, Boada FE, Shen GX, Christenson JD, Reese TG. Correction of B_1 inhomogeneities using echo-planar imaging of water. *Magn Reson Med,* 1998; 39:369–375.
4. Ding S, Wolff SD, Epstein FH. Improved coverage in dynamic contrast-enhanced cardiac MRI using interleaved gradient-echo EPI. *Magn Reson Med,* 1998; 39:514–519.

Fully Automated Registration and Warping of First-Pass Magnetic Resonance Perfusion Images

C. Gallippi, W.J. Rogers, Y.-L. Hu, N. Reichek, C.M. Kramer.
Allegheny General Hospital, Pittsburgh, PA

Introduction: Regional changes in myocardial signal enhancement after bolus administration of T1 shortening agents are useful in assessing myocardial ischemia and necrosis. However, respiration results in in-plane and through-plane motion. Cardiac cycle length variations alter when images are acquired and results in variable cardiac geometry. Together these changes limit quantification. The purpose of this study was to use image features to perform automated in-plane registration and warping to correct for physiologic motion.

Method: Short-axis perfusion images were acquired during every RR interval using an inversion prepared T1-weighted segmented k-space sequence (90 × 128 matrix, 350 mm FOV). A Sobel filter was applied to all images to highlight edge features. A Sobel image with well-visualized edges was defined as the template. Image "landmarks" within the template were determined by partitioning the myocardium into 16 blocks and identifying pixels with high edge contrast. Differences in the x-y location of landmarks between the template and nontemplate Sobel images were recorded. Differences in landmark locations were minimized by rigid-body translation of pixels within the nontemplate perfusion images. Finally, differences in landmark locations were further minimized by bilinear image warping within the acquired perfusion images. Myocardial time-intensity curves were compared between raw and processed images by placing eight equally spaced fixed regions of interest around the LV wall.

Results: Cine loops comparing processed to unprocessed short-axis perfusion images were qualitatively evaluated. Both in-plane translation and changes in LV size were minimized in the processed images. Intensity-time plots showed less beat-to-beat variation within the processed image series.

Conclusion: Fully automated registration and warping of myocardial perfusion images may improve qualitative interpretation and permit pixel-by-pixel quantitation of perfusion parameters sensitive to ischemia and infarction.

Mechanisms of Gd-DTPA Contrast Enhancement in Acute and Chronic Myocardial Infarction

W.G. Rehwald, D.S. Fieno, E.L. Chen, R.J. Kim, R.M. Judd.
Chicago, IL

Recent studies indicate that hyperenhancement is observed in patients with acute and chronic myocardial infarction following administration of Gd-DTPA. Because tissue ultrastructure changes dramatically during infarct healing, it is unclear why hyperenhancement occurs in both acute and chronic irreversible injury. To explore the mechanisms of hyperenhancement, we used electron probe x-ray microanalysis (EPXMA) to simultaneously measure relative concentrations of Gd-DTPA as well as those of Na, P, Cl, K, and Ca. Eight acute rabbits were subjected to 40 min coronary artery occlusion and 60 min reperfusion. Fourteen chronic rabbits were occluded permanently for 2 weeks. Gd-DTPA was administered and allowed to circulate for 25 min. The hearts were excised and rapidly frozen, sectioned, freeze-dried, and examined in a scanning electron microscope equipped with EPXMA. A total of 58 acute and 102 chronic x-ray spectra were acquired from randomly selected injured and normal regions. In the acute infarcts, Gd, Na, Cl, and Ca increased to 2.26 ± 0.93, 1.56 ± 0.16, 1.70 ± 0.49, and 9.69 ± 6.80 times the values in normal regions (mean ± 95% confidence interval), respectively, while P and K decreased to 0.82 ± 0.15 and 0.68 ± 0.24. Similarly, in the chronic infarcts Gd, Na, and Cl increased to 4.72 ± 1.69, 3.32 ± 0.61, and 2.81 + 0.87 times normal while P and K decreased to 0.48 ± 0.13 and 0.47 ± 0.11. These data demonstrate that although not actively transported, Gd-DTPA accumulates in regions characterized by severe disturbances in myocardial electrolytes and suggest that the mechanism of Gd-DTPA hyperenhancement in regions of both acute and chronic irreversible injury may relate to an absence of viable myocytes to exclude Gd from the MRI voxel.